



Universiteit
Leiden
The Netherlands

Microfluidic 3D cell culture for high throughput screening

Trietsch, S.J.

Citation

Trietsch, S. J. (2017, December 18). *Microfluidic 3D cell culture for high throughput screening*. Retrieved from <https://hdl.handle.net/1887/57795>

Version: Not Applicable (or Unknown)

License: [Licence agreement concerning inclusion of doctoral thesis in the Institutional Repository of the University of Leiden](#)

Downloaded from: <https://hdl.handle.net/1887/57795>

Note: To cite this publication please use the final published version (if applicable).

Cover Page



Universiteit Leiden

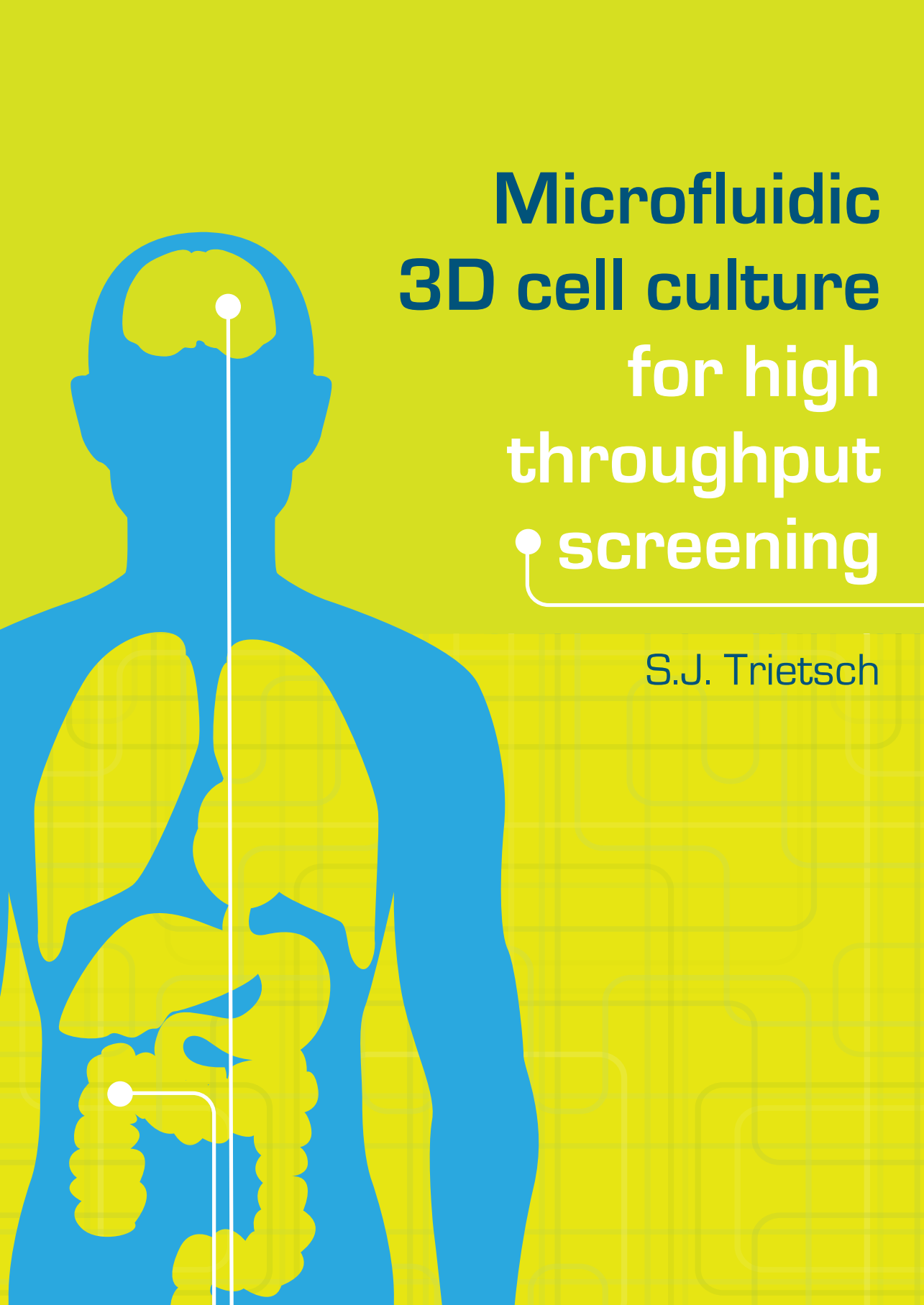


The handle <http://hdl.handle.net/1887/57795> holds various files of this Leiden University dissertation

Author: Trietsch S.J.

Title: Microfluidic 3D cell culture for high throughput screening

Date: 2017-12-18

A stylized blue silhouette of a human figure is positioned on the left side of the cover. Inside the silhouette, yellow shapes represent internal organs: a brain in the head, lungs in the chest, and a coiled large intestine in the abdominal area. Two white lines, representing microfluidic channels, originate from small white circular ports. One line starts in the brain and extends vertically down the center of the body. The other line starts in the large intestine and extends horizontally to the left before turning vertically down. The background is a solid yellow color. On the right side, the title is written in a bold, sans-serif font, with the first part in blue and the second part in white.

Microfluidic 3D cell culture for high throughput screening

S.J. Trietsch

Microfluidic 3D cell culture for high throughput screening

Sebastiaan Johannes Trietsch

The printing of this thesis was financially supported by Mimetas BV

© S.J. Trietsch, The Hague, The Netherlands

Microfluidic 3D cell culture for high throughput screening

The research described in this thesis was performed at the division of Analytical Biosciences, LACDR, Leiden University, Leiden The Netherlands

ISBN: 978-94-6233-831-9

Cover: Kitty Joore

Printed by: Gildeprint Drukkerijen, Enschede (www.gildeprint.nl)

Microfluidic 3D cell culture for high throughput screening

PROEFSCHRIFT

Ter verkrijging van
de graad van Doctor aan de Universiteit Leiden
op gezag van de Rector Magnificus Prof. Mr. C.J.J.M. Stolker,
volgens besluit van het College voor Promoties
te verdedigen op maandag 18 december 2017
klokke 12.30 uur

door

Sebastiaan Johannes Trietsch

Geboren te 's Gravenhage in 1985

Promotor:

Prof. dr. Thomas Hankemeier

Co-Promotor:

Dr. Paul Vulto

Promotiecommissie:

Prof. dr. Hubertus Irth, Universiteit Leiden (Voorzitter)

Prof. dr. Joke Bouwstra, Universiteit Leiden (Secretaris)

Overige leden:

Prof. dr. Cornelia van Duijn (Erasmus Universitair Medisch Centrum)

Prof. dr. Andreas Manz (Saarland University, Saarbrücken)

Prof. dr. Roos Masereeuw (Universiteit Utrecht)

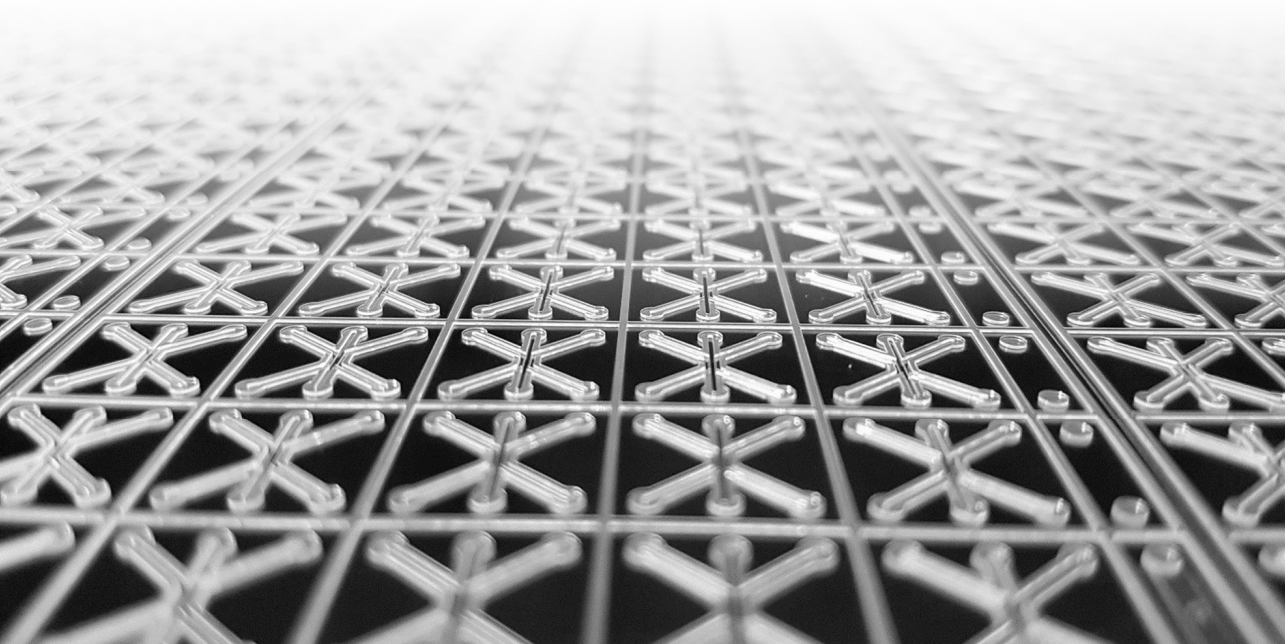
Prof. dr. Anton Jan van Zonneveld (Leids Universitair Medisch Centrum)

Content

Chapter 1	
General Introduction	7
Chapter 2	
Lab-on-a-chip technologies for massive parallel data generation in the life sciences: A review	21
Chapter 3	
Phaseguides as tunable passive microvalves for liquid routing in complex microfluidic networks	55
Chapter 4	
Microfluidic titer plate for stratified 3D cell culture	77
Chapter 5	
Membrane-free culture and real-time barrier integrity assessment of perfused intestinal epithelium tubes	95
Chapter 6	
Model development on the OrganoPlate	127
Chapter 7	
Conclusion and outlook	149
Addendum	
Summary	159
Nederlandse Samenvatting	163
Curriculum Vitae	167
List of publications	169
Acknowledgements	173

Chapter 1

General Introduction



Introduction

Development of a single new drug can take 12-15 years and costs over \$1.3bn.¹ Early in the development process large compound libraries are screened for potential new drug candidates based on fast and cost-effective tests. After extensive *in silico* evaluation of many potential molecules and ultra-high throughput molecule to molecule screening, cell based models are used for selection and prioritization of compounds for further testing. Based on these results, candidates progress towards more predictive, but also lengthier and more costly animal models and eventually human clinical trials.

Even after the extensive selection process in preclinical phases, up to 90% of drugs fail during clinical trials. As approximately 70% of the drug development costs are accrued during these clinical phases it is of vital importance to improve the selection of drug candidates that enter clinical trials. Any enhanced predictivity of preclinical models that can prevent late attrition will have a major impact on costs of drug research and development by improving research output and reducing waste of resources.

As approximately 11% of US, and 7% of global, research and development expenses are devoted to drug research and development, the importance of improving efficiency in this field cannot be overstated.²

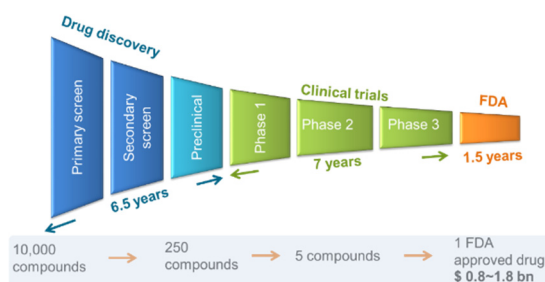


Figure 1 | The drug discovery pipeline. Over 10.000 potential new compounds enter the drug discovery pipeline to get 1 drug to market. Increasingly complex model systems are used to select which drug candidate to move forward through the pipeline towards clinical tests and the market.

Improving preclinical screening

Cell culture models have been the foundation of preclinical efficacy and toxicity screening of drug candidates. Conventional cell culture models consist of monolayers of adherent cells on plastic and are easy to culture and use in high throughput screens. However, these models fail to recapitulate many important aspects of the *in vivo* situation. A lack of physiological cell-cell interaction, 3D morphology, extracellular matrix, interaction with other cell types and complex tissue architecture leads to a poor predictivity for efficacy and safety *in vivo*.

The preclinical drug discovery pipeline shows a gradual increase in complexity and predictivity from *in-silico* modeling, to chemical molecule-to-molecule screens, to conventional cell based models, to animal models. The lack of predictivity of conventional cell based models, however, causes a gap in this selection process, leading to many inappropriate drug candidates to be passed onto animal and, much worse, clinical trials.

Many scientific efforts have been directed at overcoming this gap, and ensuring a more effective selection of drug candidates before progressing into later drug discovery stages. These efforts have consisted of biological advances in cell culture methods as well as engineering advances in devices and tools to enable implementation of new types of in-vitro models.

Advanced cell based assays

The search for better predictive models for use in pre-clinical drug development has pushed the development of more complex cell based models that better recapitulate the complexity of tissues and organs in human physiology. Primary screens make use of new insights gained from advances in genetics and molecular biology to guide compound class selections and the advent of induced pluripotent stem cell technology has provided access to previously unavailable cell types which are patient specific and have defined genotypes. However, when used in conventional 2D assays, these models still lack a large degree of the physiology found *in vivo*.

Ever since the landmark paper by Weaver et al in 1997, which showed vastly different drug response of breast cancer cells cultured in 3D rather than 2D, 3D cell culture has gained momentum.³ 3D cell culture can be performed by embedding

cells in an extracellular matrix. Synthetic hydrogels, or hydrogels extracted from tissues can be used to support cells. Cells mixed with these gels can bind in a more physiological manner. More importantly, the cells can migrate through the gel to form clusters with other cells and form larger tissue constructs. Tuning the physical and chemical properties of the cell's microenvironment, especially in combination with co-culture, can yield complex tissues that better capture the tissue complexity found *in vivo*. 3D cell culture has not only been shown to yield a different morphology, but also modified gene expression, metabolic activity and sensitivity to compounds.

Currently, the superior physiological relevance of 3D cell culture is widely recognized, but its implementation in preclinical testing and screening is still limited. Reasons for this are largely practical in nature: current technologies lack compatibility with imaging and automation and results are difficult to interpret. In addition, although platforms exist to grow tissues in hanging drops or low adhesion plates, these offer only limited advance over current status quo, as perfusion of tissues and complex co-culture options are still lacking. In other words, a platform is needed that addresses aspects of physiological relevance and end-usability in an equally satisfying manner in order to enable the end-user to make the jump towards a next generation of phenotypic models.

Microfluidics

Lab-on-a-chip (LOC) is a field of science and engineering that focusses on miniaturized tools for (analytical) chemistry and life sciences. Since its emergence in the 1990s⁴, the field of lab-on-a-Chip technology has held the promise of translating the immense advantages gained by miniaturization in electronics to the fields of chemistry and the life sciences.

By miniaturizing entire laboratory workflows on a single chip, a great reduction in labor, cost and reagent consumption is envisioned, as well as allowing large-scale parallelization of experiments in a small space. In addition, downscaling can result in unconventional physical and chemical parameters such as extreme surface to volume ratios causing dominance of surface related properties over bulk properties and laminar flow causing dominance of diffusion over advection. Leveraging these properties enables processes that would be physically impossible at conventional scale.

Downscaling of laboratory workflows into LOC devices commonly involves engineering of networks of sub-millimeter sized channels. Fluids are routed through these networks so that they interact with actuators, sensors and other fluids to achieve the desired reaction or readout. The devices can be fabricated using various techniques developed by the semiconductor industry including photolithography, thin film deposition, and wet and dry etching. In addition to utilizing semiconductor materials, other materials such as silicone rubbers have been widely utilized for their biocompatibility, flexibility and ease of processing.

Analytical chemistry is a common application of LOC devices. In addition to the obvious benefits of miniaturization for reduction in reagent use, reduced diffusion distances and proximity of analytes to sensor surfaces can vastly improve reaction speed and detection sensitivity.

Chemical synthesis can benefit from miniaturization through increased reaction speeds, access to high electrical fields, and sharp temperature gradients due to reduced thermal capacity.

Finally, biological applications can strongly benefit from the close control of the microenvironment of cells. Monitoring and manipulation of processes at the cellular level are enabled by the tight control over the microenvironment of cells in microfluidic chips, while the small volumes used avoid the vast dilution of cytokines and other signaling molecules produced by cells.

Organ-on-a-chip

The search for ever more comprehensive cell culture models has triggered efforts towards using lab-on-a-chip technologies to recapitulate organ function and physiology. This field is nicknamed 'organ-on-a-chip'. Organ-on-a-Chip adds perfusion flow, control over signaling gradients, mechanical cues as well as allows integration of actuators and sensors. Early work in combination of cell culture with microfluidics was done by the group of Linda Griffith, who added perfusion flow to a transwell type system⁵, Luke Lee, who aimed to mimic a liver lobule⁶, Mike Shuler who connected various tissues^{7,8} and Roger Kamm, who focused on vasculature aspects⁹.

A widely-lauded organ-on-a-chip publication by the Ingber group in 2010 in Science represents a milestone in Organ-on-a-Chip technology that was now regarded as a scientific discipline in its own right, alongside lab-on-a-chip. The paper by Huh et al.¹⁰ presented a lung-on-a-chip. In this device, conventional multilayer soft lithography is used to manufacture a polydimethylsiloxane (PDMS) chip that allows the culture of endothelium and alveolar epithelium on opposing sides of a porous membrane. The endothelial side is perfused with medium and the epithelial side is exposed to air. By applying a vacuum to flanking channels, the membrane can be stretched to include mechanical forces in this lung model. The exquisite control over liquid flows inside the device, as well as the inclusion of the hitherto unavailable factor of mechanical forces, are a striking demonstration of the progress that is being made in the development of such models. A downside of such devices is that they commonly contain just a single tissue and need significant of chip equipment to run.

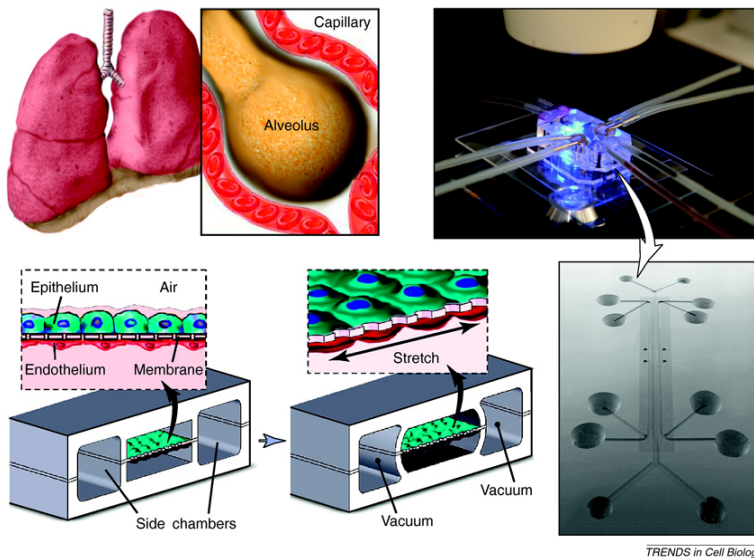


Figure 2 | Lung-on-a-chip concept showing epithelial and endothelial co-culture. Controlled fluidic flow on either side of the membrane is combined with mechanical actuation of the cells by stretching the membrane. This exquisite control over mechanical cues exerted to the cell monolayers is provided by connecting the single device to an off chip pneumatic controlled. (top right).¹¹

In the paper from Van Duinen et al.¹², we reviewed recent efforts in this field with a particular focus on 3D cell culture. We observed a predominance of vasculature and cancer related models. In addition to these, models have been described for most tissues types present in the body including brain^{13,14}, liver¹⁵, kidney^{16,17}, bone¹⁸, gut¹⁹, muscle²⁰, skin^{21,22} and many more.

In a further step, the ambition has extended to model multi-organ interaction and even develop a Human-on-a-Chip in an ambition to capture systemic effects as an alternative to animal models^{11,15,23}.

In parallel to these efforts, tremendous interest was raised amongst end-users, pharmaceutical industry in particular. The question posed itself now: how are these platforms going to be implemented in an end-user environment?

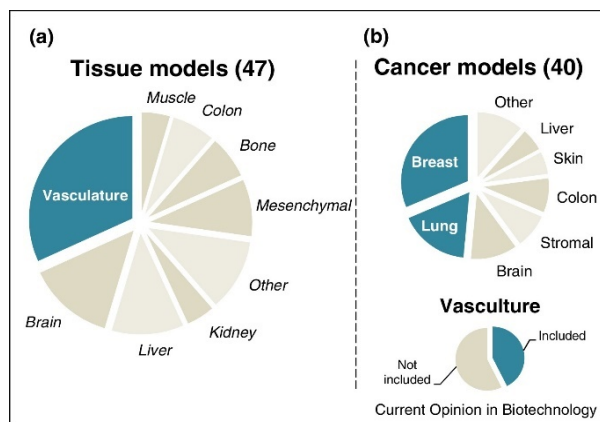


Figure 3 | Overview of the organs modeled in 87 articles published between 2012 and 2015 showing predominance of cancer related and vascular focusses models.¹²

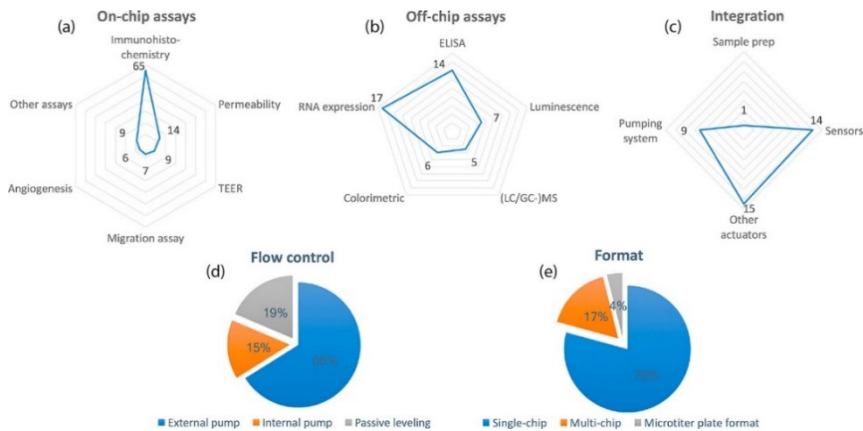


Figure 4 | Overview of assay types, flow control and formats used in 77 Organ-on-a-Chip publications published in 2014-2016. Single chip devices with external flow control make up the majority of published work resulting platforms with a high adoption barrier.²⁴

In a review by Junaid et al²⁴ it was stressed that almost none of the published models fully satisfy end-user usability requirements including assay compatibility, ease of handling and throughput. The majority of available systems are single chip devices designed to carry out experiments with a single copy of an organ model that need to be hooked up to external actuators, severely limiting throughput and scalability.

3D cell culture and organ-on-a-chip technology have the potential to alleviate the major problems facing preclinical drug development. For the strengths of both of these concepts to reach pharmaceutical industry, however, significant limitation still need to be overcome. 3D cell culture offers improved physiological relevance, but is currently associated with cumbersome techniques that are poorly compatible with automation in liquid handling and screening. Microfluidic approaches offer the exquisite control of liquids that could overcome these compatibility issues, but most developed platforms have been focusing on increased complexity instead of increased compatibility and throughput. While the level of control such devices offer is impressive, their suitability for screening, or even usability by non-expert biologists, is limited. For organ-on-a-chip technology to be widely adopted, the focus needs to shift from complex single tissue devices, towards easy to use, high throughput designs.

Scope of this thesis

The aim of the research described in this thesis was to develop a microfluidic platform that enables enhanced physiology in cell culture models by combining 3D cell culture, co-culture and perfusion flow in a single approach. Moreover, a primary guiding principle for the development has been the demand for scalable, compatible technology that is easy to implement by a non-expert end-user. To meet these demands the envisioned 3D cell culture system should meet two sets of design criteria: one for physiological relevance and one for compatibility and ease of use.

Table 1 | Design criteria defined for a 3D cell culture platform that can deliver both high physiological relevance and be easily adopted by end-users. By meeting all these criteria, a platform will be capable providing more predictive cell culture models for use in drug discovery research and screening.

Physiological relevance	End-user adoption
3D tissue morphology	Parallel data point generation
Extracellular matrix embedment	Standard lab equipment compatibility
Co-culture of multiple cell types	Stand-alone operation
Integration of tubules and vessels	Scalable throughput
Absence of artificial membranes	Inert and biocompatible materials
Continuous flow	Usable by non-experts

An overview of available microfluidic technologies for lab-on-chip platforms is described in chapter 2. While many platforms are described that could be employed for 3D cell culture, it was found that their reliance on valves, tubes and complex interfaces for a high level of control and programmability, often rendered them difficult to use and poorly suitable for high throughput screening. To overcome these difficulties, we have chosen to adopt a powerful passive liquid routing technology called phaseguiding²⁵ to control fluids, gels and cells without increasing complexity for the user.

In chapter 3, phaseguide technology was developed to enable complex liquid routing through extended microfluidic networks using only a standard pipet. This unprecedented level of passive control was achieved by choosing to hardwire the fluidic unit operations into the plate, instead of focusing on user programmability of the device. A decision that is completely in line with the needs of robustness and repeatability in a screening environment rather than flexibility of a research laboratory.

In Chapter 4, phaseguide technology was implemented in a dedicated 3D cell culture device, which we called the OrganoPlate. Up to 96 microfluidic networks were embedded in a standard 384 well titerplate. Each network connected 4 wells with specific function and enabled stratified culture of cells embedded in an extracellular matrix with continuous perfusion. The use of a standard plate format, gravity driven perfusion, inert materials and high quality optical readout ensured the platform offered all the envisioned characteristics of a high throughput screening platform.

In chapter 5, the culture of perfused, membrane free, tubular barrier tissues was added to the applications of the microfluidic 3D cell culture platform. A special focus was put on intestinal tubules with proper tissue polarization and transporter expression. The applicability and throughput of the platform was illustrated by providing the largest organ-on-a-chip dataset published to date according to our knowledge. Combining throughput and ease of use with perfused 3D (co-)culture of extracellular matrix (ECM) embedded and barrier type tissues has set the stage for wide adoption of this organ-on-chip platform in laboratories and screening facilities throughout the world.

In chapter 6, we provide an overview of the models and assays developed on the microfluidic 3D cell culture systems by our and other groups. They include models of solid tissues such as the liver, neurons and cancer, as well as barrier type tissues including endothelium and epithelium. The wide range of complex (co-)culture models as well as the described range of assays demonstrates the flexibility of the system and shows that passive microfluidics can be employed to generate culture models of highest biological complexity.

The ongoing adoption of the technology developed in this thesis by expert and non-expert users is setting the stage for the organ-on-chip platform, which we named OrganoPlate, to become a standard for perfused 3D cell culture that is now even implemented in a screening environment. At the time of writing this thesis, the OrganoPlate platform has been applied in a plethora of tissue models at over 50 different sites and is the basis of the company Mimetas, which is currently market leader in the field of organ-on-a-chip.

References

1. DiMasi, J. A., Grabowski, H. G., Hansen, R. W. Innovation in the pharmaceutical industry: New estimates of R&D costs. *J. Health Econ.* 47, 20–33 (2016).
2. Spending, D., Bernstein, E. GLOBAL R & D FUNDING FORECAST A Supplement to R & D Magazine. *IRI/R&D Magazine* 1–36 (2017).
3. Weaver, V. M., Petersen, O. W., Wang, F., Larabell, C. A., Briand, P., Damsky, C., Bissell, M. J. Reversion of the malignant phenotype of human breast cells in three-dimensional culture and in vivo by integrin blocking antibodies. *J. Cell Biol.* 137, 231–45 (1997).
4. Manz, A., Graber, N., Widmer, H. M. Miniaturized total chemical analysis systems: A novel concept for chemical sensing. *Sensors Actuators B. Chem.* 1, 244–248 (1990).
5. Powers, M. J., Domansky, K., Kaazempur-Mofrad, M. R., Kalezi, A., Capitano, A., Upadhyaya, A., Kurzawski, P., Wack, K. E., Stolz, D. B., Kamm, R., Griffith, L. G. A microfabricated array bioreactor for perfused 3D liver culture. *Biotechnol. Bioeng.* 78, 257–269 (2002).
6. Lee, P. J., Hung, P. J., Lee, L. P. An artificial liver sinusoid with a microfluidic endothelial-like barrier for primary hepatocyte culture. *Biotechnol. Bioeng.* 97, 1340–1346 (2007).
7. Viravaidya, K., Sin, A., Shuler, M. L. Development of a Microscale Cell Culture Analog to Probe Naphthalene Toxicity. *Biotechnol. Prog.* 20, 316–323 (2004).
8. Sung, J. H., Shuler, M. L. A micro cell culture analog (microCCA) with 3-D hydrogel culture of multiple cell lines to assess metabolism-dependent cytotoxicity of anti-cancer drugs. *Lab Chip* 9, 1385–1394 (2009).
9. Zervantonakis, I. K., Hughes-Alford, S. K., Charest, J. L., Condeelis, J. S., Gertler, F. B., Kamm, R. D. Three-dimensional microfluidic model for tumor cell intravasation and endothelial barrier function. *Proc. Natl. Acad. Sci.* 109, 13515–13520 (2012).
10. Huh, D., Matthews, B. D., Mammoto, A., Montoya-Zavala, M., Hsin, H. Y., Ingber, D. E. Reconstituting Organ-Level Lung Functions on a Chip. *Science* (80-.). 328, (2010).
11. Huh, D., Hamilton, G. A., Ingber, D. E. From 3D cell culture to organs-on-chips. *Trends Cell Biol.* 21, 745–754 (2011).
12. van Duinen, V., Trietsch, S. J., Joore, J., Vulto, P., Hankemeier, T. Microfluidic 3D cell culture: from tools to tissue models. *Curr Opin Biotechnol* 35, 118–126 (2015).
13. Tourovskaia, A., Fauver, M., Kramer, G., Simonson, S., Neumann, T. Tissue-engineered microenvironment systems for modeling human vasculature. *Exp. Biol. Med.* (Maywood). 239, 1264–71 (2014).
14. Wevers, N., Trietsch, S. J., Vught, R. V, Joore, J., Vulto, P., Lanz, H., Wilschut, K. 3D networks of iPSC-derived neurons and glia for high-throughput neurotoxicity screening. *Toxicol. Lett.* 258, S157 (2016).
15. Maschmeyer, I., Lorenz, A. K., Schimek, K., Hasenberg, T., Ramme, A. P., Hübner, J., Lindner, M., Drewell, C., Bauer, S., Thomas, A., Sambo, N. S., Sonntag, F., Lauster, R., Marx, U. A four-organ-chip for interconnected long-term co-culture of human intestine, liver, skin and kidney equivalents. *Lab Chip* 15, 2688–2699 (2015).

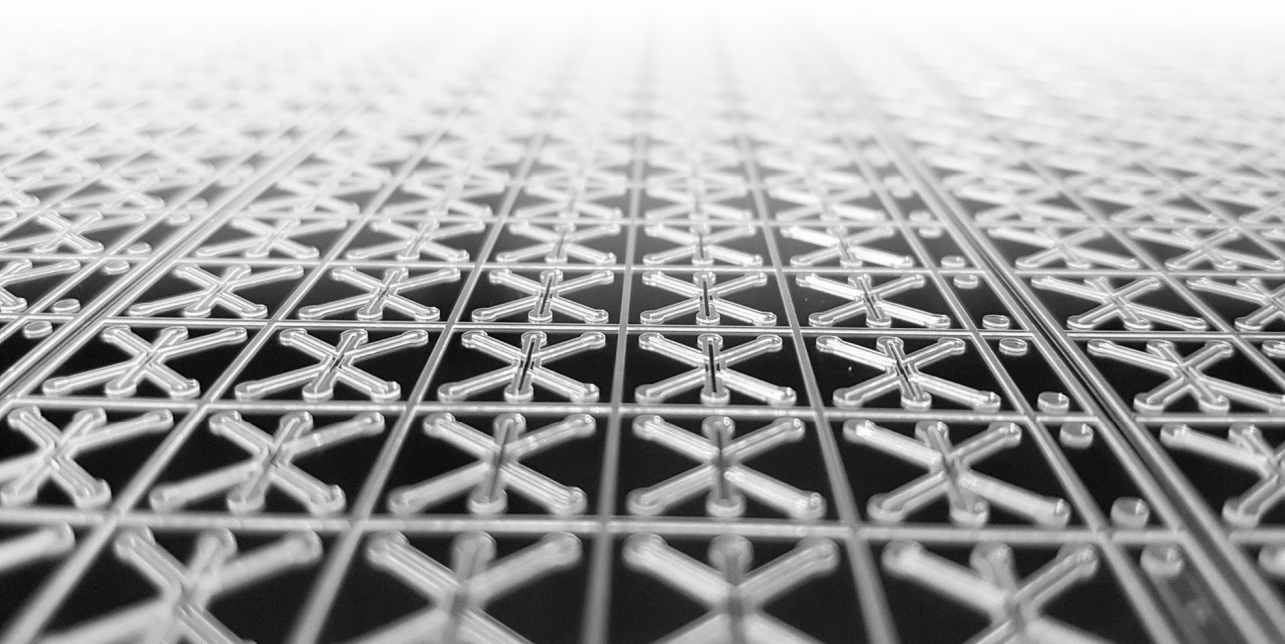
16. Jansen, J., Fedecostante, M., Wilmer, M. J., Peters, J. G., Kreuser, U. M., van den Broek, P. H., Mensink, R. A., Boltje, T. J., Stamatialis, D., Wetzels, J. F., van den Heuvel, L. P., Hoenderop, J. G., Masereeuw, R. Bioengineered kidney tubules efficiently excrete uremic toxins. *Sci. Rep.* 6, 26715 (2016).
17. Motohashi, H., Inui, K. Organic cation transporter OCTs (SLC22) and MATEs (SLC47) in the human kidney. *AAPS J.* 15, 581–8 (2013).
18. Lee, J. H., Gu, Y., Wang, H., Lee, W. Y. Microfluidic 3D bone tissue model for high-throughput evaluation of wound-healing and infection-preventing biomaterials. *Biomaterials* 33, 999–1006 (2012).
19. Kim, H. J., Huh, D., Hamilton, G., Ingber, D. E. Human gut-on-a-chip inhabited by microbial flora that experiences intestinal peristalsis-like motions and flow. *Lab Chip* 12, 2165–74 (2012).
20. Nagamine, K., Kawashima, T., Sekine, S., Ido, Y., Kanzaki, M., Nishizawa, M. Spatiotemporally controlled contraction of micropatterned skeletal muscle cells on a hydrogel sheet. *Lab Chip* 11, 513–517 (2011).
21. Wagner, I., Materne, E.-M., Brincker, S., Süßbier, U., Frädrieh, C., Busek, M., Sonntag, F., Sakharov, D. a, Trushkin, E. V, Tonevitsky, A. G., Lauster, R., Marx, U. A dynamic multi-organ-chip for long-term cultivation and substance testing proven by 3D human liver and skin tissue co-culture. *Lab Chip* 13, 3538–47 (2013).
22. Goral, V. N., Hsieh, Y.-C., Petzold, O. N., Clark, J. S., Yuen, P. K., Faris, R. a. Perfusion-based microfluidic device for three-dimensional dynamic primary human hepatocyte cell culture in the absence of biological or synthetic matrices or coagulants. *Lab Chip* 10, 3380–6 (2010).
23. Bhatia, S. N., Ingber, D. E. Microfluidic organs-on-chips. *Nat. Biotechnol.* 32, 760–772 (2014).
24. Junaid, A., Mashaghi, A., Hankemeier, T., Vulto, P. An End-User Perspective on Organ-on-a-Chip: Assays and Usability Aspects. *Curr. Opin. Biomed. Eng.* (2017). doi:10.1016/j.cobme.2017.02.002
25. Vulto, P., Podszun, S., Meyer, P., Hermann, C., Manz, A., Urban, G. a. Phaseguides: a paradigm shift in microfluidic priming and emptying. *Lab Chip* 11, 1596–602 (2011).

Chapter 2

Lab-on-a-chip technologies for massive parallel data generation in the life sciences: A review

SJ Trietsch, T Hankemeier, HJ van der Linden

Chemometrics and Intelligent Laboratory Systems



Abstract

Lab-on-a-chip (LOC) technology is an important and rapidly developing research field focused on improving experimentation and analysis in the life sciences through miniaturization of full analytical systems into (monolithic) chip substrates. Since its emergence in the 1970s¹, the field has matured, gaining tremendous momentum in the last two decades. Miniaturization and integration of analytical processes on a chip can offer enormous advantages over existing technologies and can create a range of novel opportunities in the life sciences. The developments in the field have led to significant increases in analysis throughput, more than billion-fold sample volume reductions and increased separation efficiency. Despite its potential for the life sciences, the existence and the implications of LOCs are not widely known outside its community.

The aim of this review is to introduce scientists from different disciplines to LOC technology. We will discuss the most important LOCs, their physical operating principles and the unique benefits that can be gained through miniaturization. We will conclude this review with a discussion of the potential of LOCs for massive parallel data generation and their potential implications for the life sciences.

Introduction

This review will cover lab-on-a-chip (LOC) technology and the potential of this rapidly emerging field (Fig. 1) for the life sciences. As the name 'lab-on-a-chip' implies, this technology has the ambitious goal of fabricating entire laboratory analysis workflows in small devices, using technologies similar to microelectronic chip fabrication. To achieve this goal, these (micro-) fluidic 'chips' contain a fully-integrated network of micrometer-scale fluidic components, such as channels, reactors, pumps, chromatographic columns, and detectors. The field of LOC is highly multi-disciplinary, requiring expertise from many fields, including (bio-) chemistry, physics, electronics, (micro-) engineering and (micro-) fabrication. The high level of miniaturization results in faster analyses, higher separation efficiencies, reduced sample, reagent and solvent consumption, as well as allowing unique experiments such as single-cell genomics.

Due to their inherent small size (e.g. mm²), many individual LOCs may be integrated into one larger device, still only several cm² in size, capable of performing many LOC-analyses in a rapid, parallel fashion. An analogy can be drawn with the use of integrated circuits in electronics versus the use of discrete electronic components. As the number of components and connections in an electrical circuit increases, the

chance that the failure of a single connection or component causes malfunction of the entire circuit increases dramatically. This poses a practical limit to the maximum number of discrete components that can be combined in a single functional electronic device, known as the 'Tyranny of Numbers'. Integrated circuit fabrication solved this issue by downscaling the single discrete components, allowing monolithic integration of all components, removing error-prone mechanical connections between discrete components. The same principle applies to LOCs where the monolithic fabrication process eradicates conventional, leakage-prone couplings between discrete fluidic components. Furthermore, monolithic integration can significantly reduce dead volumes and dispersion associated with conventionally constructed analysis systems. As a result, almost arbitrarily complex analysis systems can be fabricated, capable of performing massive numbers of experiments in parallel, which would otherwise not be feasible. Another aspect of monolithic integration, analogous to integrated circuit fabrication, is the strong reduction of cost as large-scale mass fabrication is used.

An example of a monolithic, highly-parallel LOC, which shows the resemblance between electronic circuits and 'large-scale integrated' microfluidics is shown in Fig. 2. This device can perform 256 enzyme expression cell assays that could not be performed with conventional components. The 30×30 mm LOC contains thousands of channels and valves, connected in a highly intricate fluidic network, used to mix reagents and culture cells in 256 separate 750 pL chambers. Fabricating the analysis setup with conventional components (i.e. capillaries, pumps and valves) would literally cost tens of thousands of dollars while LOCs based on this technique are available for less than \$100³.

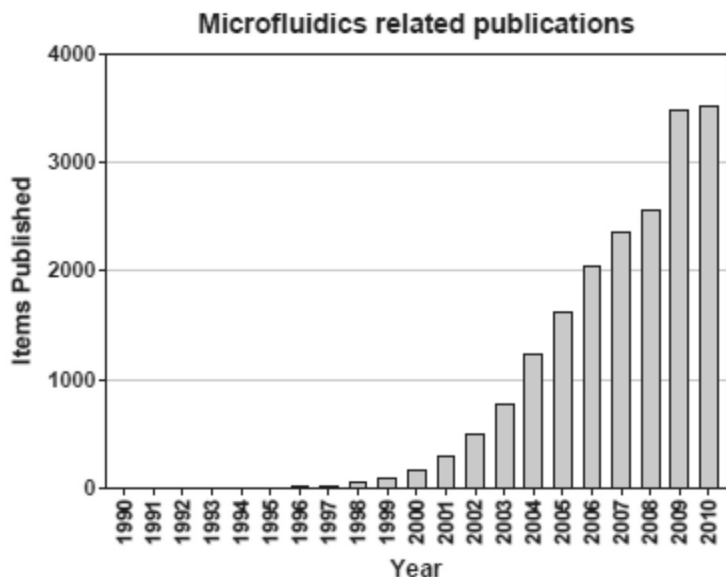


Figure 1 | Rapid growth of the number of microfluidics related publications.³⁷

Principles of downscaling

The advantages of labs-on-chips are based on the fact that miniaturization of analytical unit operations often improves the performance of analytical chemical systems as the dimensions of system components and physico-chemical principles scale positively with decreasing size (i.e. the principle of ‘positive downscaling’). In addition, different physico-chemical phenomena are dominant at a small scale (i.e. laminar flow, diffusion and electro-osmotic flow), which are employed to improve performance or obtain unique methods of operation⁶.

An obvious positive benefit of downscaling is found in the reduction of liquid volumes (i.e. samples, solvents and reagents) when performing analyses in an LOC system. Assuming x to be the characteristic length scale of a system component in an LOC system (e.g. a channel, reservoir or detection cell), the volume of the component scales as x^3 . For a ten-fold reduction in the length scale x , a thousand-fold (10^3) reduction in volume is obtained. As the dimensions of LOC components are commonly about 100 times smaller than the components in conventional analysis systems, a million-fold volumetric reduction is obtained (i.e. a reduction from milliliters to nanoliters or even less). This allows analysis of extremely small volumes (e.g. single-cell analysis, forensic trace analysis, etc.), drastically reduces

expensive reagent consumption and safely allows analysis with dangerous reagents like radio-active tracers used in assays.

The surface-to-volume-ratio (SVR) is another important scaling-dependent parameter. The SVR describes the ratio between liquid volumes in LOC components and the wall surface the liquid is contacting. When surface interactions between analytes in solution and the surfaces are important (e.g. in immuno-affinity assays, chromatographic interactions and electro-chemical detection), the SVR gives an indication of the efficiency of these interactions. The SVR commonly increases by a factor of more than ten thousand during downscaling and solute/wall interactions become dominant. This works advantageously in on-chip chromatography, but can lead to undesired results as aspecific adsorption of molecules may lead to analyte loss, carry-over and irreproducible chromatographic results. Aspecific adsorption in LOC systems can effectively be overcome by applying anti-adsorption coatings on the channel walls.

The flowing of fluids we commonly see in everyday life is characterized by turbulence (i.e. a flow pattern which constantly varies chaotically in time) as shown in Fig. 3 (left). In contrast, on the micrometer scale fluids flow in a stable, non-turbulent manner as fluid viscosity and not the fluid's inertia is dominant. An example of this non-turbulent, laminar flow is shown in Fig. 3 (right). In physics, the dimensionless Reynolds number⁷ is used to predict flow behavior. Reynolds numbers above 2000 are turbulent in nature, Reynolds numbers below 1000 are laminar in nature while values between 1000 and 2000 describe flows alternating between laminarity and turbulence. The Reynolds number becomes very small in LOC systems and is often below one (i.e. the flow is completely laminar). A positive effect of laminarity is the high predictability of the fluid flows in LOCs which is used among others to create stable and accurate gradients in chemical concentrations in cell culture LOCs⁸. On the other hand, microscale mixing is very difficult as turbulent mixing does not exist and diffusion or special mixers like stagger-herringbone mixers⁹ and chaotic advection mixers¹⁰ need to be employed.

The small Péclet numbers are also important in on-chip chromatography as the efficiency of diffusive mass transport from the analyte-carrying, liquid phase to the chromatographic solid phase greatly increases. This leads to better separations as higher flow rates can be used which limit peak broadening due to lateral diffusion during the separation.

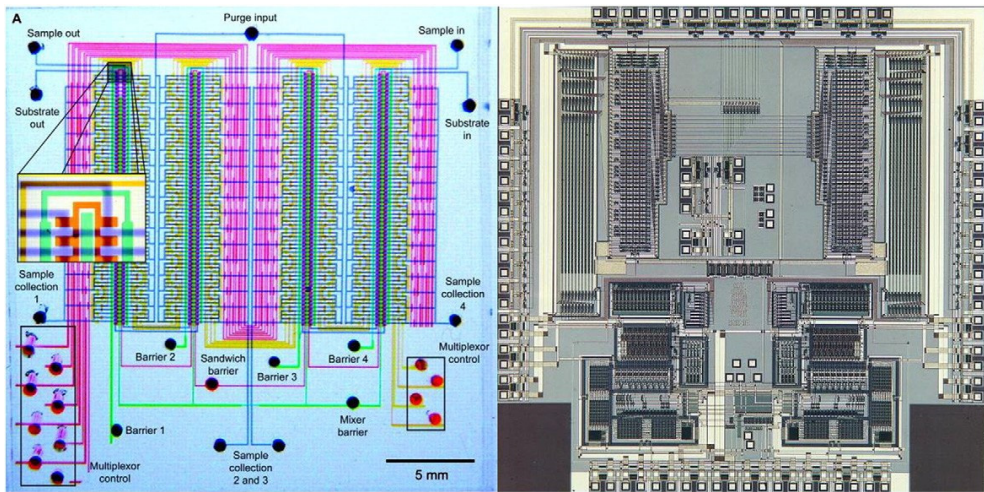


Figure 2 | A fluidic (left) and electronic (right) integrated circuit⁴. The fluidic integrated circuit shows a comparator chip, containing 2056 valves to mix reagents and assay for enzyme expression in cells in 256 separate 750 pL chambers. Adapted with permission from⁵.

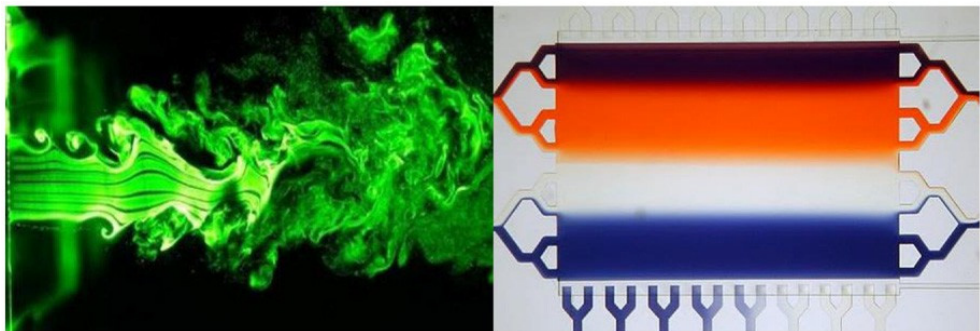


Figure 3 | Turbulence and laminar flow examples. (Right image courtesy of Greg Cooksey and Albert Folch, University of Washington, Bioengineering Dept)^{11,12}

A differentiation of lab-on-a-chip technologies

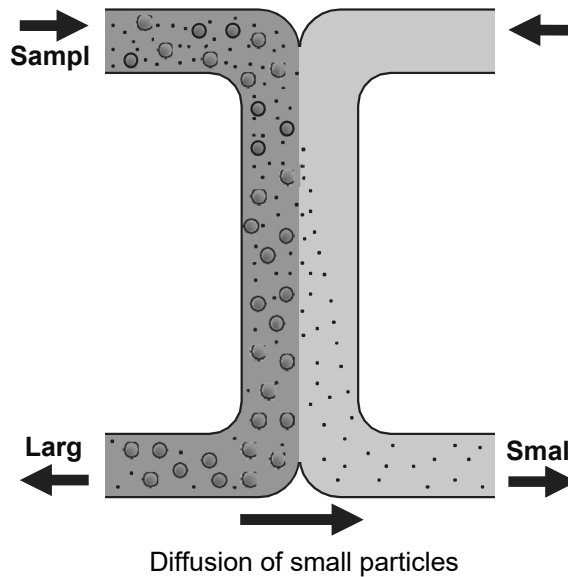
Lab-on-a-chip platforms may be categorized in a number of ways. A first categorization could be based on the separation mechanism that is employed or the detection principle that is used. However such a categorization puts different LOCs together which intuitively do not fit together. The authors have chosen a less obvious categorization, which in the end is more intuitive, namely one based on the fluid control mechanism employed. For each category, we will discuss illustrative examples which explain the working principles, the physics employed, the analytical workflows and the potential of these platforms for rapid, massive-parallel operation.

It is not our aim to provide an exhaustive overview of all available LOC platforms. Instead we will focus on the most important platforms and for further reading the interested reader is referred to other reviews covering these topics.¹⁴⁻²³ It should finally be noted that the LOC field progresses rapidly and a number of these platforms may become outdated in just a few years as new platforms and technologies emerge.

Pressure-driven platforms

As the name suggests, pressure-driven LOCs control fluid movement with differential pressures commonly applied by mechanical pumps or gas pressure. An enormous variety of micropumps for LOCs has been developed over the decades, which are discussed in several reviews.²⁴⁻²⁶

Pressure-driven LOC platforms are illustrated with the technology pioneered by Quake et al. in 1999 at the California Institute of Technology.²⁷ These platforms are made in the widely used, elastomeric silicone rubber poly-dimethyl siloxane (PDMS) by replication molding.²⁸⁻³¹ The LOCs consist of two thick layers of PDMS interspaced with a very thin, flexible PDMS membrane as depicted in Fig. 5. Microchannels in the bottom layer are used to supply gas pressure to on-chip microvalves which use the deflection of the thin membrane by the gas pressure to control liquid flow through channels in the top layer. By connecting the three microvalves in series, a peristaltic pump can be formed. In this way it is possible to create hundreds to thousands of microvalves and pumps on an LOC which measures a few square centimeters as is shown in Fig. 2 (left).⁵



2

Figure 4 | Operating principle of microfluidic H-filters. A sample (e.g. blood) containing both large species (e.g. red blood cells or large proteins) and small species (e.g. salts or metabolites) is flushed, together with a laminar co-flow, through the H-filter. As the large species diffuse very slowly compared to the rapidly-diffusing small species, different-sized sample components can be separated in the H-filter.

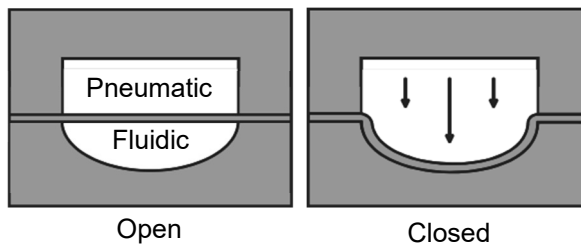


Figure 5 | Schematic of an elastomer microvalve. Pneumatic control channels are pressurized to deflect a membrane, closing of the fluidic channel.

These platforms hold the current record in the number of active components which can be integrated into one device. The device shown in Fig. 2 (left) has more than 2000 valves and more than 200 peristaltic micropumps, monolithically integrated to perform 256 single-cell analysis experiments in parallel. The challenge of individually controlling the valves and pumps is solved by connecting all the 256 experiments in parallel. In this way, all experiments are run in synchronous fashion with only 18 external pressure valves. These PDMS-based LOCs are commercially available from the company Fluidigm™.³²

Another example of pressure-driven LOCs is the Agilent HPLC-Chip, which is a miniature LC system that integrates all necessary chromatographic columns (both trapping columns and separation columns) and an electrospray interface for mass spectrometry into one small device (see Fig. 6).

Due to the positive effects of miniaturization, the LC-chip is capable of performing separations rapidly and efficiently, while at the same time allowing mass spectrometric analysis with the on-chip electrospray ion source. By efficient monolithic integration of the total system, dead volumes and peak dispersion have largely been removed. As a result, the LOC is capable of very reproducibly generating good chromatographic separations.



Figure 6 | Agilent LC-MS Chip™.³³

Electrokinetically-driven platforms

Electrokinetic flow is an important fluid control technique in LOC devices. Electrokinetic flow is more commonly known from capillary electrophoresis (CE) where the electro-osmotic flow (EOF) is used to move fluid through capillaries. Briefly, as depicted in Fig. 7, positive ions in the solution accumulate near the negatively charged wall surface. An electric field is applied between the ends of the capillary to attract the layer of ions near the wall towards the negative electrode. As viscosity is dominant on these scales (i.e. $b > 250 \mu\text{m}$), the movement of the ion layer couples into the bulk liquid, resulting in a bulk flow (i.e. the EOF). Electrokinetically-driven LOC platforms often consist of photolithographically structured glass or silicon chips on which EOF is used for a variety of operations including pumping liquids around the device, injecting minute amounts of liquid accurately, etc.³⁴⁻³⁶ By varying the electric field, the fluid flow rate can be set over a wide range and by measuring the current, the flow rate can be determined. In addition to bulk fluid control, electrokinetics can be used for very efficient separations. The field affects the analyte ions in the solution, separating them based on their charge to size ratio. The smallest and most highly-charged ions migrate fastest towards their opposite pole. An important feature of EOF is the flat flow profile resulting from the wall-driven flow as depicted in Fig. 7. The flat flow profile causes significantly less peak broadening than the parabolic flow profile seen in pressure-driven flows, resulting in very efficient separations (routinely an order of magnitude better than liquid chromatography techniques).² Electrokinetic separations can further be used for more complex separation or concentration techniques like isotachopheresis³⁸, isoelectric focusing³⁹, etc.

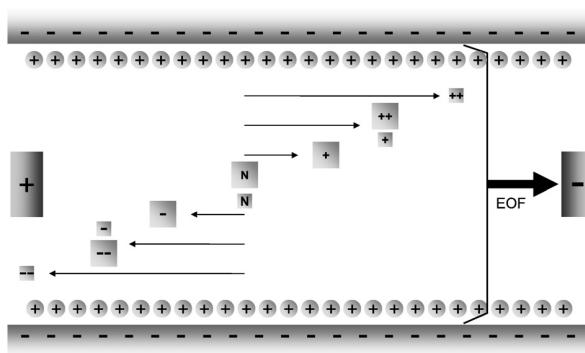


Figure 7 | Principle behind electro-osmotic flow, its flat flow profile and the mechanism of electrokinetic separation of ions based on their different size to charge ratios.

Accurate sample injection on electrokinetically-driven LOCs is not trivial and an elegant injection method using EOF to fill precise injection volume geometries (i.e. a cross- or double T-injectors) is employed. Electrokinetic sample injection with a double-T injector is shown in Fig. 8. Briefly, by applying a voltage between the sample reservoir and the waste reservoir, the sample liquid is electrokinetically pumped across the injector ($t=0$). The double-T geometry is used to accurately define the injection volume, obviating the need for valving. After loading, the sample volume is injected and separated into its constituents by applying a high voltage over the separation channel ($t=1$). The double-T injector principle can be miniaturized another three orders (i.e. nanometer scale) as was recently done in our group.⁴⁰ In a nanofluidic electrokinetic separation device we performed a 400 femtoliter analysis of fluorescently-labeled amino acids spiked into a complex biomatrix. For a consideration of size: 400 femtoliter is less than the internal volume of a single 10 μm diameter cell.

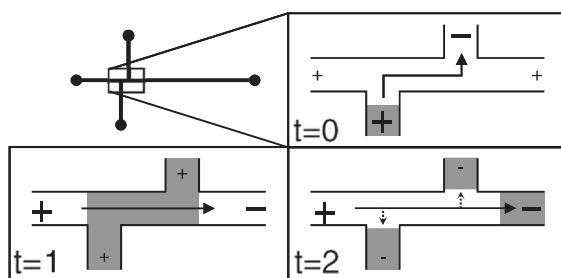


Figure 8 | Operating principle of electrokinetic injection using a double-T injector.

Chip-based electrophoresis forms the basis of the commercially available Bioanalyzer 2100™ LOC platform by Agilent™ depicted in Fig. 9. A range of chips is available for different applications including RNA⁴¹, DNA⁴², and protein analysis⁴³ or performing on-chip cell staining and flow cytometry.⁴⁴ These well-characterized chips offer an off-the-shelf system for quickly performing various analyses. Predefined methods and ready-to-use reagent kits, combined with automated use of internal standards, readout and data analysis ensure very reproducible results, allowing researchers in the life sciences to tap into the potential of LOCs without needing any LOC expertise.

2



Figure 9 | The Agilent™ LabChip™ cartridge with a view of the electrokinetic glass chip that is inside. The sample is loaded on the cartridge which is inserted into the BioAnalyzer™ for automated analysis.³³

While exploiting many of the advantages microfluidics has to offer, the Bioanalyzer 2100™ platform does not perform massive parallel analyses. The Matthies group at Berkeley University showed several systems using radial⁴⁵ or parallel channel arrays⁴⁶ fabricated in glass. A high-throughput DNA sequencing system was developed consisting of 384 radial analysis channels on a 200 mm diameter glass disc, as depicted in Fig. 10. After sample preparation, this device is capable of genotyping 384 samples in parallel in only 7 min.⁴⁷

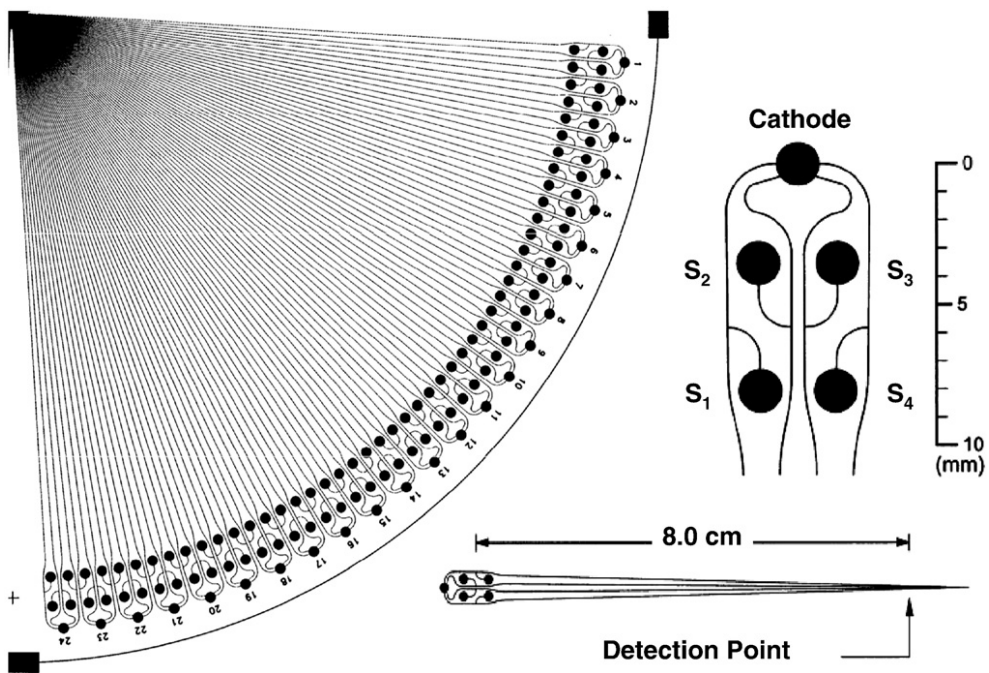


Figure 10 | Parallel genotyping device, with four sample reservoirs for each analysis channel and access for electrical connections. The transparency of the glass LOC allows detection to be performed using a rotary, confocal fluorescence scanner. Adapted from ref 47

Centrifugally-driven platforms

Centrifugally-driven lab-on-a-chip platforms are an insightful example of the ingenious methods for fluid control which may be used in LOCs. Instead of mechanical or electrokinetic pumps, centrifugal forces are used which move liquids inside circular disks containing all necessary microfluidic components for chemical analysis. Such discs are commonly manufactured from plastics using injection molding or hot embossing. In excess of one hundred parallel analyses can be performed rapidly in an LOC the size of a compact disc (see Fig. 11).

The disc is processed in a robot-operated workstation which performs all pipetting operations and handles the whole disc-based analysis workflow. The elegance of the system lies in the fact that all parallel analyses are controlled with only one global parameter: the rotational speed of the disc. By rotating the disc at different speeds, the centrifugal force and thus all liquid movements in the disc can be adjusted.

Fig. 12 graphically depicts the operating principle of the system. The samples are pipetted into sample reservoirs positioned close to the center of the disc. By rotating the disc, the liquid is forced radially outward into metering reservoirs which accurately meter the analysis volume. Excess sample is transported to waste through overflow channels. Valves are created with so-called “hydrophobic stops” which consist of small channel sections that are locally covered with a hydrophobic coating which blocks the passage of the aqueous sample liquid. By increasing the rotation speed over a critical value, equivalent to the valve's “bursting pressure”, the aqueous liquid is forced to cross the hydrophobic stop into the subsequent section of the analysis disc. On the system depicted in Fig. 11, 112 immunoassays can be performed in parallel, in less than one hour.

The disc-based analysis platforms have been commercially available for a number of years now from a number of manufacturers (i.e. Gyros and Tecan) and are in use by, for instance, pharmaceutical screening divisions at large pharmaceutical companies.

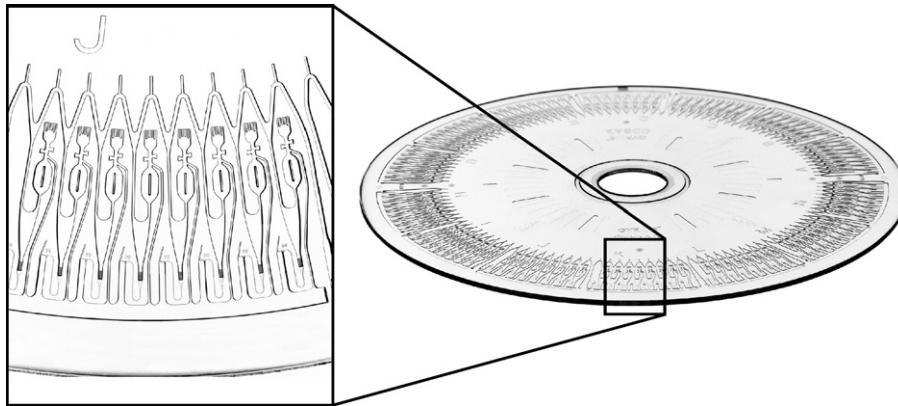
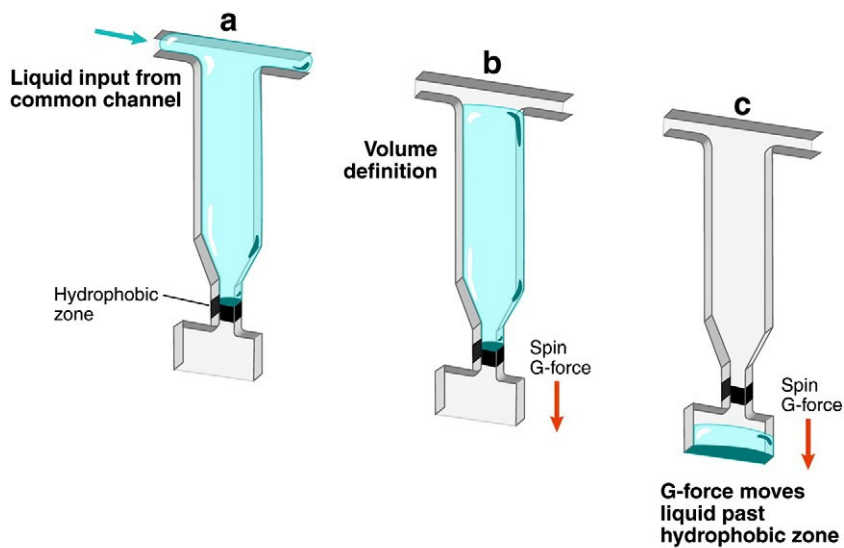


Figure 11 | A section of the Gyros™ BioaffyCD™.⁴⁸



AR Madou M, et al. 2006.
Annu. Rev. Biomed. Eng. 8:601–28

Figure 12 | A fluid dispenser in centrifugal microfluidics. The fluid fills up a reservoir with defined volume and is unable to pass the bottom valve until faster spinning of the disc provides the extra force necessary to overcome the hydrophobic barrier (Reproduced with permission from ref. 49).

Digital Microfluidics

Digital microfluidics, also called droplet-based microfluidics⁵⁰⁻⁵² or segmented-flow microfluidics is another example of an ingenious exploit of working at the small scale. Two immiscible fluids are fed through a droplet-generating geometry to form a stream of highly monodisperse, separate droplets acting as individual microreactors as shown in Fig. 13. The droplets can be produced at high frequencies (i.e. kHz), with a very accurate volume going down to the femtoliter range.

The droplets can be manipulated to perform operations such as splitting⁵³, merging⁵⁰, mixing⁵⁴, counting, sorting⁵⁵, and droplet selection⁵⁶. These actions can be performed passively (i.e. using the chip geometry) or actively (e.g. electrically⁵⁷). Because the droplets are produced so rapidly, this system is capable of performing massive amounts of discrete experiments (each contained in their individual droplet) in a small LOC. For example, by creating droplets from a liquid feed containing a chemical gradient, and subsequently merging these droplets with another droplet stream containing proteins, a huge range of protein crystallization conditions can be screened very rapidly. This screening technique is potentially a very significant step forward in the often tedious and time-consuming selection of optimal protein crystallization conditions. In a similar fashion, optimal conditions can be screened for the chemical synthesis of compounds and compound libraries.

Although not operating in a parallel fashion, digital microfluidics can be used in a similar way to massive-parallel LOCs, to perform huge numbers of experiments. If droplets are created at 3 kHz and the entire analysis takes 100 s, 300,000 samples are processed at any one time on a single chip.

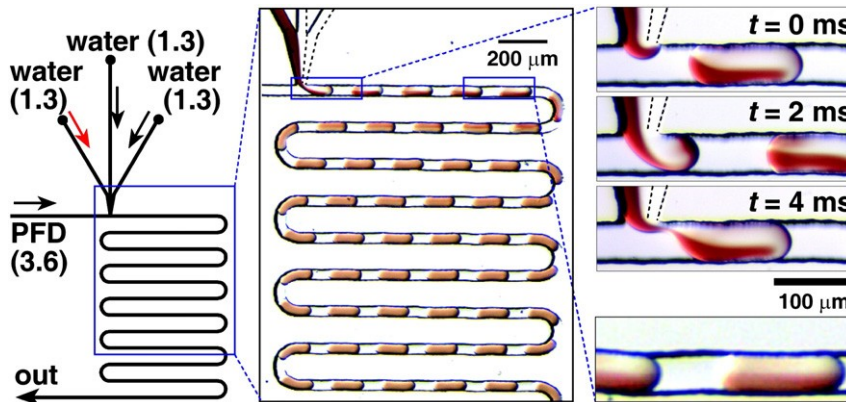


Figure 13 | A digital-microfluidics chip mixing two fluids in separate droplets at approx 250 Hz.⁵³

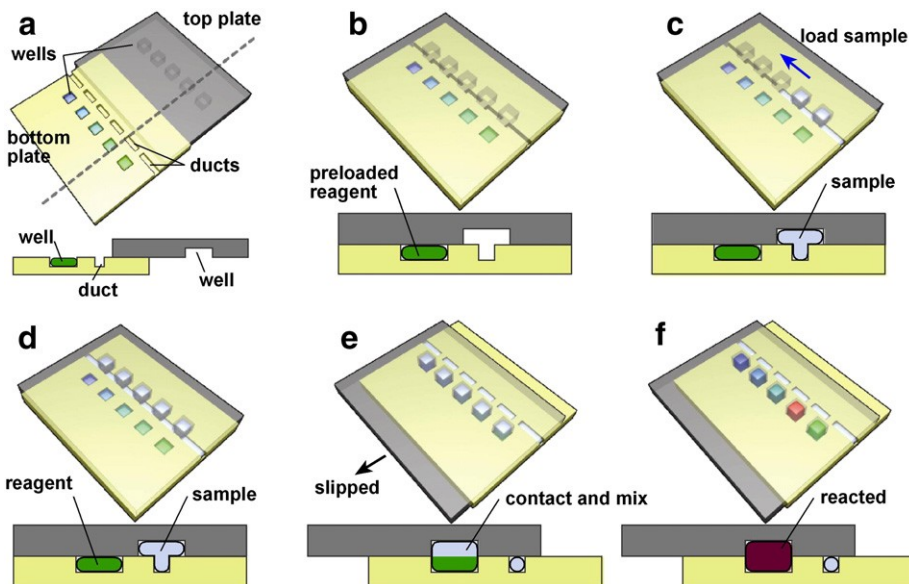


Figure 14 | Working principle of the SlipChip™ with (a) plates with pre-loaded wells and ducts (b) aligned chip ready for use (c and d) sample loading through the ducts of the bottom plate and wells of the top plate. (e) Slipping the top plate to move the sample from the duct to the separate wells. (f) Reaction of the mixed contents Reprinted with permission from ref 62.

SlipChip™

Recently, the group of Professor Ismagilov at the University of Chicago has pioneered an ingenious method to perform microfluidics without the need for an elaborate setup. The system is based on two plates containing, fluids, wells and channels (often etched in glass). The two plates are positioned on top of each other and by slipping them, fluid-containing wells in the top plate are moved to new positions over reaction wells in the bottom plate, mixing the contained volumes as shown in Fig. 14. The liquid movement can thus be controlled manually instead of with expensive pumps. This principle can be applied to perform multi-step reactions on many samples in a simple manner. Although a recent development, several promising applications have been shown including nanoliter immunoassays⁵⁸, (digital) PCR^{59,60} and water quality monitoring⁶¹.

2

Detection in lab-on-a-chip systems

Downscaling in lab-on-a-chip platforms imposes unique challenges on detection of analyte species. For instance, UV/Vis absorbance detection, which is widely used in conventional analyses, suffers from downscaling. Due to the very small optical pathlength (often around 10–100 μm), the detector's signal-to-noise ratio (SNR) will be lower and can thus be insufficient for analyses that could be performed using UV/Vis on a conventional scale. General requirements for LOC detectors include: high sensitivity/SNR, capability of detection in μL – fL volumes, and fast response time (especially in the case of massive-parallel LOCs). Often on-chip integration of the detector is preferred, which can further complicate detection. Finally, techniques are needed which deliver information-rich spectra which can be used for compound identification. As a result, many well-known detection techniques are insufficient for LOC applications and therefore often exotic and innovative detection principles are used.

In this second part of the review we will discuss the most important LOC detection techniques as well as their effect on the data generation and processing.

Laser-induced fluorescence detection

As integration of detectors or sensors inside LOCs is often very challenging, often optical microscopy techniques are used. These techniques have a number of advantages including contactless detection, suitability for detection in extremely small volumes (down to fL) and very high sensitivity. The most common optical detection technique is laser-induced fluorescence (LIF) detection. Powerful laser light is used for excitation and high-quality optical filters used in combination with extremely sensitive detectors (e.g. single-photon sensitivity photomultipliers) resulting in very low detection limits down to single molecules. In fact, LIF is such a sensitive technique that it compensates for the large decrease in detection volume caused by downscaling. The effectiveness of LIF is illustrated by the fact that most of the examples of LOCs presented above use LIF for detection.

While the most effective detection method, LIF does impose some limitations. It is limited to detection of autofluorescent or fluorescently labeled compounds (which requires sample derivatization) and does not allow broad identification of different analytes as most biologically relevant molecules do not fluoresce. The large dimensions of the detection setup and its inherent high cost limit the application of LIF to use in research laboratories and bench-top instrumentation. In these environments however LIF is by far the most widely used detection technique.

Surface-enhanced Raman spectroscopy

Raman spectroscopy is a vibrational spectroscopy technique that is based on the fact that a small portion of light is inelastically scattered from molecules (i.e. the wavelength is changed due to energy transfer to the molecule and scattered photons are emitted at longer wavelengths), resulting in a compound-specific Raman spectrum. Raman spectroscopy is an information-rich technique, but lacks sensitivity. The signal strength can however be greatly amplified using conductive (i.e. most often metallic like Au and Ag) nanostructures, resulting in a sensitive, information-rich detection technique called surface-enhanced Raman spectroscopy (SERS).

In SERS, metallic nanostructures manufactured on a surface are resonantly excited with an infrared laser, resulting in a highly amplified electromagnetic field in the gap between the nanostructures. Molecules present in the gap are strongly excited by the electromagnetic field and the Raman signal strength is greatly improved. As this enhancement is confined within nanometers from the nanostructures, SERS

measures very locally and is insensitive to downscaling. This makes SERS a very interesting information-rich detection technique for LOCs. The sensitivity of SERS is very much dependent on the quality of the nanostructures, but optimized SERS surfaces show in excess of one million-fold increases in sensitivity, compared to conventional Raman spectroscopy, resulting in detection limits down to single-molecules.^{63,64}

The compound-specific spectra acquired with SERS are comparable to infrared spectra, allowing for compound identification in addition to quantification. Although exotic, SERS is an important technique for LOC detection as its detection limit does not scale with size and SERS is one of the few detection techniques which allow compound identification. Currently, some challenges with this technique remain such as sub-optimal sensor response due to irreversible analyte binding the SERS nanostructures and the need for reproducible fabrication of SERS sensor surfaces with high sensitivities. It is foreseen that many of the challenges with SERS will be addressed in the near future as SERS is currently a very active area of research.

2

Surface plasmon resonance detection

Like SERS, surface plasmon resonance (SPR) detection is a near-field optical detection method. The technique uses the surface plasmon effect which occurs when polarized laser light at a specific angle of incidence (the surface plasmon angle) is reflected off a thin noble metal layer (e.g. gold) resulting in an absorbance at the SPR angle. Affinity molecules like antibodies or receptors are bound to the noble metal layer which is brought in contact with the sample solution. As ligand molecules bind to the receptors or antibodies, the refractive index near the metal layer is changed resulting in a change of the SPR angle. The change in SPR angle is a measure for the amount of ligand bound.^{65,66} SPR lends itself well for LOC detection as the noble metal layers can be fabricated efficiently in LOCs and SPR is an optical detection technique which like SERS is insensitive to downscaling.

Mass spectrometry

Mass spectrometry (MS) has become one of the most important techniques in conventional chemical analysis. Although also used for analyte quantification, the true power of MS lies in its enormous compound identification capabilities based on the mass-to-charge ratio of analyte ions. These ions are commonly generated with the atmospheric pressure ionization technique electrospray ionization (ESI).

In conventional ESI the analyte containing fluid is passed through a sharp capillary needle. A high voltage is applied to the needle tip causing fine spray of charged droplets to be emitted. As the solvent evaporates, the resultant ions are fed into the mass spectrometer.

Electrospray lends itself very well for interfacing LOCs with mass spectrometry. Commonly, the spray needle is monolithically integrated into the LOC as is the case with the Agilent LC–MS Chip shown in Fig. 15. As opposed to many techniques that suffer from downscaling, the ionization process is dramatically improved by downscaling electrospray to LOC dimension, resulting in more reproducible data, a better SNR, and a more linear detection response.^{67,68}

It is expected that the use of MS as a detection method for LOCs will become more widespread, as it is such a powerful identification technique and has excellent sensitivity for flow rates commonly encountered in LOCs.

Electrical detection

A number of different electrical detection methods are used in LOCs including conductivity detection, electrical impedance spectroscopy (EIS) and electrochemical detection (ECD). All these methods have the advantage that they use relatively simple electronic detection setups, and that the electrical signals are easily controlled and measured with digital acquisition systems and computers.

Conductivity detection measures changes in the electrical conductivity due to changes in the composition of the liquid flowing through the detection setup. Commonly detection is done with high frequency (up to hundreds of kHz) AC signals applied between microelectrodes. Using conductivity detection the concentration of ions can be determined as is done in the LOC for plasma lithium concentration determination shown in Fig. 15.

Another electrical detection method, widely used for on-chip cytometry, is electrical impedance spectroscopy. Individual cells are exposed to a high-frequency electric field between two electrodes in a flow-through cell. As different cells influence the electric field according to their individual size and dielectric properties, the resultant changes in the electric signal can be used to identify different types of cells.⁶⁹

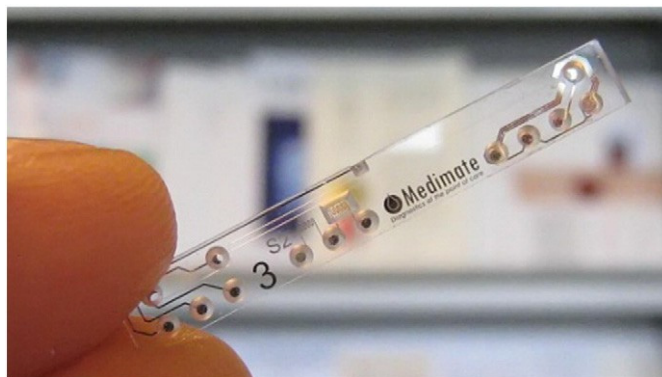


Figure 15 | Example of a commercially-available, glass LOC device for clinical applications. This commercial LOC rapidly determines plasma lithium concentration for bipolar patients by performing all necessary laboratory steps starting from whole blood.

Electrochemical detection measures current generated by the electrochemical conversion of chemical species on the surface of integrated electrodes. Depending on the molecular properties of the compounds, different potentials are needed to induce the electrochemical reactions. The required potential is compound specific and may be used for compound identification. Although not very information rich, and not suitable for all molecules, ECD has a very high sensitivity that is independent of downscaling. The sensitivity of ECD was clearly demonstrated by the detection of the exocytosis of single histamine-containing vesicles from single mast cells.⁷⁰

Surface-acoustic wave detection

Surface-acoustic wave (SAW) detection uses the changes in surface propagation of acoustic waves as they propagate along the surface of on-chip detection regions.⁷¹ Commonly, the surface of the detection region is modified with an affinity layer containing antibodies or receptors which bind to their respective substrates. Their added mass causes a change in the propagation of the acoustic surface waves. The change of the acoustic signal is a measure for substrate binding and can be used to selectively determine the concentration of a specific molecule in a sample mixture.

Cantilever detection

Cantilever detection uses micrometer-thick cantilever structures inside LOCs. One side of the cantilever is coated with a layer of affinity molecules like antibodies or receptors capable of specifically recognizing a molecular species in an analyte mixture. As the molecule of interest binds to the affinity layer on the cantilever a surface stress is developed which results in bending of the very thin cantilever structure. The amount of bending is a measure of the concentration of the analyte of interest and is measured optically by a laser beam or by integrated electrical sensors which respond to mechanical stress (piezoresistors).⁷²

Massive-parallel (bio) analytical chemistry in LOC devices

In the preceding portion of the review we have covered a wide range of important subjects for LOC systems. We have introduced the basic physical phenomena and operation and detection principles of some of the major LOC platforms. It is again noted that it is not our aim to give an exhaustive review of all available techniques, but to give insights into the current possibilities and promise of the rapidly evolving field of microfluidics and to allow the reader to judge its impact on their own field. The final part of this review will address the question of how these LOC techniques are likely to impact the life sciences in the immediate and near future. These techniques are likely to affect the life sciences in three ways, namely by enhancing research on small samples or small biological systems, by greatly increasing throughput at reduced cost, and by enabling a much higher degree of hyphenation, to allow much more comprehensive measurements. We will discuss this in some detail, but future development will show which techniques will make it to widely used LOC techniques and can truly alter the way life sciences are performed.

Small samples

The most obvious result of miniaturizing analytical systems is their improved ability to work with minute sample volumes and very small biological systems. For example, the field of single-cell analysis is very complicated when using conventional techniques. The inherent size difference between the tools used to perform experiments and the studied cells can make seemingly simple operations tedious. This size discrepancy can also lead to a high degree of dilution, making

detection difficult. Using conventional pipetting techniques, the minimum volumes that can be used accurately are normally in the μL range. When one cell is lysed in 1 μL of buffer, its contents are diluted in excess of 8 orders of magnitude, making even the most abundant analytes difficult to detect. Using LOCs, individual cells can be cultured in such small volumes that their contents or even the compounds they secrete will be kept in measurable concentrations. Additionally, it is possible to allow for communication between neighboring cells by having adjacent culture chambers in contact with each other, more closely resembling their natural environment.

The ability to work with such small biological systems will lead to unique insights into how single cells function and perform signaling in their native tissues (which may include cancerous tissues, brain tissues, organ tissues, etc.). In this and other ways it is expected that LOCs will deliver important contributions to genomics, transcriptomics, proteomics and metabolomics. With the advent of systems biology, LOC systems will probably have a strong impact in this important area of research as the functioning of organisms, organs, tissues and single cells can be studied in high resolution from the bottom up instead of the top down approaches used now.

High throughput

A second important impact these techniques will have is in the throughput of experiments and analyses. As LOC devices lead to less labor intensive, faster analyses, while consuming less chemicals and laboratory space, they can be scaled out in a massive-parallel fashion to increase the throughput by several orders of magnitude. The increase in throughput has a number of effects. First of all, experiments can be performed at lower cost. This economic aspect is further accentuated by the fact that LOC platforms use less sample, reagent and eluents. This will, for instance, also allow the performance of large numbers of experiments which require very expensive chemicals. Experiments with dangerous chemicals like radioactive materials pose less of a risk allowing these experiments to be routinely performed.

Furthermore, a high degree of automation can be incorporated in LOCs. Similar to the 'Tyranny of Numbers', there is a practical limit to the number of pipetting steps a reasonable experiment can contain (i.e. the 'Tyranny of Pipetting'). This limit can be stretched by automated pipetting, but even then experimental errors and

reagent consumption increase with the number of pipetting steps. Monolithically integrated LOCs can alleviate this problem with intricate, multiplexed networks of channels that allow for the filling of hundreds of channels or reaction chambers with a sample from one common well. One pipetting step can thus replace hundreds of individual pipetting steps. Not only can one reagent be introduced in such a manner, but the network of channels can also be designed to generate gradients of mixtures or serial dilutions allowing for the rapid screening of a huge range of experimental conditions with only a few manual steps. Afterwards it is also possible to simultaneously perform many parallel operations like metering, pumping and mixing using only one controller. These aspects might be some of the most appealing features of LOC platforms as they reduce manual labor and increase productivity.

Performing large numbers of experiments in parallel would also ensure low experimental variability and thus higher data quality, addressing one of the great hurdles of large scale -omics studies.

An important corollary of the increase in throughput is that processing and evaluation of the data generated is most likely to become a bottle neck, as is already occurring with high resolution MS– MS data or DNA sequencing. When LOCs are used with a data-intensive detection technique like high-resolution mass spectrometry, the data bottleneck will become especially prominent.

Of course, if the data bottleneck challenges are alleviated as computing power is becoming exponentially cheaper and dedicated, high-quality analysis software is developed, the full benefits of LOC systems for the life sciences can be reaped. For instance chemical compound libraries may be screened at much higher rates at a much reduced cost, which is very important for lead compound screening in the pharmaceutical drug development process. Other important areas include (personal) genetic screening, the –omics sciences, and the screening of large patient cohorts.

Multiple hyphenation

As sample consumption, dead volumes, dispersion and connections can be greatly reduced by using integrated LOCs, it becomes possible to integrate multiple separation and detection techniques into one device. The value of hyphenating several techniques can already be seen in the field of mass spectrometry, where systems consisting of several chromatographic separations, a UV detector and

multiple mass spectrometers are widely applied. The use of multiple separation and detection methods on one sample can significantly increase the coverage of an analytical system. Analytes that co-elute in one separation dimension will be separated on the second dimension and multiple detection methods will ensure that most compounds will be detected by at least one of the techniques.

Although not yet realized, this hyphenation could be put to extremes in LOC systems. A single sample could be split up and processed with different separation techniques, or multiple separation techniques can be performed sequentially in a single device. Afterwards a sample can be passed through several detectors finishing with a destructive technique like MS. It is thus not difficult to imagine extremely hyphenated techniques like LC–CE–SERS–LIF–EIS–MS (sic!). Gathering all this data in one experiment is preferable, not only because it is less labor intensive and consumes less sample, but also because it avoids inter-experimental variation.

This concept can be extrapolated even further to include a high degree of quality control in LOCs. Because of the method of manufacturing LOCs, it is not more difficult to integrate multiple electrodes in an LOC than it is to integrate one. One could thus integrate simple sensors to monitor for example, the temperature, pH, ion strength and other experimental conditions. Recording and potentially regulating all these experimental variables would allow for a large degree of control of the experimental conditions and thus significantly higher data quality.

It is envisioned that a new data format would be needed, to include all the experimental conditions and results, to allow for better comparison of results between experiments and especially between different laboratories. Such a standard, comprehensive data format would greatly increase the possibilities for meta-analyses of results of different studies, yielding large scale information. Especially in the -omics sciences, such analyses could be extremely useful to give insight into networks and pathways.

Conclusions

In this review we have introduced the basic concepts in microfluidics including the associated physics, the different microfluidic platforms, and the different detection techniques. Furthermore, we have discussed the concept of massive-parallel microfluidics, the potential for multiple hyphenations, and the opportunity for chemometrics. We hope that by reading this review, readers have gained a basic working knowledge on microfluidic systems, which may allow them to judge the

impact on their own respective fields and potentially select the most suitable microfluidic technology for their endeavors.

Due to the wide range of physical phenomena available for fluid propulsion on the small scale, very different microfluidic platforms are available (e.g. electrokinetic, pressure driven and centrifugal platforms). Thus, specific platforms have different properties more suitable for certain applications. For example, digital microfluidics is very well suited for rapidly testing high numbers of different experimental conditions, but intrinsically does not allow for compound separation as is inherently possible in electrokinetic systems. On the detection side, an even more impressive array of choices is available as the detectors may use the optical, chemical, mechanical, or electromagnetic domain. In addition it is possible to incorporate many detectors into one microfluidic device to achieve a multi-hyphenated device. As opposed to on the macroscale, monolithic integration can largely remove dead volumes and leakage-prone connections, allowing in-line coupling of multiple detectors without significant loss of performance. LOCs with multi-hyphenated detection could be very useful as they allow much more comprehensive screening of chemical samples. Especially the -omics sciences, which often process very complex samples, could benefit from such comprehensive screening methods to increase analyte coverage.

In addition to the inherent short run times seen in microfluidics, a significant benefit of microfluidic systems is their potential for performing many analyses of small volumes in parallel. Such massive parallel operation is very interesting for the life sciences as both sample throughput and reproducibility are drastically increased due to the parallel operation.

The massive amount of data generated by such techniques, does not only pose a challenge for chemometrics, but the increases in data quality and data coverage also offers huge opportunities for benefiting the life sciences with very reliable, comprehensive information.

Abbreviations

CE	Capillary electrophoresis	ECD	Electrochemical detection
EIS	Electrical impedance spectroscopy	EOF	Electro-osmotic flow
ESI	Electrospray ionization		
LIF	Laser-induced fluorescence	LOC	Lab-on-a-chip
MS	Mass spectrometry		
PDMS	Poly-dimethyl siloxane		
SAW	Surface acoustic wave		
SERS	Surface enhanced Raman spectroscopy		
SNR	Signal-to-noise ratio		
SPR	Surface plasmon resonance	SVR	Surface-to-volume ratio

Acknowledgments

This project was (co)financed by the Netherlands Metabolomics Centre (NMC) which is part of the Netherlands Genomics Initiative/ Netherlands Organization for Scientific Research.

References

1. S.C. Terry, J.H. Jerman, J.B. Angell, A gas chromatographic air analyzer fabricated on a silicon wafer, *IEEE Trans. Electron Devices* 26 (1979) 1880–1886.
2. ISI Web of Knowledge, Thomson Reuters, search results for "topic=(microfluidic*) or topic=(microtas) or topic=("micro total analysis system*") or topic= ("lab on a chip") or topic=("lab on chip") or topic=(lab-on-a-chip) or topic= (lab-on-chip)", accessed on 21/02/2011.
3. S.R. Quake, <http://www.stanford.edu/group/foundry/pricing%20information.html>, accessed on 10/10/2010.
4. <http://www.aztex.biz/general-computer/integrated-circuit-work/>, accessed on 10/11/2010.
5. T. Thorsen, S.J. Maerkl, S.R. Quake, Microfluidic large-scale integration, *Science* 298 (2002) 580–584.
6. T.M. Squires, S.R. Quake, Microfluidics: fluid physics at the nanoliter scale, *Rev. Mod. Phys.* 77 (2005) 977–1026.
7. E.M. Purcell, Life at low Reynolds number, *Am. J. Phys.* 45 (1977).
8. T.M. Keenan, A. Folch, Biomolecular gradients in cell culture systems, *Lab Chip* 8 (2008) 34–57.
9. A.D. Stroock, S.K.W. Dertinger, A. Ajdari, I. Mezic, H.A. Stone, G.M. Whitesides, Chaotic mixer for microchannels, *Science* 295 (2002) 647–651.
10. D.J. Beebe, G.A. Mensing, G.M. Walker, Physics and applications of microfluidics in biology, *Annu. Rev. Biomed. Eng.* 4 (2002) 261–286.
11. S.R.H.L. Kim, S.J. Lee, Experimental study on the flow characteristics of sinusoidal nozzle jet, *J. Korean Vis.* 7 (2010) 28–34.
12. A. Folch, LabART, <http://faculty.washington.edu/afolch/FolchLab-ART.html> accessed on 12/9/2010.
13. P. Yager, T. Edwards, E. Fu, K. Helton, K. Nelson, M.R. Tam, B.H. Weigl, Microfluidic diagnostic technologies for global public health, *Nature* 442 (2006) 412–418.
14. T.H. Schulte, R.L. Bardell, B.H. Weigl, Microfluidic technologies in clinical diagnostics, *Clin. Chim. Acta* 321 (2002) 1–10.
15. J.R. Kraly, R.E. Holcomb, Q. Guan, C.S. Henry, Review: microfluidic applications in metabolomics and metabolic profiling, *Anal. Chim. Acta* 653 (2009) 23–35.
16. D. Mark, S. Haeberle, G. Roth, F.v. Stetten, R. Zengerle, Microfluidic lab-on-a-chip platforms: requirements, characteristics and applications, *Chem. Soc. Rev.* 39 (2010) 1153–1182.
17. K.B. Mogensen, H. Klank, J.P. Kutter, Recent developments in detection for microfluidic systems, *Electrophoresis* 25 (2004) 3498–3512.
18. J. Voldman, M.L. Gray, M.A. Schmidt, Microfabrication in biology and medicine, *Annu. Rev. Biomed. Eng.* 1 (1999) 401–425.
19. S. Haeberle, R. Zengerle, Microfluidic platforms for lab-on-a-chip applications, *Lab Chip* 7 (2007) 1094–1110.

20. N. Lion, T.C. Rohner, L. Dayon, I.L. Arnaud, E. Damoc, N. Youhnovski, Z.Y. Wu, C. Roussel, J. Josserand, H. Jensen, J.S. Rossier, M. Przybylski, H.H. Girault, Microfluidic systems in proteomics, *Electrophoresis* 24 (2003) 3533–3562.
21. P.S. Dittrich, A. Manz, Lab-on-a-chip: microfluidics in drug discovery, *Nat. Rev. Drug Discov.* 5 (2006) 210–218.
22. H. Becker, L.E. Locascio, Polymer microfluidic devices, *Talanta* 56 (2002) 267–287.
23. G.M. Whitesides, The origins and the future of microfluidics, *Nature* 442 (2006) 368–373.
24. N. Nguyen, H. XIAOYANG, C. TOH KOK, Mems-micropumps: a review: pump analysis and design, *J. Fluids Eng.* 124 (2002) 384–392.
25. D.J. Laser, J.G. Santiago, A review of micropumps, *J. Micromech. Microeng.* 14 (2004) R35.
26. W.O. Kwang, H.A. Chong, A review of microvalves, *J. Micromech. Microeng.* 16 (2006) R13.
27. M.A. Unger, H.-P. Chou, T. Thorsen, A. Scherer, S.R. Quake, Monolithic microfabricated valves and pumps by multilayer soft lithography, *Science* 288 (2000) 113–116.
28. D.C. Duffy, J.C. McDonald, O.J.A. Schueller, G.M. Whitesides, Rapid prototyping of microfluidic systems in poly(dimethylsiloxane), *Anal. Chem.* 70 (1998) 4974–4984.
29. S.K. Sia, G.M. Whitesides, Microfluidic devices fabricated in poly(dimethyl-siloxane) for biological studies, *Electrophoresis* 24 (2003) 3563–3576.
30. J.C. McDonald, G.M. Whitesides, Poly(dimethylsiloxane) as a material for fabricating microfluidic devices, *Acc. Chem. Res.* 35 (2002) 491–499.
31. J.C. McDonald, D.C. Duffy, J.R. Anderson, D.T. Chiu, H. Wu, O.J.A. Schueller, G.M. Whitesides, Fabrication of microfluidic systems in poly(dimethylsiloxane), *Electrophoresis* 21 (2000) 27–40.
32. www.fluidigm.com, accessed on 08/10/2010.
33. www.agilent.com, accessed on 10/09/2010.
34. A. Manz, D.J. Harrison, E.M.J. Verpoorte, J.C. Fetters, A. Paulus, H. Lüdi, H.M. Widmer, Planar chips technology for miniaturization and integration of separation techniques into monitoring systems: capillary electrophoresis on a chip, *J. Chromatogr.* 593 (1992) 253–258.
35. D.J. Harrison, A. Manz, Z. Fan, H. Luedi, H.M. Widmer, Capillary electrophoresis and sample injection systems integrated on a planar glass chip, *Anal. Chem.* 64 (1992) 1926–1932.
36. C.S. Effenhauser, A. Manz, H.M. Widmer, Manipulation of sample fractions on a capillary electrophoresis chip, *Anal. Chem.* 67 (1995) 2284–2287.
37. D.C. Harris, Quantitative chemical analysis, 5th Edition W.H. Freeman and Company, New York, 1998.
38. B. Jung, R. Bharadwaj, J.G. Santiago, On-chip million fold sample stacking using transient isotachopheresis, *Anal. Chem.* 78 (2006) 2319–2327.

39. A.E. Herr, J.I. Molho, K.A. Drouvalakis, J.C. Mikkelsen, P.J. Utz, J.G. Santiago, T.W. Kenny, On-chip coupling of isoelectric focusing and free solution electrophoresis for multidimensional separations, *Anal. Chem.* 75 (2003) 1180–1187.
40. K.G.H. Janssen, J. Li, H.T. Hoang, R.J.B.H.N. v.d. Berg, H.S. Overkleeft, J.C.T. Eijkel, N.R. Tas, H.J. v.d. Linden, T. Hankemeier, Nanofluidic Isotachopheresis for attomole separations of amino acids in sub-picoliter volumes (in preparation).
41. K. Dheda, Validation of housekeeping genes for normalizing RNA expression in real-time PCR, *Biotechniques* 37 (2004) 112.
42. N.J. Panaro, P.K. Yuen, T. Sakazume, P. Fortina, L.J. Kricka, P. Wilding, Evaluation of DNA fragment sizing and quantification by the Agilent 2100 bioanalyzer, *Clin. Chem.* 46 (2000) 1851–1853.
43. L. Bousse, S. Mouradian, A. Minalla, H. Yee, K. Williams, R. Dubrow, Protein sizing on a microchip, *Anal. Chem.* 73 (2001) 1207–1212.
44. P. Tobias, L. Gerd, D.H.C. Samuel, N.W. Benjamin, D. Robert, B. Carsten, Detection of cellular parameters using a microfluidic chip-based system, *J. Assoc. Lab. Automation* 7 (2002) 85–89.
45. B.M. Paegel, C.A. Emrich, G.J. Wedemayer, J.R. Scherer, R.A. Mathies, High throughput DNA sequencing with a microfabricated 96-lane capillary array electrophoresis bioprocessor, *PNAS* 99 (2002) 574–579.
46. J.H. Aborn, S.A. El-Difrawy, M. Novotny, E.A. Gismondi, R. Lam, P. Matsudaira, B.K. McKenna, T. O'Neil, P. Streechon, D.J. Ehrlich, A 768-lane microfabricated system for high-throughput DNA sequencing, *Lab Chip* 5 (2005) 669–674.
47. C.A. Emrich, H. Tian, I.L. Medintz, R.A. Mathies, Microfabricated 384-lane capillary array electrophoresis bioanalyzer for ultrahigh-throughput genetic analysis, *Anal. Chem.* 74 (2002) 5076–5083.
48. <http://www.gyros.com>, accessed on 11/10/10.
49. M. Madou, J. Zoval, G. Jia, H. Kido, J. Kim, N. Kim, Lab on a CD, *Annu. Rev. Biomed. Eng.* 8 (2006) 601–628.
50. S.-Y. Teh, R. Lin, L.-H. Hung, A.P. Lee, Droplet microfluidics, *Lab Chip* 8 (2008) 198–220.
51. A. Huebner, S. Sharma, M. Srisa-Art, F. Hollfelder, J.B. Edel, A.J. deMello, microdroplets: a sea of applications? *Lab Chip* 8 (2008) 1244–1254.
52. H. Song, D.L. Chen, R.F. Ismagilov, Reactions in droplets in microfluidic channels, *Angew. Chem. Int. Ed.* 45 (2006) 7336–7356.
53. H. Song, J.D. Tice, R.F. Ismagilov, A microfluidic system for controlling reaction networks in time, *Angew. Chem.* 115 (2003) 792–796.
54. A. Günther, M. Jhunjunwala, M. Thalmann, M.A. Schmidt, K.F. Jensen, Micro-mixing of miscible liquids in segmented gas — liquid flow, *Langmuir* 21 (2005) 1547–1555.
55. W. Shi, J. Qin, N. Ye, B. Lin, Droplet-based microfluidic system for individual *Caenorhabditis elegans* assay, *Lab Chip* 8 (2008) 1432–1435.
56. X. Niu, M. Zhang, S. Peng, W. Wen, P. Sheng, Real-time detection, control, and sorting of microfluidic droplets, *Biomicrofluidics* 1 (2007) 044101–044112.

57. J.-C. Baret, O.J. Miller, V. Taly, M. Ryckelynck, A. El-Harrak, L. Frenz, C. Rick, M.L. Samuels, J.B. Hutchison, J.J. Agresti, D.R. Link, D.A. Weitz, A.D. Griffiths, Fluorescence-activated droplet sorting (FADS): efficient microfluidic cell sorting based on enzymatic activity, *Lab Chip* 9 (2009) 1850–1858.
58. W. Liu, D. Chen, W. Du, K.P. Nichols, R.F. Ismagilov, Slipchip for immunoassays in nanoliter volumes, *Anal. Chem.* 82 (2010) 3276–3282.
59. F. Shen, W. Du, E.K. Davydova, M.A. Karymov, J. Pandey, R.F. Ismagilov, Nanoliter multiplex PCR arrays on a slipchip, *Anal. Chem.* 82 (2010) 4606–4612.
60. F. Shen, W. Du, J.E. Kreutz, A. Fok, R.F. Ismagilov, Digital PCR on a SlipChip, *Lab Chip* 10 (2010) 2666–2672.
61. J.C. Gertsch, S.D. Noblitt, D.M. Crokek, C.S. Henry, Rapid analysis of perchlorate in drinking water at parts per billion levels using microchip electrophoresis, *Anal. Chem.* 82 (2010) 3426–3429.
62. W. Du, L. Li, K.P. Nichols, R.F. Ismagilov, Slipchip, *Lab Chip* 9 (2009) 2286–2292.
63. K. Kneipp, Y. Wang, H. Kneipp, L.T. Perelman, I. Itzkan, R. Dasari, M.S. Feld, Single molecule detection using surface-enhanced Raman scattering (SERS), *Phys. Rev. Lett.* 78 (1997) 1667–1670.
64. S.M. Nie, S.R. Emery, Probing single molecules and single nanoparticles by surface-enhanced Raman scattering, *Science* 275 (1997) 1102–1106.
65. J. Homola, S.S. Yee, G. Gauglitz, Surface plasmon resonance sensors: review, *Sens. Act. B Chem.* 54 (1999) 3–15.

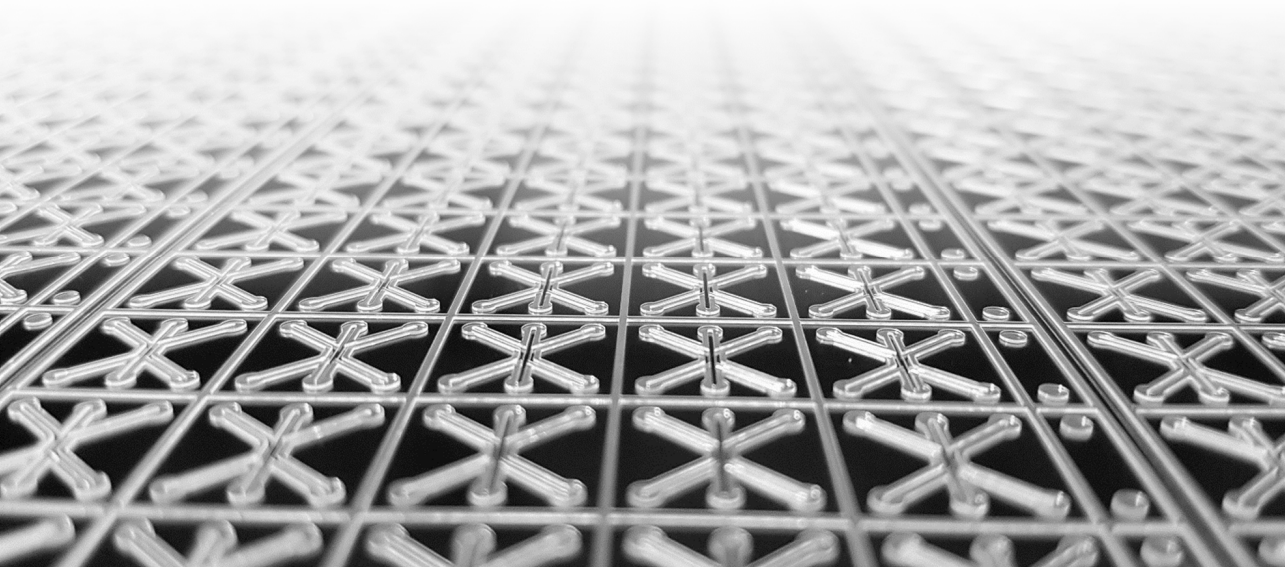
Chapter 3

Phaseguides as tunable passive microvalves for liquid routing in complex microfluidic networks

E Yildirim*, SJ Trietsch*, J Joore, A van den Berg, T Hankemeier, P Vulto

*Authors contributed equally

Lab on a Chip



Summary

A microfluidic passive valving platform is introduced that has full control over the stability of each valve. The concept is based on phaseguides, which are small ridges at the bottom of a channel acting as pinning barriers. It is shown that the angle between the phaseguide and the channel sidewall is a measure of the stability of the phaseguide. The relationship between the phaseguide–wall angle and the stability is characterized numerically, analytically and experimentally. Liquid routing is enabled by using multiple phaseguide with different stability values. This is demonstrated by filling complex chamber matrices. As an ultimate demonstration of control, a 400-chamber network is used as a pixel array. It is the first time that differential stability is demonstrated in the realm of passive valving. It ultimately enables microfluidic devices for massive data generation in a low-cost disposable format.

3

Introduction

Passive valves have been a major focal point in microfluidics since the emergence of the field in the '90s.^{1–4} Passive valves hold the promise to control routing of liquids in complex microfluidic channel networks without the use of moving parts or complex actuation schemes. The idea that microfluidic functionality could be “preprogrammed” in the device, rather than using *ad hoc* control over valve states, is alluring. It would eliminate the need for user interference and/or bulky control equipment. It also holds the promise of cheaper fabrication than active valving platforms. Passive valve-based microfluidic systems are therefore the most amenable to make microfluidics available as a low-cost laboratory disposable.

Passive valves can be largely subdivided into two types: hydrophobic barriers and pinning barriers. The first type is typically created by patterning a hydrophobic material such as Teflon, parylene or self-assembled monolayers on one or more of the channel walls.^{5,6} Given that the wettability of a channel suddenly changes from hydrophilic to hydrophobic, additional energy is required to breach the barrier. The pressure required for breaching such valves is typically higher than that for pinning barriers.

The mechanisms behind pinning barriers are less intuitive to understand. Retarding effects due to pinning are sometimes erroneously explained as occurring due to hydrodynamic resistance of channels. Pinning effects occur due to a change in geometry, such that advancement of a liquid–air meniscus causes an increase in its principal radii of curvature to such an extent that this would require an increased

applied external pressure. Impressive examples of pinning barriers were shown by Zimmermann *et al.*, Melin *et al.* and Ahn *et al.*^{7–9}

Alternatives to passive valve-based systems are autonomous capillary systems that use capillarity as a driving force and/or control hydrodynamic resistance of channels for liquid routing.^{10,11}

However, none of these systems could achieve a level of complexity that is achieved by active valving systems such as PDMS microvalves^{12,13} or electrowetting platforms.¹⁴ The aspect that is lacking so far is differential control over the stability of passive valves. For complex geometries, valves should be breached in a certain, preprogrammed order. For this, precise control over the stability of each valve is necessary. So far, however, differential stability has not been demonstrated in the realm of passive valves.

We introduced the concept of “phaseguides” almost a decade ago.¹⁵ Phaseguides are a type of pinning barriers that allow controlled filling and emptying of microfluidic chambers of any shape. Phaseguide-based microfluidic systems have gained widespread use over the recent years, leading to applications in 3D cell culturing, RNA extraction, recombinase polymerase amplification, concentration of bacteria, sandwich immunoassays, electroextraction and magnetic bead-based assays.^{16–24} In ref. 25 we suggested that phaseguides would ultimately enable complex liquid routing schemes.

Here we show for the first time that the stability of passive valves in general and phaseguides in particular could be differentially controlled. The burst pressure of the phaseguide was precisely controlled by varying the angle between the phaseguide and the wall. A smaller phaseguide–wall angle leads to a lower burst pressure, while a larger angle leads to an increased stability of the phaseguide. This concept was applied to create pinning barriers with differential stability and utilized to fill complex arrays of chambers in one pipetting step only. As a demonstration of selectivity we show a 400-chamber array in which we selectively fill the chamber while leaving the others empty to ultimately ‘write’ the word μ TAS.

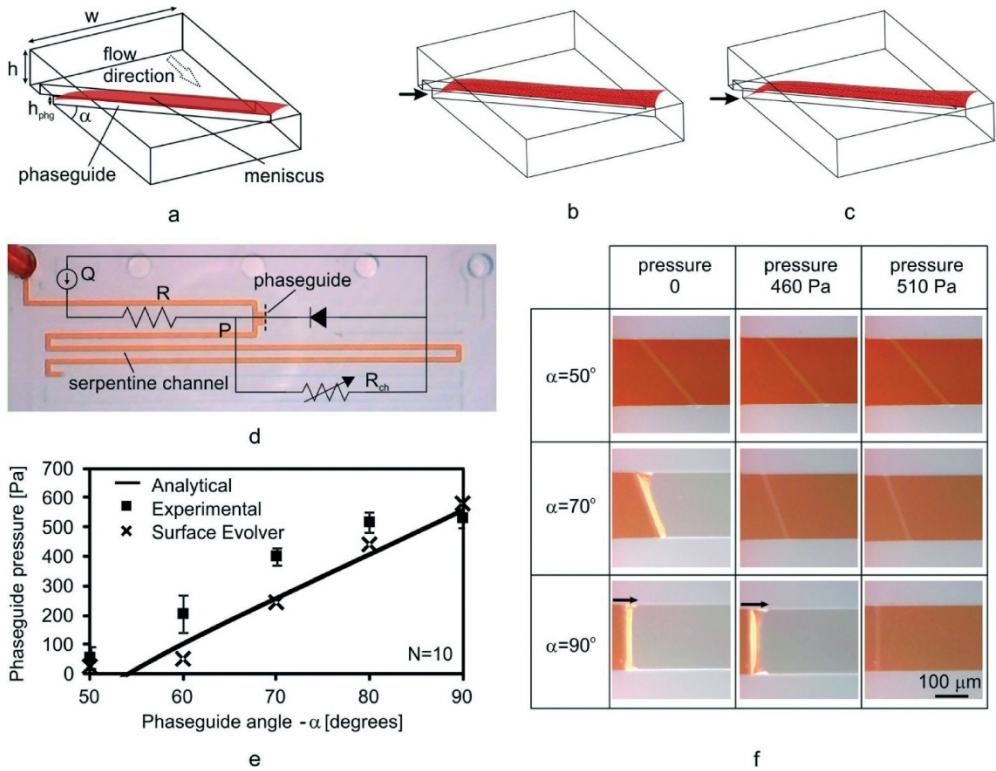


Figure 1 | Quantification of the phaseguide stability as a function of the phaseguide wall angle (a) schematic of the liquid air meniscus that is pinned on a phaseguide (b, c) snapshots of the Surface Evolver simulation showing meniscus advancement at the location of the smallest angle, α (depicted by the arrow); overflow occurs when the tip of the meniscus touches the channel bottom. (d) test structure used to experimentally determine the phaseguide pressure by equivalent electrical circuit analogy; (e) quantification of phaseguide stability as a function of the angle by experimental, numerical and analytical methods. All three methods show a clear increase in phaseguide stability with increasing phaseguide–wall angle. Below a certain angle the phaseguide loses its barrier function, which is designated the critical angle. Error bars indicate the standard error with $n = 10$ observations. See ESI† for experimental and simulation results. (f) frames captured at different pressures for three different phaseguide–wall angles during one set of experiments. For $\alpha = 50^\circ$ no alignment was observed. Arrows indicate the stretching of the meniscus before overflow. See ESI† for Video S1

Results

Phaseguide stability

In this work, a phaseguide is patterned as a shallow barrier at the bottom of the microfluidic channel (Fig. 1a). An advancing liquid meniscus first aligns along the phaseguide and then overflows it at its weakest point if sufficient pressure is built up across the meniscus.²⁵ This weakest point is typically the smallest angle along the phaseguide (phaseguide–wall angle α in Fig. 1a). This is typically the angle between the phaseguide and an intersecting sidewall. Control over this angle implies control over the stability of the phaseguide.

To assess the relationship between phaseguide stability and the angle between the phaseguide and a sidewall, a simulation was performed using Surface Evolver (a software package developed to examine interfaces under surface tension,²⁶ see Fig. 1b–c). The simulation shows that the meniscus moves downwards along the sidewall of the phaseguide. We define the overflow of the phaseguide as the point where the barrier function is relieved, *i.e.* when the meniscus touches the bottom substrate.

In addition to the simulation, we developed an analytical model to estimate the principal radii of curvature of the meniscus. The Laplace pressure developed across the meniscus at the instant of overflow, given by the Young–Laplace equation (eqn (1)), is defined as the phaseguide pressure (P_{phg}) and used as a measure of phaseguide stability.

$$P_{phg} = \gamma \left(\frac{1}{R_1} + \frac{1}{R_2} \right) \quad 1$$

Here, γ is the surface energy of the liquid and R_1 and R_2 represent the principle radii of curvature of the meniscus at the instant of overflow. R_1 and R_2 could be derived from the various contact angles and geometrical aspects (see the ESI† text for details).

To validate the analytical model and simulation results, we fabricated test structures (Fig. 1d) including phaseguides with phaseguide–wall angles varying from 50° to 90°. The phaseguides were positioned adjacently to a meandering channel close to the fluid inlet. Application of a constant flow rate resulted in gradual filling of the meander, thereby increasing the hydrodynamic resistance and

thus the back pressure over the meniscus that is pinned on the phaseguide. By electrical analogy (Fig. 1d), this backpressure (P) can be calculated as

$$P = R_{ch}Q \quad 2$$

with constant flow (Q) and channel resistance, R_{ch} , that increases with the length of the serpentine channel wetted by the liquid. The back pressure at the instant of overflow was recorded as the phaseguide pressure. Contact angles of the phaseguide and the channel wall material were assumed to be 70° , while top and bottom substrate contact angles were 20° . Channel height, phaseguide height, and channel width were set to $120\text{ }\mu\text{m}$, $30\text{ }\mu\text{m}$, and $200\text{ }\mu\text{m}$, respectively. Fig. 1e compares the analytical model and the simulation results with the experimental results. There is a close correlation between the analytical model and the simulation model. The experimental results show slightly higher phaseguide pressures than predicted by the analytical and numerical models. The trend, however, is comparable to these models. We assume this is due to the fact that the corner between the phaseguide and the side wall is not infinitely sharp as well as to a deviation in the contact angle with respect to measured values.

Both analytical and simulated models show that below a certain angle, the phaseguide immediately overflows without meniscus alignment. This is in accordance with the observation of Concus and Finn, who stated that a liquid under surface tension would wet a wedge with an angle less than a critical value.²⁷ This critical angle can be found as $(180^\circ - \theta_1 - \theta_2)$, where θ_1 and θ_2 are the contact angles of water on the phaseguide and the wall material, respectively. The critical angle was also found experimentally. In 6 out of 10 observations for 50° phaseguides, the liquid immediately overflowed the phaseguide without alignment (see ESI† Video S1). The fact that the meniscus alignment does not occur indicates the absence of a barrier function. This result implies a phaseguide pressure of less than or equal to zero. Since the test structure (Fig. 1d) does not allow measuring negative phaseguide pressures, we defined the phaseguide pressure as zero for these cases. For a material contact angle of 70° , the Concus–Finn theorem yields a critical angle of 40° . The discrepancy with the modeled and experimental values might be due to a range of causes, including meniscus stretching, corner flow effects and the fact that the angles are not infinitely sharp.

Complex liquid routing

Differential stability of the phaseguides implies that upon pinning of a meniscus on multiple phaseguides, the phaseguide with the lowest stability will overflow first²⁵ (Fig. 2a). To demonstrate this concept for liquid routing, we designed a microfluidic network composed of 14 parallel chambers placed as rungs between common inlet and outlet channels (Fig. 2b). The design is such that the hydrodynamic resistance between the inlet and the outlet measured across any of the chambers is the same. For bubble-free routing of liquid through this network, overflow must occur at the outlet of the first chamber only after all the chambers are filled.

This was achieved by placing relatively stable phaseguides (phaseguide #3 in Fig. 2b) at the outlets of chambers 2–14, while placing a less stable phaseguide (phaseguide #2 in Fig. 2b) at the outlet of chamber 1. Phaseguide #2 must be stable enough to prevent a premature overflow due to the increasing back pressure during the filling process. To satisfy these criteria, phaseguide #3 was designed as a curve protruding into the outlet channel such that the phaseguide–wall angle is 150°. Phaseguide #2 was designed as a straight line making a 90° angle with the channel wall. In addition to these phaseguides, curved phaseguide #1 was utilized at the inlet of chambers 1–13 to ensure sequential filling of the chambers. These phaseguides were designed as a smooth curve having a 30° angle with the chamber wall. Fig. 2d shows a detail of the filling process. The complex shaped phaseguides at the inlets ensure that overflow occurs only after the meniscus has advanced into the chamber. The relatively stable phaseguides at the chamber outlets keep the relating menisci pinned, while another meniscus proceeds in the downstream direction for filling the remaining chambers. As the meniscus reaches the last chamber (see Fig. 2e), overflow of phaseguide #2 occurs. The meniscus advances through the outlet channel and sequentially merges with the menisci pinned at the stable #3 phaseguides.

The result is that the complete network is filled without any air entrapped in the channels or chambers (Fig. 2f). The density of parallel data generation can be further increased by successively placing multiples of these ladder-like structures in parallel. This is shown in Fig. 2g–k. The figures show an array composed of 5 rows each of which comprise 15 chambers to create a total of 75 identical microfluidic chambers. In this configuration, the same phaseguide pattern is used as shown in Fig. 2a–f. In addition, 150° phaseguide #5 was utilized to block the outlet channel of each row at the common outlet channel. To ensure that overflow occurs at the outlet of the

first row, a less stable phaseguide #3 of 90° was used here. To ensure that this 90° phaseguide is not overflowed before all the rows are filled, the stability of phaseguide #2 was reduced, utilizing a 75° angle.

As a visual demonstration of the level of control that could be exerted using differential phaseguiding, we utilized a chamber array as a pixel array. Selective filling and non-filling of chambers due to the phaseguide shape result in the word μ TAS (in reference to the micro total analysis system, the original name for Lab-on-a-Chip,²⁸ see Fig. 3f and ESI† Video S4). The pixel array consists of 20 hairpin loops. Each loop contains 20 microchambers connecting the upstream and downstream channels of the loop. The outlet of each chamber contains a stable phaseguide of 90°, with the exception of the last chamber of each loop that does not contain a phaseguide. Each chamber that is to be filled with liquid contains a phaseguide #1 similar to the one shown in Fig. 2. Each chamber that is meant to stay empty contains a straight phaseguide of 90° at the inlet. Fig. 3b–e show the selective filling of chambers in a single loop. Fig. 3f shows the complete array filled, depicting the word μ TAS.

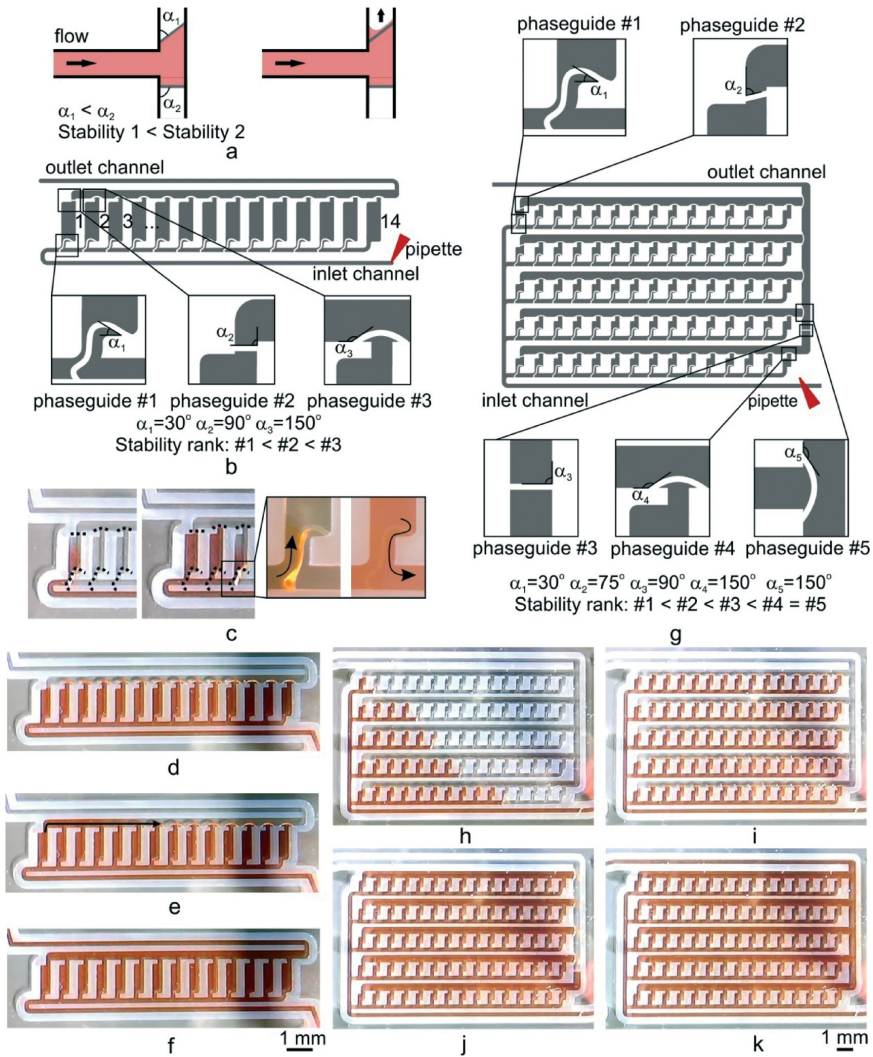


Figure 2 | Liquid routing through differential phaseguiding: (a) concept of differential phaseguiding: a liquid that is pinned on multiple phaseguides will overflow the least stable phaseguide, i.e., the phaseguide with the smallest phaseguide-wall angle; (b) a string of 14 chambers containing phaseguides of 3 different stability values: phaseguide #1 serves to fill each chamber consecutively, phaseguide #3 is not intended to be overflowed, while phaseguide #2 is to be overflowed only after filling all 14 chambers; (c) close-up of the filling sequence of the first 3 chambers; (d) the channel system upon filling all 14 chambers; (e) overflow of phaseguide #2; (f) the channel network upon complete filling; see also the ESI+ Video S2. g) Multitude of chamber rows in parallel containing phaseguides of 4 different stabilities; h–k) filling of a matrix of chambers, see also ESI+ Video S3.

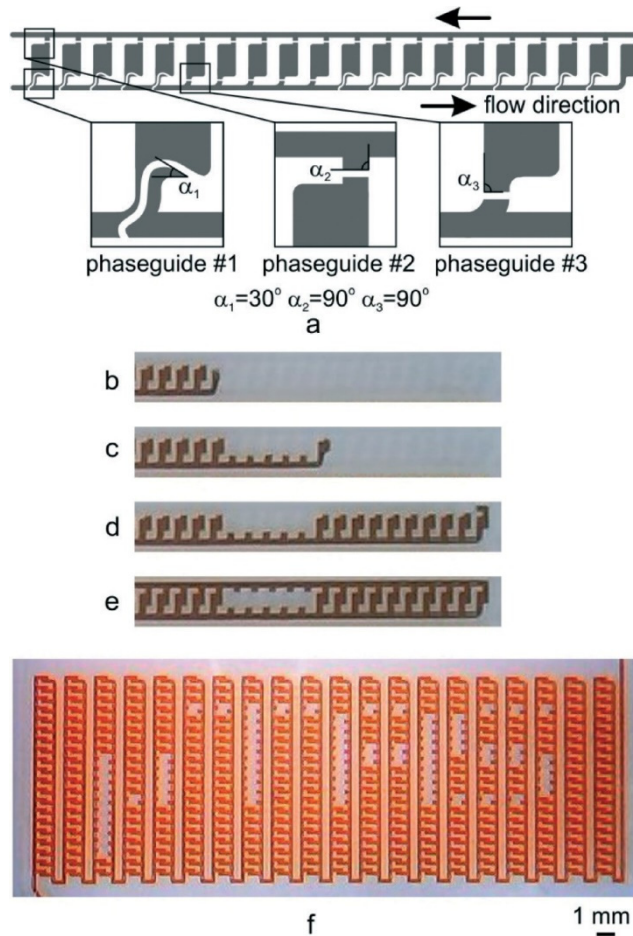


Figure 3 | Filling of a 20 × 20 pixel array: (a) one of the loops in the array containing 3 types of phaseguides. Phaseguide #1 is of lower stability than phaseguide #3 enabling selective filling of each chamber. Phaseguides #2 and #3 are not intended to be overflowed. b–e) Close-up of the filling of a single loop in which 3 chambers are deliberately left empty; (f) filling of the entire pixel array displaying the word μ TAS. See also the ESI,[†] Video S4.

Discussion

The above results, to our knowledge, are the first to demonstrate differential valving using passive pinning barriers, which was made possible by varying the angle between the phaseguide and the sidewall. However, a sharp bend in the phaseguide itself or a branching structure making a similar V-shape would also enable tuning of the stability.²⁵ This finding is a consequence from the insight that the pinning barrier stability is governed by both its vertical and horizontal cross-sectional shapes. Earlier literature typically describes a pinning barrier as governed by a two-dimensional cross-sectional shape.^{1,29} Others did include the third dimension in their analysis, but failed to observe the importance of the V-shaped grooves at the edges of the barriers.³⁰ As clearly shown in the above results, it is of critical importance to take both the horizontal and vertical cross-sectional shapes into account when assessing the stability of a pinning barrier. In our case, when the pinning barrier is positioned as a ridge on the bottom of a channel, the variation of the horizontal cross-sectional shape is more interesting than that of the vertical cross-sectional shape. As most microfabrication techniques are 2.5D at best, horizontal variations of design are strongly preferable over difficult to vary vertical geometries. Variations in the horizontal plane, such as used above, are usually part of the routine design and fabrication procedures, while adjusting the shape in the vertical cross section is typically limited by the fabrication technique and cannot be varied at will.

This innovation may have important consequences for the applicability of passive valves. Whereas active valves (PDMS microvalves in particular¹²) have largely lived up to their promises to enable massively parallel operations, passive valve-based platforms have failed to do so despite their inherent advantages such as ease of fabrication, stand-alone operation and wide material compatibility. This was mainly caused by the fact that active valve-based platforms offer selective liquid progression, while this was not possible in passive valve platforms. By introducing differential stability concepts, selective liquid progression is now possible in passive systems by preprogramming the barrier stability. This enables sequentially controlled filling of the channel networks.

In this paper we demonstrated the principle of differential valving using phaseguides without referring to any particular application. An example of the potential application of the technique is in performing combinatorial assays. Recently, it was shown that phaseguides can be used to laminate static volumes of liquids in a common chamber.²⁰ This concept can be combined with the one-shot

dispensing techniques described here in order to obtain an array of chambers filled in parallel with different combinations of reagents. Further extrapolation towards multi-layer microfluidic channel networks enables applications in combinatorial PCR, library preparation for next-generation sequencing, or single-cell analysis that are currently performed in active valving platforms.³¹

The primary interest of our research groups goes towards increasing the data density of the microfluidic 3D cell cultures or Organs-on-a-Chip.¹⁶ These devices today suffer from the typical microfluidics paradox, where the actual active area is much smaller than the surrounding chip and equipment used for world-to-chip interfacing. Multiplexing of tissues, combinatorial screening techniques and one-shot perfusion of cell cultures would greatly assist in increasing the density of tissues on a single plate.

Experimental

Fabrication

The structures were fabricated as previously described.²⁵ Briefly, phaseguides and channels walls were made from dry film resist (Ordyl SY330, Elga Europe) on glass substrates using standard photolithographic techniques. The microfluidic device was covered with a glass wafer on which the inlets and outlets were created by ultrasonic drilling. Nominal heights of the channels and the phaseguides were set to 120 μm and 30 μm , respectively.

Phaseguide characterization

To determine the back pressure at the instant of overflow, we measured the length of the serpentine channel wetted by the liquid and inserted in the equation for the pressure drop (ΔP) in rectangular channels³² (eqn (3))

$$\Delta P = \frac{12\mu QL}{h^3 w} \left(1 - 0.630 \frac{h}{w}\right)^{-1} \quad 3$$

where μ is the dynamic viscosity of the liquid, Q is the volumetric flow rate, L is the wetted length of the serpentine channel, h is the channel height, and w is the channel width. To determine the wetted length of the serpentine channel, the flow was recorded using a digital microscope. The wetted length was determined by processing the captured image at the instant of overflow using ImageJ. During the tests, the flow rate was set to 20 $\mu\text{L min}^{-1}$.

Testing of the chips

To test the microfluidic device, food-dye-colored de-ionized water was dispensed with a pipette. Pipette tips precisely fit the access holes such that they can be used for active pumping of liquids in the channels.

Conclusion

A passive liquid routing platform was introduced based on differential phaseguiding. Differential stability was achieved by variation of the angle between the phaseguide and the channel wall. Stability was quantified experimentally, numerically and analytically. A 400-pixel array could be filled in a controlled manner in one pipetting step only. Differential phaseguiding resolves a critical bottleneck in microfluidics,

making it available as an affordable laboratory disposable for massive parallel data generation.

Acknowledgements

Authors like to thank Koen Sweering and Athanasios Giannitsis for fabrication of microfluidic chips. Our gratitude also goes to the Technology Foundation STW, the Netherlands Metabolomics Centre and the Scientific and Technological Research Council of Turkey for funding this research.

Notes and references

1. P. Man, C. Mastrangelo, M. Burns and D. Burke, Proceedings of the 11th Annu. Int. Work. Micro Electro Mech. Syst., Heidelberg, 1998.
2. M. R. McNeely, M. K. Sputea, N. A. Tusneem and A. R. Oliphant,
3. J. Assoc. Lab. Autom., 1999, 4, 30.
4. K. W. Oh and C. H. Ahn, J. Micromech. Microeng., 2006, 16, R13.
5. A. K. Au, H. Lai, B. R. Utela and A. Folch, Micromachines, 2011, 2, 179.
6. P. Man, C. Mastrangelo, M. Burns and D. Burke, Proceeding of Transducers, Sendai, 1999.
7. Y. Feng, Z. Zhou, X. Ye and J. Xiong, Sens. Actuators, A, 2003,
8. 108, 138.
9. M. Zimmermann, P. Hunziker and E. Delamarche,
10. Microfluid. Nanofluid., 2008, 5, 395.
11. J. Melin, N. Roxhed, G. Gimenez, P. Griss, W. van der Wijngaart and G. Stemme, Sens. Actuators, B, 2004, 100, 463.
12. C. H. Ahn, A. Puntambekar, S. M. Lee, H. J. Cho and C. C. Hong, Proceedings of Micro Total Anal. Syst., Enschede, 2000.
13. D. Juncker, H. Schmid, U. Drechsler, H. Wolf, M. Wolf, B. Michel, N. de Rooij and E. Delamarche, Anal. Chem., 2002, 74, 6139.
14. R. Safaviieh and D. Juncker, Lab Chip, 2013, 13, 4180.
15. M. A. Unger, H. P. Chou, T. Thorsen, A. Scherer and S. R. Quake, Science, 2000, 288, 113.
16. T. Thorsen, S. J. Maerkl and S. R. Quake, Science, 2002, 298, 580.
17. B. Hadwen, G. R. Broder, D. Morganti, A. Jacobs, C. Brown, J. R. Hector, Y. Kubota and H. Morgan, Lab Chip, 2012, 12, 3305.
18. P. Vulto, G. Medoro, L. Altomare, G. A. Urban, M. Tartagni, R. Guerrieri and N. Manaresi, J. Micromech. Microeng., 2006, 16, 1847.
19. S. J. Trietsch, G. D. Israëls, J. Joore, T. Hankemeier and P. Vulto, Lab Chip, 2013, 13, 3548.
20. J. W. Schoonen, V. Van Duinen, A. Oedit, P. Vulto, T. Hankemeier and P. W. Lindenburg, Anal. Chem., 2014, DOI:10.1021/ac500707v.
21. P. Vulto, G. Dame, U. Maier, S. Makohliso, S. Podszun, P. Zahn and G. A. Urban, Lab Chip, 2010, 10, 610.
22. R. Gottheil, N. Baur, H. Becker, G. Link, D. Maier, N. Schneiderhan-Marra and M. Stelzle, Biomed. Microdevices, 2013, 16, 163.
23. C. Phurimsak, E. Yildirim, M. D. Tarn, S. J. Trietsch,
24. T. Hankemeier, N. Pamme and P. Vulto, Lab Chip, 2014, 14, 2334.
25. C. Y. Chen, T. C. Chiang, C. M. Lin, S. S. Lin, D. S. Jong, F. S. Tsai, J. T. Hsieh and A. M. Wo, Analyst, 2013, 138, 4967.
26. D. Puchberger-Enengl, C. Krutzler, F. Keplinger and M. J. Vellekoop, Lab Chip, 2014, 14, 378.

26. C. Tung, O. Krupa, E. Apaydin, J.-J. Liou, A. Diaz-Santana, B. J. Kim and M. Wu, *Lab Chip*, 2013, 13, 3876.
27. P. Vulto, P. Kuhn and G. A. Urban, *Lab Chip*, 2013, 13, 2931.
28. P. Vulto, S. Podszun, P. Meyer, C. Hermann, A. Manz and G. A. Urban, *Lab Chip*, 2011, 11, 1596.
29. K. A. Brakke, *Exp. Math.*, 1992, 1, 141.
30. P. Concus and R. Finn, *Proc. Natl. Acad. Sci. U. S. A.*, 1969, 63, 292.
31. A. Manz, N. Graber and H. M. Widmer, *Sens. Actuators, B*, 1990, 1, 244.
32. S. Chibbaro, E. Costa, D. I. Dimitrov, F. Diotallevi, A. Milchev, D. Palmieri, G. Pontrelli and S. Succi, *Langmuir*, 2009, 25, 12653.
33. T. S. Leu and P. Y. Chang, *Sens. Actuators, A*, 2004, 115, 508.
34. J. Melin and S. R. Quake, *Annu. Rev. Biophys. Biomol. Struct.*, 2007, 36, 213.
35. H. Bruus, *Theoretical Microfluidics*, Oxford University Press, New York, 2008, pp. 48–51.

Supplementary Information

Analytical Model

The phaseguide pressure was calculated using the Young-Laplace pressure given by

$$P_{phg} = \gamma \left(\frac{1}{R_1} + \frac{1}{R_2} \right)$$

where γ is the surface tension, R_1 and R_2 are the principle radii of curvature of the meniscus at the instant of overflow. Figure S1 illustrates the cut-out section of the channel with phaseguide at the instant of overflow, showing the global coordinate frame, the phaseguide, and the meniscus.

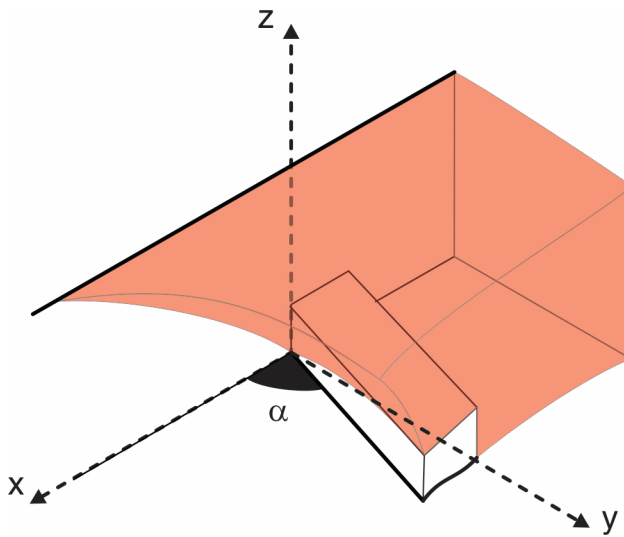


Figure S1 | Cut out section of the microchannel with phaseguide. The global coordinate system is located such that the z axis is directing upward and collinear with the edge created by the phaseguide and the channel wall, and x is directing the liquid advancing direction.

To determine the principle curvatures, a local frame was defined as shown in Figure S2.a. This frame was defined such that $x'z'$ plane dissects the wedge created by the phaseguide and the channel wall to make a dihedral angle of $\alpha/2$ with the channel wall.

Assuming that this plane passes normal to the contact line on the channel top, it can be concluded that the angle between the curve C1 and the top substrate measured on $x'z'$ plane is equal to the advancing contact angle θ_1 between the liquid and the top substrate (Figure S2.b). On the other hand, angle θ_2' between the edge created by intersection of the phaseguide and the channel wall, and curve C1 can be found as:

$$\cos \theta_2' \cos \left(90^\circ - \frac{\alpha}{2} \right) = \cos \theta_2$$

where θ_2 is the advancing contact angle between the liquid and the wedge material. Since the phaseguide and channel wall, which constructs the wedge, are made of the same material (dry-film-photoresist in our case) we assumed a single contact angle θ_2 in our derivations.

As a result, referring Figure S2.b it can be written that:

$$\begin{aligned} \sin \theta_2' &= \frac{l_2}{R_1} & \cos \theta_2' &= \frac{l_1 + x'}{R_1} \\ \sin \theta_1 &= \frac{l_1}{R_1} & \cos \theta_1 &= \frac{l_2 + h}{R_1} \end{aligned}$$

Since

$$l_2 = R_1 \sin \theta_2'$$

then it can be written that

$$R_1 \cos \theta_1 = R_1 \sin \theta_2' + h$$

As a result R_1 can be found as

$$R_1 = \frac{h}{\cos \theta_1 - \sin \theta_2'}$$

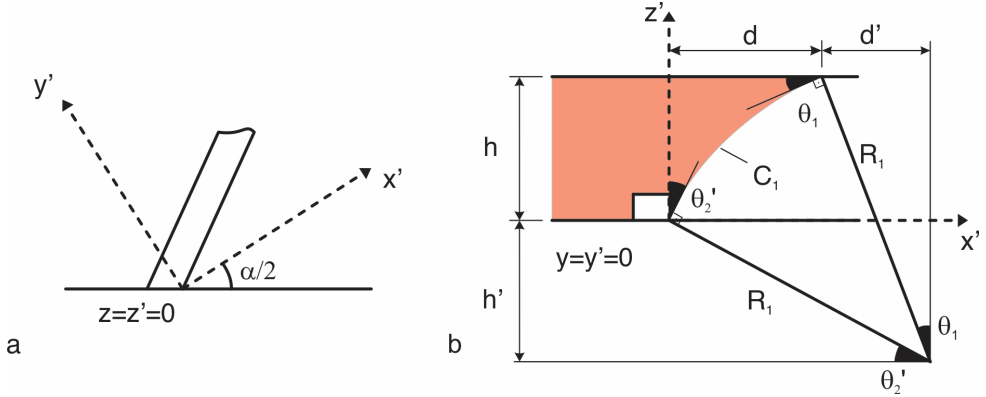


Figure S2 | (a) Orientation of the local coordinate frame for calculation of R_1 . (b) Curve C_1 lying on $x'z'$ plane.

By definition, principal curves on a surface are perpendicular to each other. To find the other principal curvature, a secondary frame is defined such that the x'' , whose extension intersects the front edge of the phaseguide, lies on $x'z'$ plane and is normal to the curve C_1 (Figure S3.a). Assuming a shallow phaseguide, this distance δ between the origin of this local frame and the front edge of the phaseguide along x'' can be approximated as:

$$\delta = h_{phg} \sin \theta_2'$$

Referring to Figure S3.b, it can be written that

$$\frac{R_2}{\sin \alpha'} = \frac{R_2 + \delta}{\sin (90^\circ + \theta_2')}$$

As a result the radius of curvature of curve C_2 can be found as:

$$R_2 = \frac{\delta \sin \alpha'}{\sin (90^\circ + \theta_2') - \sin \alpha'}$$

Here α' is the half phaseguide angle tilted approximately by θ_2' , which can be states as:

$$\tan \alpha' = \tan \frac{\alpha}{2} \cos \theta_2'$$

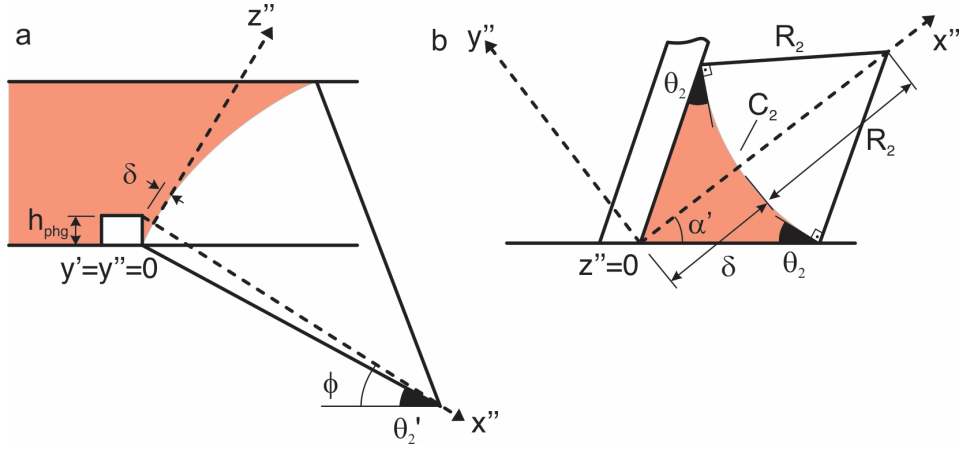


Figure S3 | (a) Orientation of the local coordinate frame for calculation of R_2 . (b) Curve C_2 lying on $x'z'$ plane.

As a result, inserting the expressions derived for the radii of curvature into Young-Laplace equation, the phaseguide pressure can be found.

By rearranging the terms, Young-Laplace equation for the phaseguide pressure can be rewritten as:

$$P_{phg} = \frac{\gamma}{R_1} + \frac{\gamma}{R_2}$$

Here γ/R_1 and γ/R_2 can be interpreted as the pressure contribution of the first principle curve C_1 and the second principle curve C_2 respectively. Plotting γ/R_1 , γ/R_2 , and P_{phg} (Figure S4) reveals that P_{phg} is dominated by γ/R_2 , which is mainly controlled by the phaseguide angle.

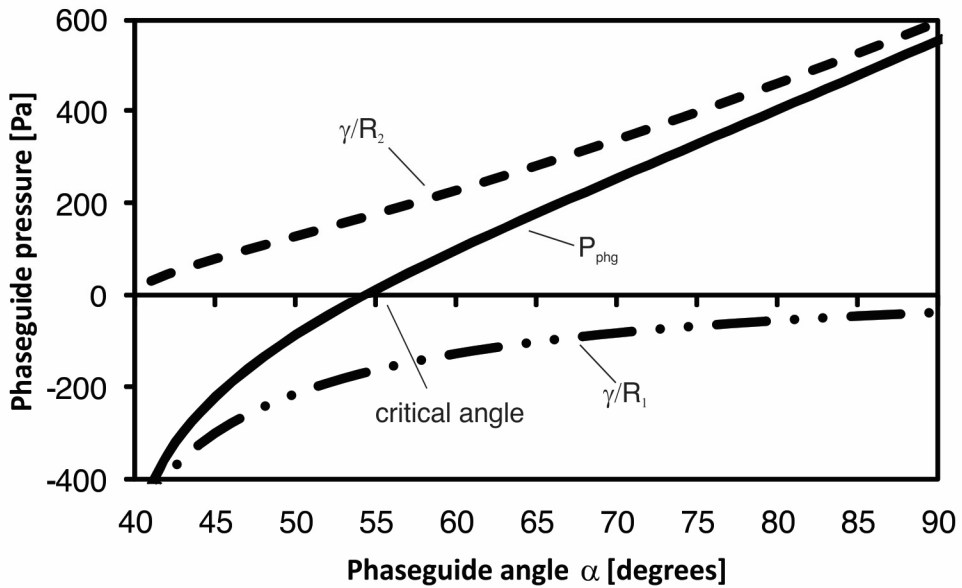


Figure S4 | Contribution of the first principle curve represented by the radius R_1 and the second principle curve represented by the radius R_2 on phaseguide pressure. θ_1 and θ_2 are 20° and 70° respectively. Channel height and phaseguide height are $30\ \mu\text{m}$ and $120\ \mu\text{m}$ respectively. Intersection of μ/R_2 gives the critical angle prescribed by the Concus-Finn criterion. However, we found a slightly larger critical angle, which is caused by the effect γ/R_1 .

Simulation Model

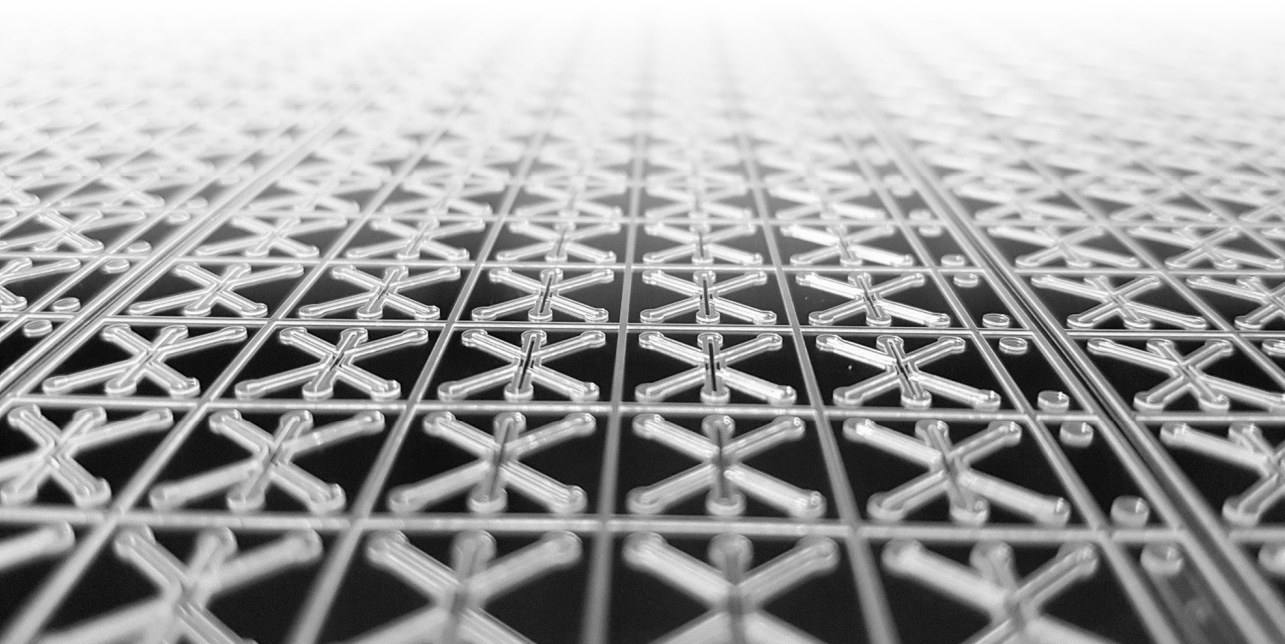
To determine the phaseguide pressure using Surface Evolver, the meniscus, the channel, and the phaseguide were geometrically modeled. Surface Evolver was used to find the meniscus geometry at zero pressure by evolving this initial meniscus. The new meniscus was re-evolved by incrementally changing the pressure. These iterations were carried out until the meniscus reaches the bottom of the channel. The pressure on the meniscus at this instant was recorded as the phaseguide pressure.

Chapter 4

Microfluidic titer plate for stratified 3D cell culture

SJ Trietsch, GD Israëls, J Joore, T Hankemeier, P Vulto

Lab on a Chip



Abstract

Human tissues and organs are inherently heterogeneous. Their functionality is determined by the interplay between different cell types, their secondary architecture, vascular system and gradients of signaling molecules and metabolites. Here we propose a stratified 3D cell culture platform, in which adjacent lanes of gels and liquids are patterned by phaseguides to capture this tissue heterogeneity. We demonstrate 3D cell culture of HepG2 hepatocytes under continuous perfusion, a rifampicin toxicity assay and co-culture with fibroblasts. 4T1 breast cancer cells are used to demonstrate invasion and aggregation models. The platform is incorporated in a microtiter plate format that renders it fully compatible with automation and high-content screening equipment. The extended functionality, ease of handling and full compatibility to standard equipment is an important step towards adoption of Organ-on-a-Chip technology for screening in an industrial setting.

4

Introduction

There is a great need for more predictive *in vitro* screening models for early de-risking in drug discovery and development. A trend towards better mimicry of the *in vivo* microenvironment is to culture relevant tissues in three dimensions instead of conventional monolayers.¹ Cells are suspended in a surrogate extracellular matrix (ECM), which results in more natural morphology and has a tremendous effect on gene expression, metabolism and ultimately drug efficacy² and toxicology.^{3,4}

Efforts are ongoing to add further organotypic functionality to these 3D cell cultures by considering the structural, mechanical and chemical complexity of tissues. With roots in the fields of tissue engineering and lab-on-a-chip, “Organs-on-Chips”⁵ aim to exploit the precise control of liquids in the microfluidic space to control the tissue microenvironment.

Over the past years, a wide variety of mono and co-culture⁶ models have been developed including liver,^{7–11} kidney,^{12,13} colon,^{14,15} lung,^{16,17} cornea,¹⁸ heart,¹⁹ breast,^{20,21} neuronal,^{22,23} and vascular models.²⁴ Different models have been combined to achieve multi-organ integration^{25–27} and have been adapted to disease specific models.^{28–30}

The essence of improving translatability of *in vitro* models is to capture the complexity of heterogeneous tissues. This includes perfusion flow aspects, co-culture flexibility and communication between various distinct microenvironments. Today's preferred method to achieve heterogeneous tissue complexity is by compartmentalization of the microfluidic space using physical separations. Compartmentalization techniques reported include usage of membranes,^{31,32} valves,³³ tightly placed pillars,¹⁰ long narrow channels,³⁴ or other tight gaps.³⁵ However compartmentalization can severely hamper communication, because of long diffusion distances or prevention of direct cell–cell interactions.

Here we propose a stratified 3D cell-culture platform in which tissues and perfusion lanes are patterned adjacently, without physical separation. We employ a two- and three-lane bioreactor in which lanes are separated by phaseguides. As described previously,^{36–39} phaseguides are geometric features that act as pressure barriers due to meniscus pinning. One or more lanes are filled with gel-embedded cells. Remaining lanes are employed for a perfusion flow, a challenge compound or staining reagents. Perfusion by leveling of reservoirs supplies nutrients, oxygen and removes waste metabolites. Co-cultures enable studying cell–cell interaction and construction of complex tissues.

Here we present a proof of concept by culturing HepG2 liver cells in 3D under continuous perfusion. The cells exhibit excellent survival, and are used for hepatotoxicity assessment of rifampicin. Mixed and side-by-side cultures of hepatocytes and fibroblasts demonstrate co-culture flexibility of the system. Invasion and aggregation of tumor cells demonstrates migration assay capabilities. Arrays of 40 or 96 microchambers are embedded in a microtiter-based screening plate that is pipette-operatable and fully compatible with industrial readout and liquid handling equipment. The phaseguide-stratified 3D culture platform provides a complete toolbox for modeling tissues of arbitrary complexity. It is among the most elegant approaches for constructing complex heterogeneous tissues and Organ-on-a-Chip models.

Materials & methods

Chips fabrication

Microfluidic chips were fabricated using a dry film resist (DFR) based process as extensively described previously.^{40–43} Briefly, a 30 μm thick permanent dry film resist (Ordyl SY330, Elga Europe, Italy) was hot laminated on 175 μm thick glass substrates and exposed using a Karl Suss MA45 mask aligner through a transparency foil mask of the phaseguides printed on an AGFA Accuset 1500 photo plotter at 3000 dpi. Three additional layers were laminated on top and exposed with a second mask in order to pattern microfluidic channel walls. After post baking, the chips were developed using BMR developer (Elga Europe, Italy). Chips were capped with a glass substrate with predrilled access holes in a hot press (5 min, 95°C, 60 N cm⁻²), resulting in 120 μm high microfluidic chambers with 30 μm high phaseguides. Bottomless 384-wells plates were glued on top of the inlets using non-cytotoxic medical grade glue (Loctite M-31 CL, Henkel, Germany).

Cell culture

HepG2 and 4T1 cells were cultured in Dulbecco's Modified Eagle Medium (DMEM) supplemented with 10% fetal calf serum (FCS), 50 U mL⁻¹ Penicillin and 50 mg mL⁻¹ Streptomycin (P/S) and stable glutamine (PAA Laboratories GmbH, Cölbe, Germany). 3T3 cells were cultured in DMEM/ FCS/P/S with added stable glutamine, both wild type and transfected with mCherry-LifeAct. Unless otherwise specified all cell culture reagents were acquired from Life Technologies, Carlsbad, CA, USA.

For 3D cell culture, cells were harvested, washed once in full medium, pelleted and resuspended in the appropriate ECM on ice. Unless stated otherwise, Matrigel was used at 9 mg mL⁻¹ concentration (BD Matrigel, lot 2152611 and 23060, BD Bioscience, Franklin Lakes, NJ USA). Type I collagen (rat tail) was neutralized with Na₂CO₃ (Alfa Aesar, Karlsruhe, Germany) buffered with 100 mM HEPES and diluted to 3 mg/mL using medium, before resuspending cells. Unless otherwise specified, cells were resuspended at 2.5·10⁷ cells mL⁻¹. For mixed co-culture, HepG2 and 3T3 cells were mixed in a 4 : 1 ratio for a total cell count of 2.5·10⁷ cells mL⁻¹.

Plate loading

The gel with cells is patterned adjacent to one or two flanking empty lanes. Cells suspended in liquid ECM were loaded into the microfluidic chips, where it is sucked into the phaseguide defined space by capillary force. After gelation (10 min at 37°C), the flanking lanes are filled with media, which can either be static or passively perfused by leveling of two connected wells. Due to the hydrodynamic resistance of the small connecting channels between the wells and the culture chamber, an average fluid flow of $1.5 \mu\text{L h}^{-1}$ is achieved, allowing for 24 h of perfusion with 100 μL of medium. In most cases media was exchanged three times per week for convenience reasons.

Assays

For toxicity assays, rifampicin was dissolved in DMSO and diluted in the perfusion media resulting in medium with 0.5% DMSO and varying rifampicin concentrations up to 640 mM. Live/dead assays were performed by washing the culture chamber twice with PBS before incubating for 30 min with 2 μM calcein AM and 4 μM ethidium homodimer-1 in phenol red and serum free medium (Invitrogen L3224 LIVE/DEAD1 Viability/Cytotoxicity Kit for mammalian cells, Life Technologies, USA). The stained cells were imaged using an Olympus IX81 inverted fluorescence microscope with automated stage and analyzed using CellM and ImageJ (Fiji) software. Confocal images were obtained using a Leica SP5 confocal microscope and analyzed using LAS-AF software and ImageJ.

Results and discussion

Device

Fig. 1 shows the microtiter plate setup for 3D heterogeneous cell and tissue culture. The 384 well plate has been modified on the bottom-side with microfluidic structures. Two designs have been used. The plate depicted in Fig. 1 contains 40 culture chambers, each with three inlets and three outlets that are connected to corresponding wells. A second plate is also used containing 96 culture chambers, each with two inlets and one outlet. Each chamber is 4.5 mm in length and consists of three resp. two 200 μm wide, 120 μm high lanes that are separated by 50 μm wide, 30 μm high phaseguides. A gel is patterned in one of the three lanes by simply pipetting the gel in the corresponding inlet well. The gel is sucked into the microfluidic chamber by capillary force, but the meniscus pinning effect prevents

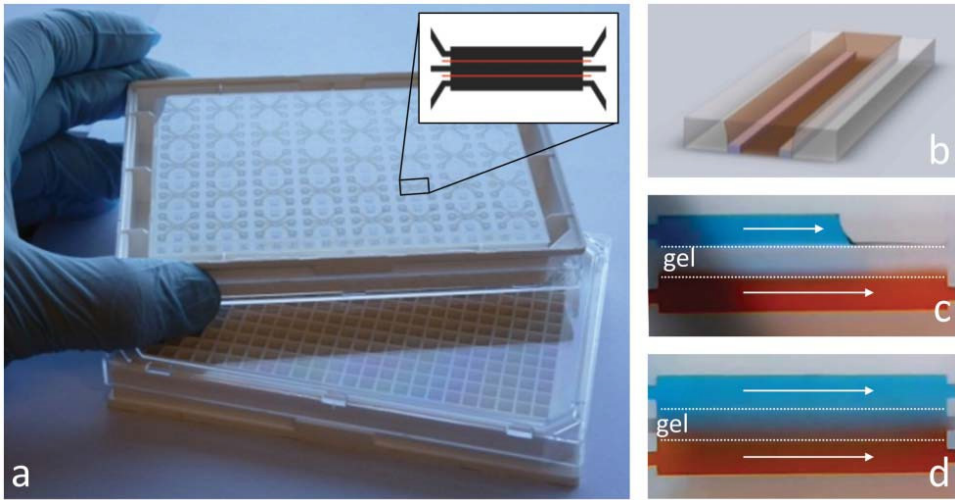


Figure 1 | (a) 384-well format 3D cell culture plate with 40 three-lane culture chambers manufactured in the bottom plate. Inset depicts the design of a single culture chamber with phaseguide positions in red. (b) Artist impression of culture chamber with gel confined in middle lane between phaseguides, flanked by perfusion lanes. (c) Food dye being filled in flanking lanes, dotted line indicates phaseguide position. (d) Perfused media forming a gradient across gel.

the gel from overflowing into one of the flanking lanes. Upon gelation, adjacent lanes can be filled with a second gel or be used for perfusion. Since the phaseguide is merely a pinning barrier that is not higher than one fourth of the channel height, free communication between the three lanes through diffusion is maintained. This is demonstrated in Fig. 1c and d by patterning matrigel (middle lane) flanked by a red and blue food dye. The red and blue dyes are diffusing into the matrigel to form a gradient. Various gradient regimes are possible. When both lanes are perfused continuously, a constant transverse gradient is formed. Without perfusion, the gradient equilibrates over time, ultimately resulting in a homogeneous mixture.

As opposed to often-used silicone rubber (polydimethylsiloxane, PDMS) based systems, the hybrid glass–DFR system is impermeable to gasses giving complete control over gas pressure in the tissues. The plate is equipped with a thin

175 μm bottom glass plate to ensure compatibility with imaging techniques such as phase contrast, fluorescence, confocal, and multi-photon microscopy as well as with high content screening (HCS) automated readers.

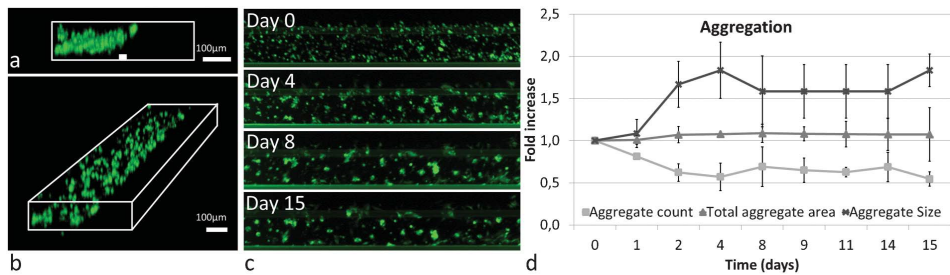


Figure 2 | Fluorescent HepG2 cells in an extracellular matrix gel in a two-lane microfluidic chamber: (a, b) confocal analysis of cells 48 h after seeding demonstrates a 3D distribution of cells throughout the chamber; (c) image sequence showing clustering of cells over time; (d) quantification of clustering and proliferation behavior of cells in a microfluidic 3D environment: cells aggregate into clusters, while proliferation becomes near zero.

Perfused 3D cell culture

Fig. 2 shows GFP transfected HepG2 human hepatocytes in matrigel flanked by a perfusion flow up to 15 days in culture. Fig. 2a shows confocal image of the cell culture upon 48 h in culture. Notwithstanding the relatively shallow chamber height of 120 μm, cells and aggregates are observed throughout the microfluidic space. This indicates that sedimentation does not significantly affect the distribution of cells in the gel. Fig. 2b and c shows the behavior of cells over time. The size of aggregates increases over time, the number of aggregates decreases, but no change in the overall area of the sum of aggregates is observed. This indicates that no significant proliferation occurs in 3D, as opposed to the high proliferation in conventional 2D culture. The formation of low proliferative three-dimensional cell clusters when culturing cells embedded in surrogate extracellular matrices is well documented in

literature. The clustering is associated as a first step in the process towards a more metabolic competent model.^{44–46} After 7 days the number and size of clusters stabilized. The clusters maintained near complete viability as confirmed by fluorescent live/dead staining.

As a proof of principle for a toxicity assay, hepatotoxicity of rifampicin was assayed. HepG2 cells were perfused with varying concentrations of up to 640 μM rifampicin for 48 and 96 h and at least three replicates were assayed for viability using a fluorescent live/dead stain at day 7 after seeding. Fig. 3a shows a series of images

of cells exposed to different doses of rifampicin, acquired using automated microscopy on a single plate. Viability of the cell clusters was scored and normalized to the number of clusters. Fig. 3b shows the dose response curve for viability of clustered hepatocytes upon rifampicin exposure. The results demonstrate the expected dose-dependent cell death, increasing with dose and exposure time.

Conventional 2D cell cultures need to be passaged up to several times a week in order to maintain viability, often requiring harsh treatments like trypsinization and scraping. 3D cell cultures under perfusion form stable tissues that show full viability for several weeks, circumventing the need to passage. The perfusion flow provides nutrients and oxygen and removes waste metabolites. This yields stable culture conditions, whereas conventional static culture systems often undergo cycles of acidification, nutrient depletion, waste build-up and evaporation. In the results of Fig. 2, however, media were exchanged three times a week for convenience reasons, resulting in perfusion for approximately half of the time before liquid levels equalized. Nonetheless we observed no significant effect on the stability of the cell culture. The reason may be that effects are limited by the presence of a relatively large volume of media in the connected wells that can act as a source and sink for nutrients and metabolites in the microchamber. Clearly in a future design, perfusion times will be extended by increasing the hydrodynamic resistance of the channels.

The gel lane has a width of 200 μm , reflecting the physiological distance between two capillary vessels in a human body. The gel matrix protects cells from shear stress generated by the perfusion flow. In contrast to non-gel based perfusion systems, the gel matrix limits rapid efflux of signaling molecules and thus maintains a biologically relevant microenvironment.

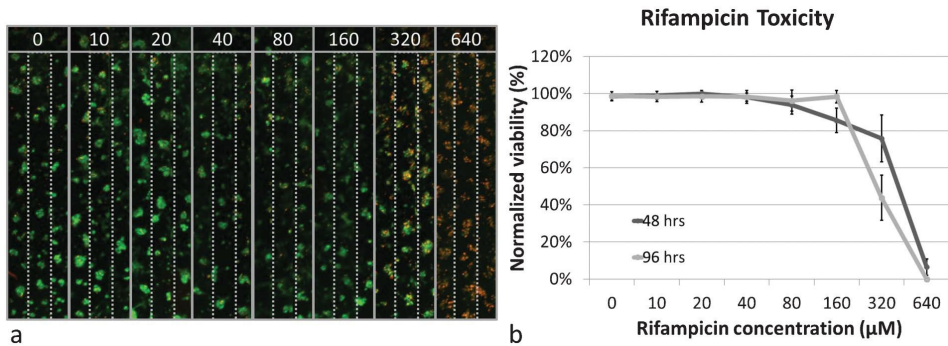


Figure 3 | (a) Image array of one-week old HepG2 spheroids exposed to varying concentrations of rifampicin for 96 h, followed by fluorescent live/dead staining (green/red); (b) dose response curve of rifampicin toxicity upon 48 and 96 h of exposure.

The image stack of Fig. 3a was acquired by automated fluorescence microscopy of one single plate containing 96 microchambers. Due to the shallow chamber height, all cells and clusters are sufficient in focus for quantification. The fact that standard 2D imaging techniques can be applied to 3D cultures in these shallow culture chambers offers an excellent balance between superior 3D functionality and the ease of imaging associated with 2D cultures.

The above results convincingly demonstrate that the microfluidic plates presented here are fully compatible with advanced imaging techniques such as confocal, phase contrast, and fluorescent imaging. This is largely facilitated by the thin 175 μm bottom glass. Fluorescent and phase contrast images were acquired by automated microscopy, demonstrating compatibility of the titer-plate based microfluidic platform with high content screening (HCS) assays.

Co-culture and cell migration

The three-lane reactor setup facilitates different types of co-cultures, including cells mixed in the same ECM (mixed co-culture), different cell types patterned in adjacent lanes (adjacent co-culture) and different cell types patterned in lanes that are not in direct contact but communicate, e.g. through a perfusion flow or third gel (separated co-cultures). Fig. 4a–c illustrates these different co-culture methods. To demonstrate co-culture functionality of the plate, HepG2 hepatocytes were co-cultured with 3T3 fibroblasts cells in both mixed and adjacent modes (see Fig. 4d, e). The two co-cultures with fibroblasts result in very different tissue types. In the mixed mode, dense aggregates of fibroblasts and hepatocytes are formed. No

significant change in hepatocyte morphology is observed in adjacent cell culture. As supported by fibril formation observed in 3T3 mono-culture, the aggregates in the mixed co-culture are thought to be formed by fibroblasts that mechanically contract and support hepatocytes. The absence of any contraction of the hepatocytes in adjacent co-culture illustrates the ability to distinguish between changes in morphology by excreted signaling molecules and direct cell–cell interaction. Comparison of adjacent and separated co-cultures could be used to distinguish between local (paracrine) signaling and long distance (endocrine) cell–cell communication. An example of an endocrine system would be a liver–kidney co-culture or a liver–heart co-culture. Such cultures can for example be used to study liver mediated nephro- or cardiotoxicity.

Here we describe devices with two or three lanes, but it is clear that an arbitrary number of lanes can be patterned in order to increase the level of complexity of the model. One could try to capture the secondary architecture of an organ up to the level of a “living coupe”; a carefully designed architecture of lanes containing cell types and perfusion sites behaving like a section of an organ in a living organism.

4

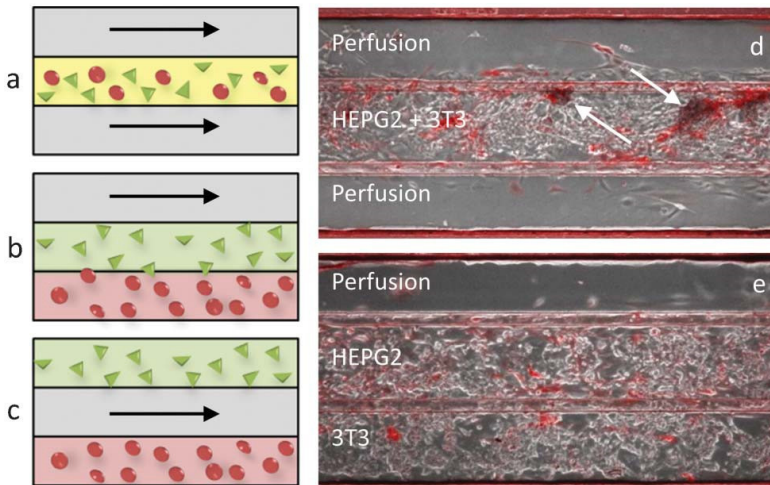


Figure 4 | Schematic representation of (a) mixed co-culture, (b) adjacent co-culture, (c) separate co-culture configurations with perfusion through empty lanes. (d) Mixed and (e) adjacent co-culture of HepG2 hepatocytes and 3T3 mCherry fibroblasts, with mixed co-culture resulting in tighter aggregates as indicated by

Contraction and invasion

The potential of the platform to support migration assays was investigated using 4T1 breast cancer cells cultured in collagen (Collagen 1, rat tail). A 4T1 cell loaded collagen gel was patterned adjacent to a clean collagen lane. Invasion of the 4T1 cells into the adjacent lane was monitored using time lapse imaging. Initial contraction towards the empty collagen lane caused formation of a boundary, followed by invasion into the empty collagen lane. Fig. 5 depicts this invasion process as quantified by the area of the middle lane that is covered by invaded cells. Additionally, 4T1 cells in a single lane showed strong contraction (see Fig. S1, ESI3). Within 48 h dense aggregates are formed and in prolonged cultures, cells grow out of these aggregates that ultimately disintegrate. In single-lane collagen gels, centric aggregation into spheroids was observed. Such spheroids can become very dense showing increased cell death in the center of the spheroid. This effect indicates that even on this scale necrotic core formation might be induced by hampered nutrient diffusion, resulting in an interesting model for tumor formation and angiogenesis. Examples of practical applications are wound healing-, chemotaxis- and invasion assays. In combination with the above described co-culture and gradient flexibility, a range of invasion assays can be designed under precisely controlled conditions.

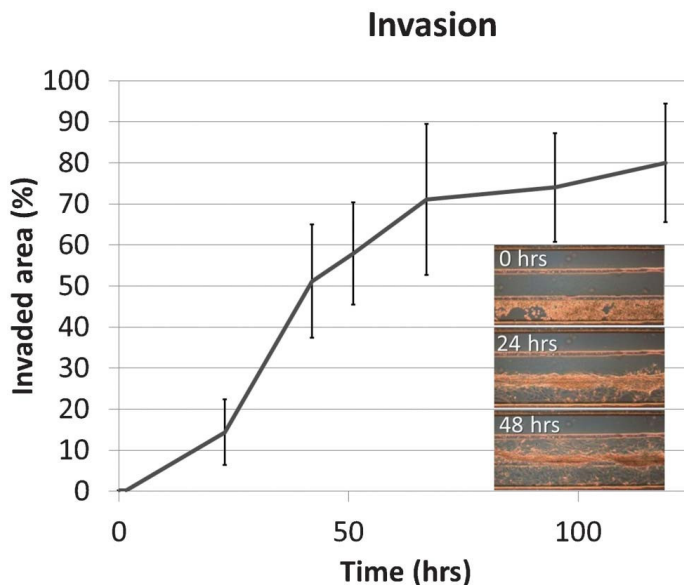


Figure 5 | 4T1 cells cultured in collagen I next to a cell free collagen lane are invading into the adjacent lane. Invasion was quantified as the area of the central lane covered with invaded cells

Organ-on-a-Chip: bridging the technology acceptance gap

In the section above we introduced a platform technology for heterogeneous tissue modeling in a 3D configuration. We expect that the stratified culture approach using phaseguides will provide the basis for a range of culture models implemented by ourselves and others and ultimately become available for the pharmaceutical industry and the clinic. The success of the platform greatly depends on whether the technology acceptance gap is efficiently bridged. Both Lab-on-a-Chip technology and 3D cell culture have been around since the early 1990's. Although there is a clear trend towards acceptance by the pharmaceutical industry, their uptake is still limited. Clearly improved performance over current technologies, unique capabilities and/or reduced costs will ultimately drive acceptance, provided these advantages outweigh the cost of implementing a new technology (Table 1). Prerequisites include a good ease of use, low initial investments and the availability of well documented, fully validated applications.

During the design of the platform presented in this paper, we have paid careful consideration to address these aspects. The platform offers improved performance with respect to standard cell culture due to the well-documented and proven superiority of 3D cell cultures. In addition, the system boasts capabilities that are hardly available in modern cell culture, including continuous perfusion, co-culture capabilities and gradient functionalities, all aspects are fully scalable in throughput due to the microtiter plate footprint. An inherent benefit of miniaturization is the reduced consumption of reagents, which significantly reduces costs or enables screening of more data points. For example, ECM matrix preparations and cell material can be extremely costly and/or scarce, especially when working with primary cells or stem cell derived cells.

The platform offers ease of use comparable to conventional microtiter plates, as it is fully pipette-operated and can be used with standard readout equipment. The microtiter plate format reduces initial investment to near-zero as it renders the system fully robot and HCS equipment compatible, thus alleviating the need for customized equipment. A point of attention remains full validation of the system. Efforts are on-going for implementation and full validation of a range of tissue models against both state-of-the-art assays, as well as retrospective and ultimately prospective clinical validation studies. The ultimate goal is to provide a better alternative to both animal testing as well as conventional cell culture techniques.

Table 1 Overview of incentives and prerequisites required to bridge the technology acceptance gap

Incentives	Projection on phaseguide-stratified approach
Improved performance:	Better predictive data points through 3D ECM embedment
Unique capabilities:	Full co-culture capabilities, perfusion flow, gradients
Cost reduction:	Reduced reagent consumption (gel, cells, compounds) Increased numbers of data points
Prerequisites	
Ease of use:	Pipette operation, passive perfusion, standard readout
Low initial investment:	No external equipment required, fully compatible with robot handling and HCS readouts.
Validation:	Full validation for a range of tissue models is ongoing

Conclusion

In this paper, we introduce a novel platform for organ and tissue-on-a-chip culture of deliberate complexity. The platform employs phaseguides to pattern lanes with gels and liquids in a stratified manner. We demonstrate the functionality of the platform for 3D cell culture under continuous perfusion, co-culture and invasion. The microtiter-plate format is shown to be compatible with fluorescent assays as well as confocal and automated microscopy. As such, phaseguide-stratified 3D tissue culture makes Organ-on-a-Chip technologies amenable to screening in an industrial setting.

Acknowledgements

We thank Prof. Dr Hans Tanke for the use of the imaging facilities at the Department of Molecular Cell Biology, Leiden University Medical Center. We thank Rafael Zwier and Martijn Witlox of the Fine Mechanical Department of the Faculty of Science of Leiden University as well as Dr Athanasios T. Giannitsis for their assistance in chip fabrication. We thank Dr Sandrine L. Ellero for valuable discussions on cell biology and assay development. This work is (co)financed by Technologiestichting STW and the Netherlands Metabolomics Centre (NMC) which is a part of The Netherlands Genomics Initiative/Netherlands Organization for Scientific Research.

References

1. A. Abbott, *Nature*, 2003, 424, 870–2.
2. V. M. Weaver, *J. Cell Biol.*, 1997, 137, 231–245.
3. P. A. Kenny, G. Y. Lee, C. A. Myers, R. M. Neve, J.R. Semeiks, P. T. Spellman, K. Lorenz, E. H. Lee, M. H. Barcellos-Hoff, O. W. Petersen, J. W. Gray and M. J. Bissell, *Mol. Oncol.*, 2007, 1, 84–96.
4. B. Weigelt and M. J. Bissell, *Semin. Cancer Biol.*, 2008, 18, 311–21.
5. D. Huh, G. A. Hamilton and D. E. Ingber, *Trends Cell Biol.*, 2011, 21, 745–54.
6. S. Chung, R. Sudo, P. J. Mack, C.-R. Wan, V. Vickerman and R. D. Kamm, *Lab Chip*, 2009, 9, 269–75.
7. K. Domansky, W. Inman, J. Serdy, A. Dash, M. H. M. Lim and L. G. Griffith, *Lab Chip*, 2010, 10, 51–8.
8. V. N. Goral, Y.-C. Hsieh, O. N. Petzold, J. S. Clark, P. K. Yuen and R. A. Faris, *Lab Chip*, 2010, 10, 3380–3386.
9. Y. Nakao, H. Kimura, Y. Sakai and T. Fujii, *Biomicrofluidics*, 2011, 5, 22212.
10. P. J. Lee, P. J. Hung and L. P. Lee, *Biotechnol. Bioeng.*, 2007, 97, 1340–6.
11. Y. Hsu, M. Moya, C. Hughes, S. George and A. Lee, in *MicroTAS 2011*, 2011, vol. 1, pp. 1382–1384.
12. K.-J. Jang and K.-Y. Suh, *Lab Chip*, 2010, 10, 36–42.
13. K.-J. Jang, H. S. Cho, D. H. Kang, W. G. Bae, T.-H. Kwon and K.-Y. Suh, *Integr. Biol.*, 2011, 3, 134–41.
14. H. J. Kim, D. Huh, G. Hamilton and D. E. Ingber, *Lab Chip*, 2012, 12, 2165–74.
15. J. H. Sung, J. Yu, D. Luo, M. L. Shuler and J. C. March, *Lab Chip*, 2011, 11, 389–92.
16. N. J. Douville, P. Zamankhan, Y.-C. Tung, R. Li, B. L. Vaughan, C.-F. Tai, J. White, P. J. Christensen, J. B. Grotberg and S. Takayama, *Lab Chip*, 2011, 11, 609–19.
17. D. Huh, B. D. Matthews, A. Mammoto, M. Montoya-Zavala, H. Y. Hsin and D. E. Ingber, *Science*, 2010, 328, 1662–8.
18. C. M. Puleo, W. McIntosh Ambrose, T. Takezawa, J. Elisseeff and T.-H. Wang, *Lab Chip*, 2009, 9, 3221–7.
19. A. Grosberg, P. W. Alford, M. L. McCain and K. K. Parker, *Lab Chip*, 2011, 11, 4165–73.
20. M. M. G. Grafton, L. Wang, P.-A. Vidi, J. Leary and S. Lelièvre, *Integr. Biol.*, 2011, 3, 451–459.
21. K. E. Sung, N. Yang, C. Pehlke, P. J. Keely, K. W. Eliceiri, Friedl and D. J. Beebe, *Integr. Biol.*, 2011, 3, 439–50.
22. J.-M. Peyrin, B. Deleglise, L. Saias, M. Vignes, P. Gougis, S. Magnifico, S. Betuing, M. Pietri, J. Caboche, P. Vanhoutte, J.-L. Viovy and B. Brugg, *Lab Chip*, 2011, 11, 3663–73.
23. D. Majumdar, Y. Gao, D. Li and D. J. Webb, *J. Neurosci. Methods*, 2011, 196, 38–44.
24. J. W. Song and L. L. Munn, *Proc. Natl. Acad. Sci. U. S. A.*, 2011, 108, 15342–7.
25. J. H. Sung and M. L. Shuler, *Lab Chip*, 2009, 9, 1385–94.
26. J. H. Sung, C. Kam and M. L. Shuler, *Lab Chip*, 2010, 10, 446–55.
27. Y. Imura, K. Sato and E. Yoshimura, *Anal. Chem.*, 2010, 82, 9983–8.

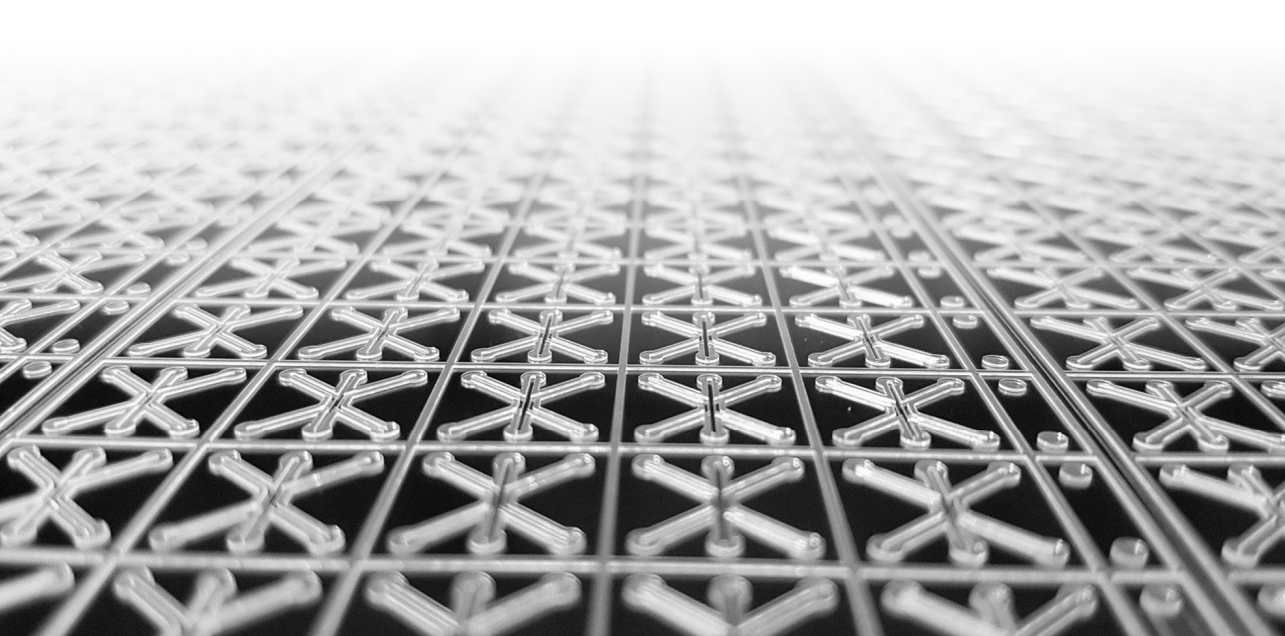
28. E. Westein, A. D. van der Meer, M. J. E. Kuijpers, J.-P. Frimat, A. van den Berg and J. W. M. Heemskerk, *Proc. Natl. Acad. Sci. U. S. A.*, 2013, 110, 1357–1362.
29. J. W. Song, S. P. Cavnar, A. C. Walker, K. E. Luker, M. Gupta, Y.-C. Tung, G. D. Luker and S. Takayama, *PLoS One*, 2009, 4, e5756.
30. D. Huh, D. C. Leslie, B. D. Matthews, J. P. Fraser, S. Jurek, G. A. Hamilton, K. S. Thorneloe, M. A. McAlexander and D. E. Ingber, *Sci. Transl. Med.*, 2012, 4, 159ra147–159ra147.
31. W.-M. Hsu, A. Carraro, K. M. Kulig, M. L. Miller, M. Kaazempur-Mofrad, E. Weinberg, F. Entabi, H. Albadawi, M. T. Watkins, J. T. Borenstein, J. P. Vacanti and C. Neville, *Ann. Surg.*, 2010, 252, 351–7.
32. A. Carraro, W.-M. Hsu, K. M. Kulig, W. S. Cheung, M. L. Miller, E. J. Weinberg, E. F. Swart, M. Kaazempur, Mofrad, J. T. Borenstein, J. P. Vacanti and C. Neville, *Biomed. Microdevices*, 2008, 10, 795–805.
33. A. Zijlstra, D. J. Webb and D. Li, *Biomed. Microdevices*, 2011, 13, 539–48.
34. H. Ma, T. Liu, J. Qin and B. Lin, *Electrophoresis*, 2010, 31, 1599–605.
35. S.-Y. C. Chen, P. J. Hung and P. J. Lee, *Biomed. Microdevices*, 2011, 13, 753–8.
36. S. Podszun, P. Vulto, H. Heinz, S. Hakenberg, C. Hermann, T. Hankemeier and G. A. Urban, *Lab Chip*, 2012, 12, 451–7.
37. D. Puchberger-Enengl, S. Podszun, H. Heinz, C. Hermann, P. Vulto and G. A. Urban, *Biomicrofluidics*, 2011, 5, 44111–4411110.
38. P. Vulto, G. Dame, U. Maier, S. Makohliso, S. Podszun, P. Zahn and G. A. Urban, *Lab Chip*, 2010, 10, 610–6.
39. P. Vulto, S. Podszun, P. Meyer, C. Hermann, A. Manz and G. A. Urban, *Lab Chip*, 2011, 11, 1596–1602.
40. P. Vulto, G. Medoro, L. Altomare, G. A. Urban, M. Tartagni,
41. R. Guerrieri and N. Manaresi, *J. Micromech. Microeng.*, 2006, 16, 1847–1853.
42. P. Vulto, N. Glade, L. Altomare, J. Bablet, L. Del Tin,
43. G. Medoro, I. Chartier, N. Manaresi, M. Tartagni and
44. R. Guerrieri, *Lab Chip*, 2005, 5, 158–62.
45. P. Vulto, T. Huesgen, B. Albrecht and G. A. Urban, *J. Micromech. Microeng.*, 2009, 19, 077001
46. T. Huesgen, G. Lenk, B. Albrecht, P. Vulto, T. Lemke and
47. P. Woias, *Sens. Actuators, A*, 2010, 162, 137–144.
48. K. Wrzesinski and S. J. Fey, *Toxicol. Res.*, 2013, 2, 123.
49. S. Ramaiahgari, M. Den Beaver, B. Herpers, J. N.
50. M. Commandeur, B. van de Water and L. Price, 2013, submitted.
51. S. J. Fey and K. Wrzesinski, *Toxicol. Sci.*, 2012, 127, 403–11.

Chapter 5

Membrane-free culture and real-time barrier integrity assessment of perfused intestinal epithelium tubes

SJ Trietsch, E Naumovska, D Kurek, MC Setyawati, MK Vormann, KJ Wilschut, HL Lanz, A Nicolas, CP Ng, J Joore, S Kustermann, A Roth, T Hankemeier, A Moisan, P Vulto*

Nature Communications



Abstract

In vitro models that better reflect *in vivo* epithelial barrier (patho-)physiology are urgently required to predict adverse drug effects. Here we introduce extracellular matrix-supported intestinal tubules in perfused microfluidic devices, exhibiting tissue polarization and transporter expression. Forty leak tight tubules are cultured in parallel on a single plate and their response to pharmacological stimuli is recorded over 125 hours using automated imaging techniques. A study comprising 357 gut tubes is performed of which 93% are leak tight before exposure. EC50-time curves could be extracted that provide insight in both concentration and exposure time response. Full compatibility with standard equipment and user-friendly operation, make this the first Organ-on-a-Chip platform that is readily applicable in routine laboratories.

Introduction

Dysfunction of epithelial barriers as a result of pathological states or drug-induced toxicity can lead to life-threatening conditions and halt drug development at all clinical stages. Epithelial barrier disruption is mainly manifested by an increased para-cellular permeability of the epithelium. *In vitro* testing of para-cellular permeability of epithelial barriers is most commonly achieved by cultivating cells on a rigid membrane that separates two medium-containing chambers under static conditions. Such conventional Transwell systems are poorly suited for high-resolution kinetic measurements and image-based readouts and therefore provide only limited information on the underlying mechanisms leading to barrier disruption. More importantly, it does not comply with the current paradigm in cell culture that is steadily shifting towards three-dimensional cultures, extracellular matrix (ECM) embedment and addition of perfusion flow.^{1–5}

The field of microfluidics has rapidly gained momentum in the realm of *in vitro* modelling.³ Inherent to its dimensions, microfluidic techniques are uniquely suitable to connect with epithelia of tubular shapes in order to provide shear stress and continuous medium refreshment through perfusion. Typical microfluidic solutions make use of artificial membranes to enable apical-basal access to the epithelia⁶, thus not accommodating an ECM that is a crucial parameter in cell signaling involved in differentiation and epithelial-to-mesenchymal transition. Also, microfluidic techniques, which are typically presented as single chips⁷, need to be parallelized in order to deliver readouts for multiple compounds, dilutions,

replicates and controls. User-friendly operation and compatibility with state-of-the-art readouts, such as high content imaging-based multiplexed cellular and molecular analyses are crucial prerequisites for perfused ECM embedded cell culture techniques to become a new standard.⁸

We developed a methodology to culture perfused, ECM-supported epithelia and interrogate their barrier function in a membrane-free manner. As an example, we developed a model of intestinal tract epithelium that exhibits cellular polarization, tight junction formation and expression of key receptors. Forty gut models were grown in a tubular shape in the OrganoPlate platform that were accessible from both the apical and basal sides. The tubes were assessed for barrier integrity and exposed to staurosporine and acetylsalicylic acid (aspirin) for 125 hours. From 330 tubes used in these experiments, 93% were leak tight before exposure. The experiment was repeated using real-time parallel time-lapse imaging in which tubes were stable up till 6 to 8 hours. EC50-time curves provide insight in concentration response at increasing exposure time in one single experimental run.

Results

Figure 1 shows the OrganoPlate platform, which encompasses 40 microfluidic cell culture structures embedded in a standard 384-well microtiter plate format (Fig. 1a-b).^{9,10} Each microfluidic channel structure is comprised of three lanes that are connected to corresponding wells of a microtiter plate that function as inlets and outlets to access the microfluidic culture. The lanes join in the centre of the structure where two capillary pressure barriers are present called phaseguides.¹¹ Figure 1c-j show a schematic representation of vertical and horizontal cross-sections of the centre of a microfluidic structure and the method of growing a tubular structure. First an ECM gel is introduced in the central lane (Fig. 1c-d). The phaseguides are used to selectively pattern the ECM gel in the central lane by meniscus pinning. The meniscus stretches beyond the phaseguide, leading to a curved shape. After ECM gelation, epithelial cells are seeded in one lateral lane, allowing them to sediment directly against the ECM gel by placing the titre plate in a vertical position, i.e. standing on one side (Fig. 1e-h). Upon attachment of the cells, the plate is horizontally placed on an interval rocker that induces flow by reciprocal leveling between reservoirs (SI1). Upon application of flow, cells proliferate and start lining all surfaces of the perfusion channel, forming a confluent tubular structure (Fig. 1i-j). The tubules have a lumen that is connected to the in- and outlet of the respective lane

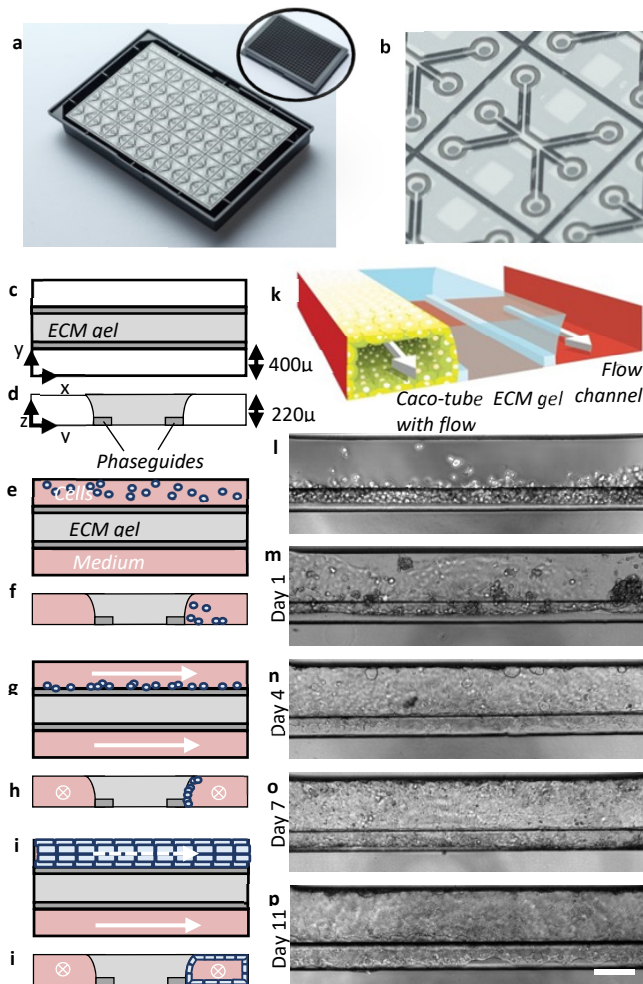


Figure 1 | Overview of the method for modeling intestinal tubules in the OrganoPlate platform.

(a) Photograph of the bottom of an OrganoPlate showing 40 microfluidic channel networks with inlay showing the top view of the 384 well plate format device; (b) Zoom-in on a single microfluidic channel network comprising three channels that join in the center. (c, e, g, i) Horizontal projection and (d, f, h, j) vertical cross section of center region for subsequent steps in establishing the gut model: (c, d) an extracellular matrix gel (light grey) is patterned by two phaseguides (dark grey); (e, f) Culture medium is introduced in the two lanes adjacent to the ECM gel, one of which comprises

cells. (g, h) Cells are allowed to settle against the ECM gel surface, by placing the plate on its side; (i, j) Upon application of flow, cells form a confluent layer lining the channel and gel surfaces, resulting in a tubular shape. (k) 3D artist impression of the center of a chip comprising a tubule, an extra cellular matrix gel and a perfusion lane; two phaseguides (white bars) are present that define the three distinct lanes in the central channel. The tubule has a lumen at its apical side that is perfused. (l-p) Phase contrast images of the formation of the tubular structure at day 0, 1, 4, 7 and 11 respectively. Scale bars are 100µm

making it accessible for perfusion with medium and for apical compound exposure. The basal side of the epithelium is facing the ECM gel and can be accessed by the second perfusion lane on the opposite side of the ECM gel lane. Fig. 1k depicts an artist impression of the 3D configuration of the tube, showing that the tube is grown directly against the extracellular matrix, without presence of artificial membranes (Fig. 1k).

For modeling of the intestinal barrier, the human intestinal colorectal adenocarcinoma cell line (Caco-2) was used. Figure 1l-p show phase contrast pictures of tube formation at day 0, 1, 4, 7, and 11 respectively. On day 0, cells are seeded against the ECM and start colonizing the glass walls to form a confluent tube (Fig. 1n-p). Perfusion was crucial for tube formation. Tubes were formed in 3 days and optimal barrier function was found at day 4 (SI1).

Differentiation and polarization marker expression

Figure 2a shows a 3D reconstruction of confocal fluorescence micrographs of the gut tube. The tube has a clear lumen and lines the perimeter of the gel and perfusion lane. Caco-2 cells in the confluent tubule display tight junctions and brush border formation as shown by immunofluorescence staining of ZO-1 and Ezrin respectively¹² (Fig. 2a-d, g). Figure 2e shows localization of acetylated tubulin (microtubules) and occludin (tight junctions)¹³. Dome-formation is observed, indicative of active fluid transport and intact epithelial barrier function^{14,15} (Fig. 2f). Fig. 2h-j show maximum intensity projection images of tubes stained for Glut-2, MRP2, ErbB1, and ErbB2. Cells in contact with the ECM showed a strongly increased expression of the transporters Glut-2, MRP2 and to a lesser extend ErbB1 and ErbB2 receptors.¹⁶

These staining results illustrate the crucially instructive role that the extracellular matrix plays in cellular differentiation and protein expression. Furthermore, characteristics of the ECM gel surface, such as its (bio-)chemical composition and mechanical characteristics, allow the formation of tissue structures observed *in vivo*.¹⁷ Polarization of the cell layer against the gel is best visualized at the contact line between the gel meniscus and the phaseguide, at the bending point of the cell layer where apical-basal polarization is in the horizontal plane. This is the most right-hand part of the tube in Fig. 2a or the bottom side of the tube in Fig. 2b. Fig. 2g and SI2 show single z-slices at this bending point, just above the phaseguide.

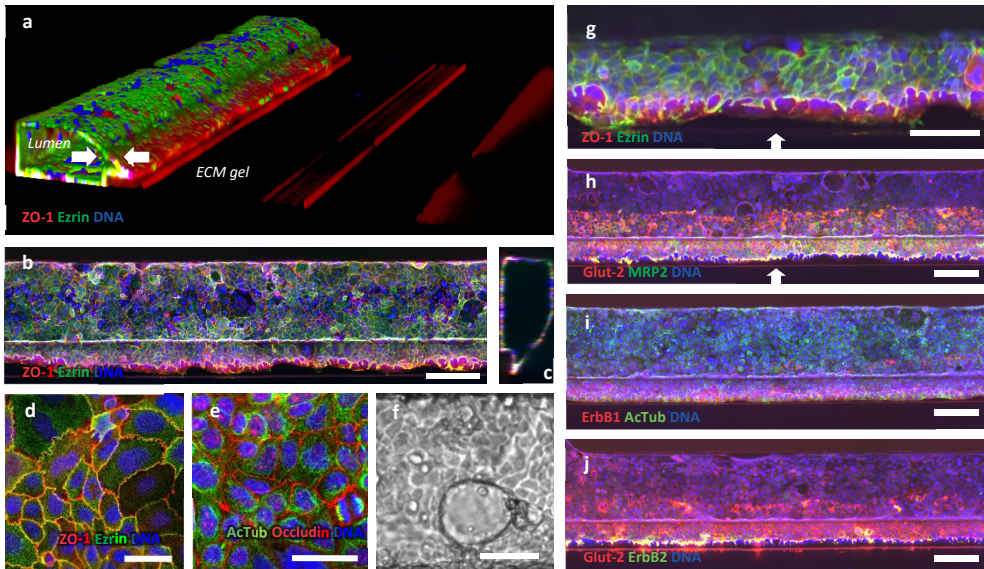


Figure 2 | Tubule characterization by immunofluorescent staining. (a) 3D reconstruction of a confocal z-stack showing tubular morphology with a lumen. White arrows indicate the apical (A) and basal (B) sides. The tube is stained for tight junctions (ZO-1 in red) and brush borders (Ezrin in green). (b) max projection and (c) vertical cross section of the tubular structure in (a); (d, e) Zoom of the epithelial layer at the bottom of the tube exhibiting (d). tight junctions (ZO-1 in red) and brush borders (Ezrin in green) and (e) acetylated tubulin (green) and occludin (red). (f) Phasecontrast image showing dome formation. (g) Zoom of a z-slice of the tube in (a) of the cell layer on top of the phaseguide showing apical positioning of Ezrin indicating polarization of the tube (white arrow indicates basal side B). (h) expression of glucose and MRP2 transporters respectively stained with Glut-2 in red and MRP2 stain in green. Both Glut-2 and MRP2 show significantly higher signal against the collagen gel compared to the regions that are not exposed to the collagen indicating increased expression levels. Both stains clearly stain the apical side of the tube. For z-slices above the phaseguide at a higher magnification see SI2b (i) ErbB1 (red) and acetylated tubulin (green) expression. ErbB1 expression levels appear higher against the collagen. (j) Co-staining of Glut-2 transporter and ErbB2 receptor; both stains show higher signal levels against the collagen gel. ErbB2 is primarily expressed pericellularly (see also SI2d for a zoom)). All tubes are fixated after four days in culture. Nuclei are stained blue with DraQ5 (a-c, g-j) and DAPI (d, e). Scale bars in white are 100µm with the exception of (d, e, f) and (g), where they are 50µm. Z-slices just above the phaseguide at higher magnification of the images (g-j) are available in SI2

Tubes are the same as the images of Fig. 2b, h-j, but depicted as single z-slices and at higher magnification. Polarization is confirmed by localization of brush borders (ezrin) and the MRP2 transporter on the apical side as shown in fig. 2g, and SI2a, b, while ErBb2 is positioned pericellularly (see SI2d). At least ten Caco-2 tubes were stained with each marker, figures show a representative selection of results.

Barrier integrity

Barrier function of the Caco-2 tubes was assessed by perfusion with a fluorescent probe in culture medium through the tube lumen, followed by the determination of fluorescence levels in the basal gel region, normalized to the fluorescence in the lumen. This is illustrated in Fig. 3a-i. Both a high molecular weight fluorescent probe (150kDa FITC-dextran) and a lower molecular weight probe (4.4kDa TRITC-dextran) were added to the medium that is perfused through the lumen of the tube. In absence of an intact tubular structure, the fluorescent probes leak into the gel and the basal side perfusion channel (Fig. 3a, d, g), while for a fully intact barrier the fluorescent probes are retained in the lumen of the tube (Fig. 3b, e, h). Upon (partial) loss of barrier function, e.g. through drug-induced toxicity, the fluorescent probe leaks out of the lumen towards the basal side, yielding a higher signal in the ECM (Fig. 3c, f, i). Barrier integrity was measured using a high content imaging (HCI) system allowing monitoring of 40 tubes in parallel. To quantify the integrity of the barrier, the fluorescence level was measured in the gel region and normalized to the fluorescence level in the luminal side to compensate for bleaching effects. Upon reaching a fluorescence value of 0.4, barrier integrity of a tube was considered lost. The barrier integrity of 24 tubes was tracked on day 4, 7 and 11 of culture. As depicted in SI1c, it was found that on day 4 all tubes were leak tight, while at day 7 and 11, three and seven tubes were leaky respectively. Therefore, barrier integrity measurements are performed at 4 days of culture.

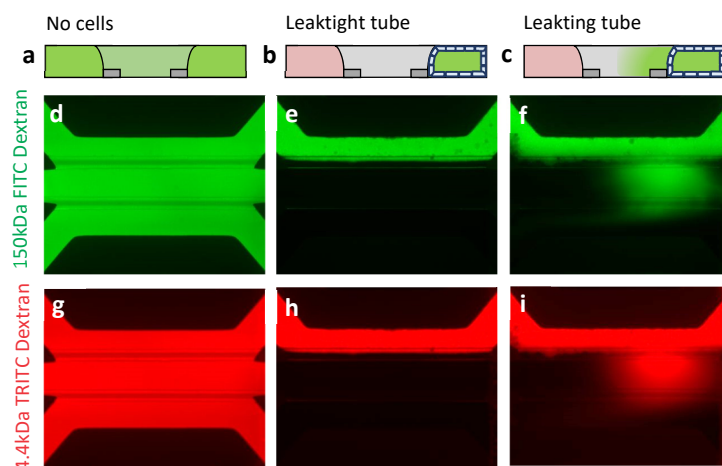


Figure 3 | Barrier integrity assay in OrganoPlate: a fluorescent dye is inserted in the channel comprising the tube. Integrity of the tube barrier is quantified by measuring the amount of dye that is leaking out of the tube into the adjacent gel channel. (a-c) Sketch in vertical cross section showing fluorescence distribution: (a) in absence of a tube, (b) for the case of a leak tight tube and (c) for a leaky tube. (d-i) Fluorescent images of microfluidic chips perfused with fluorescent molecules show experimental results for: gel only (d, g), leak-tight tube (e, h) and leaky tube (f-i) using both a 150kDa FITC-dextran and a 4.4kDa TRITC-Dextran during the same experiment.

Drug induced barrier disruption

Barrier integrity of 4-day-old Caco-2 tubes was assessed during a 125-hour apical exposure to various concentrations of staurosporine (0.4 to 90 μ M), an inducer of apoptosis¹⁸ and aspirin which affects tight junctions¹⁹ (0.16 to 40 mM). Fluorescence levels were measured at 1-hour intervals from 1 to 12 hours, and 24 to 36 hours, as well as at 16, 48, 53, 60, 72, 82, 96 and 125 hours. Between measurements the OrganoPlate was placed back on the rocker platform to maintain flow. Fig. 4a-d depict arrays of images showing the fluorescence in the gel at each time-point for both FITC- and TRITC-dextran. Measurements for each compound were taken on a single OrganoPlate with 5 replicates per concentration. The staurosporine and aspirin studies were executed five and three times respectively on different days (see SI3 and SI4).

Fluorescence images of one single OrganoPlate depicted in the arrays of Fig. 4a-d and their quantification as depicted in Fig 4e, h show that barrier integrity was gradually diminished over time for all concentrations of staurosporine and for the

two highest concentrations of aspirin. Results can also be visualised by generating Kaplan-Meier plots for loss of barrier integrity, in which events are defined as the fluorescence ratio reaching 40% (Fig. 4f, i). This approach is particularly useful for less potent toxicants where EC50 determination suffers from a lack of data of high effect. Aspirin, which has a different mode of action involving tight junction disruption and proliferation inhibition, instead of apoptosis induction^{20,21}, causes much less barrier disruption at relevant concentration. The Kaplan-Meier curve, however, does show a highly significant trend of loss-of-barrier function at higher concentration ($P < 0.0001$ for both curve difference and trend significance) (Fig 4i). An EC50 value was estimated for each time point by fitting the concentration response curve based on non-linear regression of the logarithm of the compound concentration versus the normalized fluorescence assuming a top and bottom plateau at 0 and 100% fluorescence. With increasing exposure times, a shift of EC50 towards lower compound concentrations was observed (Fig. 4g, j). The 95% confidence interval of the extracted EC50 values indicates robust data over the entire exposure time. EC50 values extracted at time points before the first event in the Kaplan Meier plots should be interpreted with caution as baseline fluorescence is likely to dominate the curve fitting rather than a biologically relevant signal.

SI4 shows an overlay of the EC50 curves for 5 independent experimental series of staurosporin (SI4a, b) and aspirin (SI4 c, d), based on both 150kDa FITC-dextran (SI4a, c) and 4.4kDa TRITC-dextran (SI4b, d) analysis. The high degree of similarity between the EC50 time curves for the full replicate series are a powerful illustration of the robustness of the method.

In parallel to fluorescence images, phase contrast pictures were taken at selected time points. An example of tube morphology as a response to 96 hours of staurosporine exposure is included in the supplementary information (SI5). Tubes are fully deteriorated for the highest concentration staurosporine and damages can be observed for exposure to 30 μ M staurosporine. For lower concentrations tubes appear intact, while fluorescence images show that barrier integrity is lost. This indicates that loss of barrier function at higher concentrations of staurosporin is primarily due to cell death. Dead cells are flushed away by the perfusion flow.

For comparison, a similar experiment in a conventional Transwell was performed, which revealed a lower sensitivity for barrier disruption compared to the OrganoPlate showing no significant difference between controls and staurosporine exposed wells after 4 hours (SI6), while a clear effect is already apparent in the OrganoPlate results. In addition to improved morphological maturity of the 3D perfused culture, the increased sensitivity of the model can be attributed to a decreased dead volume and higher surface to volume ratio of the microfluidic system as compared to Transwell systems. In a Transwell the FITC-dextran was strongly diluted in the large target volume when crossing the barrier. By contrast, in OrganoPlates the fluorescence is measured directly in the ECM after crossing the epithelial membrane. Since no dilution step is involved here, a much higher signal-to-noise ratio is obtained. Sensitivity of the microfluidic assay is such, that it can be used as a binary assay, in which the exposure time at which leakage is observed is indicative of the toxicity of the compound.

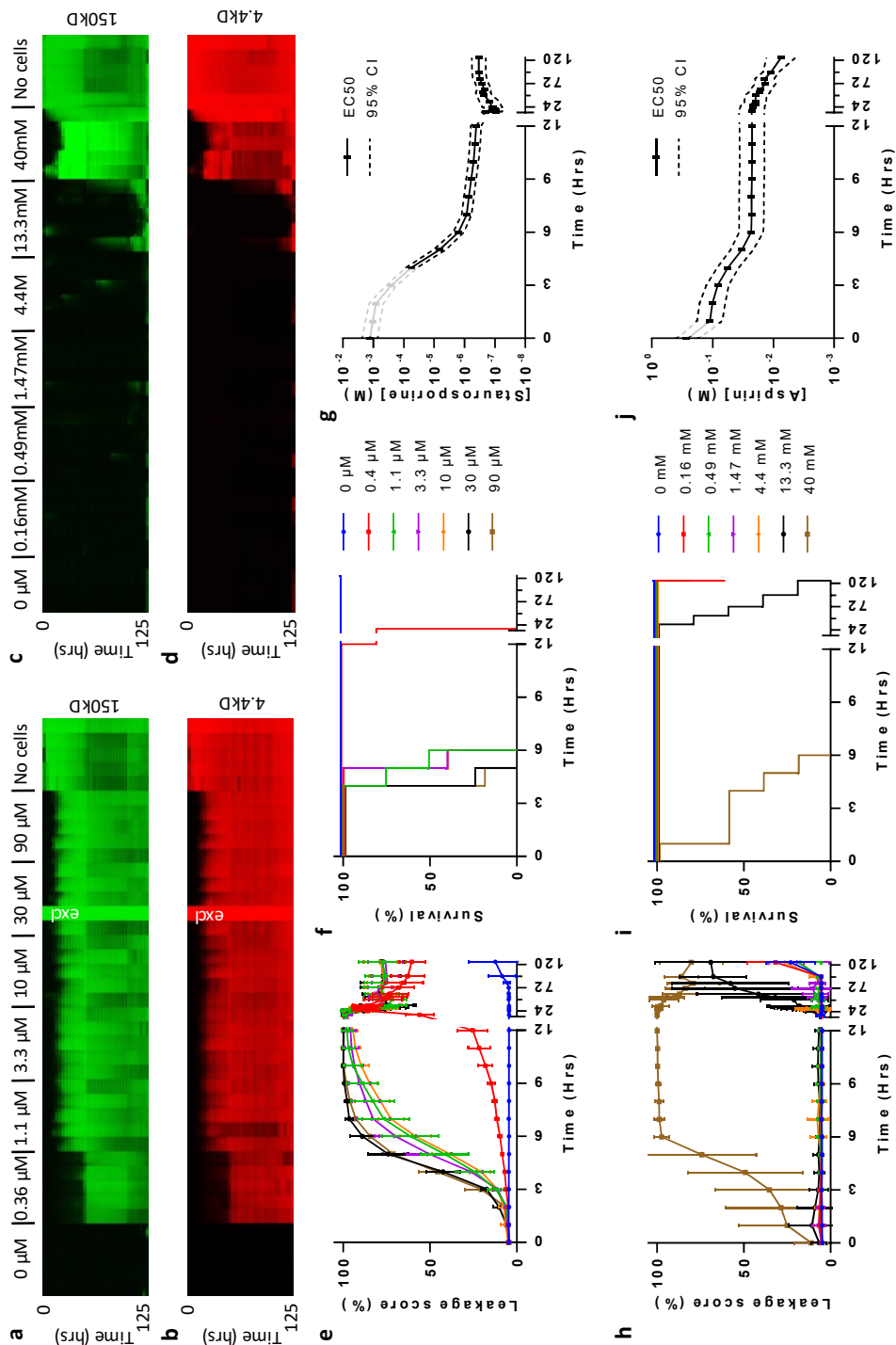


Figure 4 | Drug induced loss of barrier integrity is observed over time in a concentration-dependent manner for staurosporine (a, b, e-g) and aspirin (c, d, h-j). (a-d) Array of fluorescence micrographs of the gel region showing distribution of the 150kDa FITC-Dextran (a, c) and 4.4kDa TRITC-Dextran (b, d) over time and for various compound concentrations; the loss of barrier integrity results in an increased fluorescent signal. Measurements are taken at 1-hour intervals up to 12 hours, at 16 hours, from 24 to 36 hours at 1 hour interval, and at 48, 53, 60, 72, 82, 96 and 125 hours. In between each interval, the OrganoPlate was placed back into the incubator on the interval rocker platform to maintain the perfusion flow. Five replicates of each concentration of a compound were measured on a single plate. One well was excluded from further data analysis, because of a pipetting error (marked with “excl” in white). (e, h) The progression of the loss of barrier function over time is plotted as the ratio between fluorescent signal in apical and basal regions for the various concentrations of staurosporine (e) and aspirin (h), where the plotted line is the mean of 5 replicate exposures and error bars depict the standard deviation. (f, i) Kaplan-Meier curves were generated where survival was defined as showing a leakage score below 40%. Overlapping curves were shifted by 1% for clarity purposes. (g, j) EC50 values are plotted as a function of exposure time. EC50 values were obtained by fitting a concentration response curve at each time point based on non-linear regression of leakage scores using normalized response and standard slope and were plotted including 95% confidence interval (CI). EC50 values obtained from time points before the first event in the Kaplan-Meier plot, as indicated by grayed out line, should be interpreted with caution as the curve fit could be dominated by noise rather than biological effect. All shown graphs were derived from data acquired using 150kDa FITC dextran. Full replicate series were run for both staurosporine and aspirin on different days that are displayed in **S13 and S14**

Real-time measurement

Fig. 5 shows another concentration response experiment with staurosporine, but this time the OrganoPlate was continuously kept inside the microscope throughout the experiment. A conditioned high content imager was used to maintain appropriate CO₂, temperature and humidity. Flow was absent in this experiment, as the high content imager did not provide for rocking. As can be observed in fluorescent images and quantification thereof, vehicle control tubes started leaking after 6 to 8 hours of imaging. This can most likely be attributed to suboptimal conditions, including a lack of perfusion flow. Nevertheless, a clear concentration-response effect could be observed. An EC50-time curve was extracted and overlaid in red with the curve from the experiments with rocking in black (as shown previously in Fig. 4g) showing similar curves for up to 8 hours (Fig. 5c). The advantage of incubation in the microscope is that a higher time resolution can be obtained.

In the experimental series of Fig. 4, 5, SI3 and SI4 ten OrganoPlates were used, comprising a total of 357 gut tubes and 33 ECM-only negative controls in total. Two tubes were excluded because of pipetting errors and 26 because of insufficient barrier function after one hour, yielding 93% of leak tight tubes at the onset of drug exposure.

Discussion

In summary, we present a unique methodology for assessing the barrier integrity of 40 leak-tight, polarized epithelial gut tubes in parallel using high content imaging. It is for the first time that a comprehensive method is presented to interrogate perfused epithelia tubules that are exposed to an ECM. The system allows sensitive, real-time interrogation of compound effects on barrier integrity, yielding insight in both exposure concentration and exposure time effects. The method has been robustly demonstrated for over 350 gut tubes and over 20,000 datapoints, making this to our knowledge the largest published Organ-on-a-Chip dataset so far. The method can be applied to other epithelia as well as translated to disease models. The co-culture capabilities of the platform⁹ can be explored to create complex tissue configurations, for example by incorporating mesenchymal and immune cells in the ECM adjacent to the epithelial tubes. The system outperforms classical techniques such as Transwell systems in terms of sensitivity, ease of use and

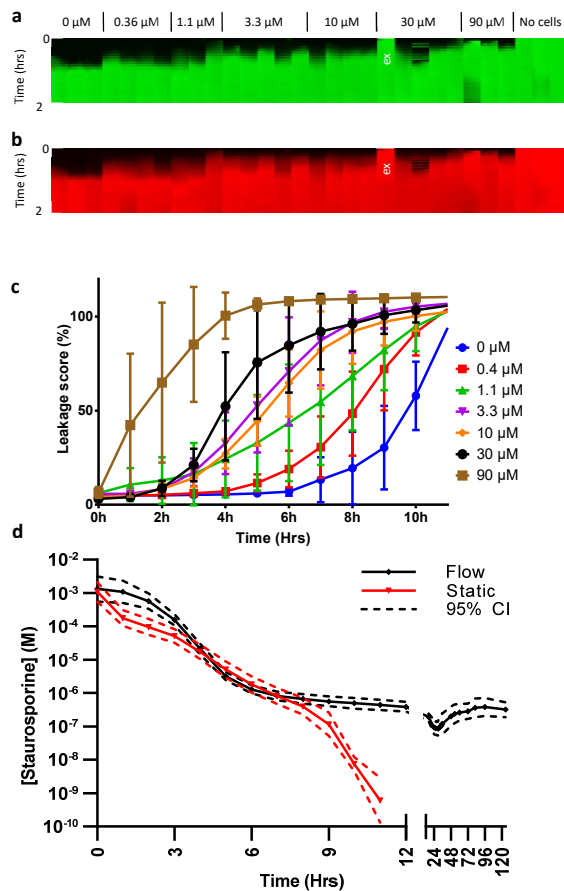


Figure 5 | Drug induced loss of barrier integrity as a function of staurosporine concentration measured in real-time. (a, b) Array of fluorescence micrographs of the gel region showing distribution of the 150kDa FITC-Dextran **(a)** and 4.4kDa TRITC-Dextran **(b)** over time and as a function of compound concentration; The OrganoPlate was continuously kept in an incubated automated microscope. Pictures were taken at 1 hour intervals. One data point was excluded for the fact that the tube appeared leaky at the first time point (marked with “excl” in white) **(c)** The progression of the loss of barrier function over time shows that untreated controls lose barrier integrity at 6-8 hours due to lack of flow. The plotted line is the mean of 3 to 5 replicate exposures and error bars depict the standard deviation. **(d)** EC₅₀ values over time for real time measurement without flow and for measurement in intervals with flow induced between measurement (overlay with the graph of **Figure 4g**). EC₅₀ values with and without flow are similar for the initial 8 hours of measurement.

(multiplexed) readout flexibility, as well as reagent, cell and time consumption. More importantly, it allows for the first-time non-expert end-users to adopt organ-on-a-chip technology in their laboratories, without need for specific microfluidic skills or dedicated equipment.

Materials and Methods

Cell culture

The human colon adenocarcinoma cell line Caco-2 (86010202, Sigma-Aldrich) was cultured on T75 flasks in EMEM (#30-2003, ATCC), 10% FBS (#F4135, Sigma), 1% NEAA (#11140-050, Life technologies) and 1% penicillin/streptomycin (Sigma #P4333). Caco-2 cells between passage 45 and 60 were used for all experiments.

OrganoPlate culture

OrganoPlate culture was performed using 3-lane OrganoPlates with 400 μm x 220 μm (w x h) channels (Mimetas BV, the Netherlands). Phaseguides had dimensions of 100 μm x 55 μm (w x h). Gel and perfusion channels have a length of 9 mm and 13 mm respectively. 2 μL of gel composed of 4 mg/mL Collagen I (AMSBio Cultrex 3D Collagen I Rat Tail, 5 mg/mL, Cat. 3447-020-01), 100 mM HEPES (Life Technologies, 15630-122) and 3.7 mg/mL NaHCO_3 (Sigma, Cat. S5761) was dispensed in the gel inlet and incubated 30-45 min at 37°C. Caco-2 cells were trypsinized using 0.5% trypsin in PBS/EDTA (Sigma, T3924), aliquoted and pelleted (5 min, 100 x g). The cells were applied to the system by seeding 2 μL of 1×10^7 of cells/mL in the outlet of the top medium channel. Subsequently, the OrganoPlate was put on the side for 20 minutes to allow the cells to sediment against the ECM. This was followed by addition of 50 μL medium to the outlet of the top medium channel and the OrganoPlate was again incubated on the side for 3-4 hours at 37°C to complete cell attachment. After incubation, medium was added up to a total of 50 μL on both inlets and both outlets. The OrganoPlate was placed horizontally in the incubator (37°C 5% CO_2) on an interval rocker switching between a +7° and -7° inclination every 8 minutes (Mimetas Rocker Mini) allowing bi-directional flow. Medium (50 μL each on inlet and outlet) was refreshed every 2 to 3 days.

Transwell culture

Caco-2 cells (60×10^3 cells/ cm^2) were seeded on Transwell inserts (24-well, Transwell, Costar #3470-Clear, 0.4 μM pore size) and cultured for 21 days in EMEM supplemented with 10% fetal calf serum (FCS), and penicillin/streptomycin (Sigma #P4333). Medium was refreshed every 2 to 3 days, both 100 μL on apical (insert) and 500 μL on basal side of the Transwell.

Immunohistochemistry

Caco-2 tubules were fixed with 3.7% formaldehyde (Sigma # 252549) in PBS (phosphate-buffered saline, Life tech # 20012068) for 15 min washed twice for 5 min with PBS and permeabilized with 0.3% Triton X-100 (Sigma # T8787) in PBS for 10 min. After washing with 4% FCS in PBS, cells were incubated with blocking solution (2% FCS, 2% bovine serum albumin (BSA) (Sigma # A2153), 0,1% Tween 20 (Sigma # P9416) in PBS) for 45 min. Subsequently, cells were incubated with primary antibodies for 60 min or at 4°C overnight, washed 3 times, incubated with secondary antibodies for 30 min and washed 3 times with 4% FCS in PBS. The following antibodies were used for immunohistochemistry: Rabbit a-ZO-1 (Invitrogen #617300, 1:125), Mouse a-acetylated tubulin (Sigma #T6793, 1:2000), Rabbit a-ErbB1 (Novusbio #NBP-1-51439, 1:200), Mouse a-MRP-2 (Santa cruz #SC-59608, 100 $\mu\text{g}/\text{ml}$, 1:10), Rabbit a-Glut-2 (Santa cruz #SC-9117, 200 $\mu\text{g}/\text{ml}$, 1:20), Mouse a-Ezrin (BD Transduction #610602, 1:50), Mouse a-ErbB2 (Thermo scientific #MS-229-P0, 200 $\mu\text{g}/\text{ml}$, 1:20), Rabbit a-Occludin (ThermoFisher #71-1500, 0.25 mg/ml , 1:100), Rabbit isotype (Life tech #86199), Mouse isotype (Life tech #86599), Goat isotype (Life tech #02-6202), Goat a-Rabbit AlexaFluor 488 (ThermoFisher, #A11008, 1:250), Goat a-Rabbit AlexaFluor 555 (LifeTechnologies, A21428, 1:250), Goat a-Mouse AlexaFluor 488 (LifeTechnologies, A11001, 1:250), Goat a-Mouse AlexaFluor 555 (LifeTechnologies, A21422, 1:250), Goat a-Mouse AlexaFluor 647 (LifeTechnologies, A-21236, 1:250), Donkey a-Rabbit AlexaFluor 647 (LifeTechnologies, A-31573, 1:250). After nuclear stain (DraQ5, Abcam # ab108410 or DAPI, H-1200, Vector Laboratories) cells were stored in PBS or Vectashield (H-1200, Vector Laboratories). All steps were performed at room temperature (RT). Cells were imaged with ImageXpress Micro XLS and Micro XLS-C High Content Imaging Systems (Molecular Devices, US) and SP5 laser point scanning confocal microscope (Leica).

Compound exposure

Caco-2 cells in OrganoPlates and Transwells were exposed to staurosporine or aspirin and barrier integrity was measured. Cells were exposed for 125 hours for interval measurements and for 24 hours for real-time measurements. Concentrations of aspirin were 0, 0.1, 0.33, 1.11, 3.67, 12.12, 40 mM (Sigma # A5376), and concentrations of staurosporine were 0, 0.4, 1.1, 3.3, 10, 30, 90 μ M (Sigma # S4400). Aspirin was dissolved in medium. Staurosporine was dissolved in medium with 0.9% DMSO (Sigma, #D8418) for 90 μ M and 0.3% for the other concentrations. Staurosporine preparations for the shorter term exposure also contain 3% tox medium (500 mL of MEM α (Sigma #M4526) with 6.25 mL of L-glutamine (Sigma #G7513), 6 mL Tox Supplement (Sigma #MTOXRTSUP).

Barrier integrity assay in OrganoPlate

Medium in the apical perfusion channel was replaced by medium containing 0.5 mg/mL FITC-dextran (150 kDa, Sigma # 46946) and TRITC-dextran (4.4 kDa, Sigma # T1037) and increasing concentrations of staurosporine or aspirin. Leakage of the fluorescent probe from the lumen of the tubular structure into the ECM compartment was automatically imaged using an ImageXpress XLS Micro High content imaging system at 37°C and 5% CO₂. For long term exposure, imaging was performed at 1-hour intervals up to 12 hours, and from 24 to 36 hours, and at 16, 35, 36, 48, 53, 60, 72, 82, 96 and 125 hours. Between each interval, the OrganoPlate was placed back into the incubator on the interval rocker platform in order to maintain perfusion flow. For real time measurement, automatic imaging was performed every hour for 24 hours without removing the OrganoPlate from the HCI system. The ratio between the fluorescent signal in the basal and apical region of the tube was analyzed using Fiji²².

Barrier integrity assay in Transwell

14-21h prior to start of the experiment, media was changed to Phenol-red free media (DMEM F12 (Gibco, 11039-021), 10% FBS HI (Sigma, F4135), 1% NEAA (Life tech, 11140050), 1% pen/strep (Sigma, P4333)). At the start of the compound exposure medium was replaced. 550 μ L was added to the basolateral side, 250 μ L of FITC-dextran solution (0.125mg/mL medium) mixed with the compound of choice was added to the apical side. At timepoints a 75 μ L aliquot was collected from the basolateral side. 75 μ L of fresh medium was added to the basolateral side

after the 2hr aspirin timepoint. The fluorescence intensity was measured with a multi-well plate fluorimeter (Fluoroskan Ascent FL, Thermo Fisher) with excitation at 485 nm and emission at 535 nm.

Statistics and data analysis

Barrier integrity assay images were analyzed using Fiji²². Fluorescence intensities were measured in the apical and basal regions of the tubes and the ratio between these was reported. Tubes that reached a 40% fluorescent intensity ratio at first hour of measurement were considered non-leak-tight and discarded. GraphPad Prism 6 (GraphPad Software Inc., La Jolla, CA) was used to generate Kaplan-Meier curves using the Survival Analysis – Survival Curve function defining an event as showing a basal to apical fluorescence intensity ratio over 40%. To prevent overlapping data, curves were nudged by 1 data point each for clarity. Curve difference was estimated using Log-rank (Mantel-Cox) test. Trend significance was evaluated using Log rank test.

Concentration response curves were fit using nonlinear regression of the logarithm of the compound concentration versus the normalized fluorescence assuming a top and bottom plateau at 0 and 100% and standard slope (hill slope=1). The estimated EC50 values and 95% confidence interval were plotted versus time.

Acknowledgements

We thank Prof. Dr. Hans Tanke for the use of the imaging facilities at the Department of Molecular Cell Biology, Leiden University Medical Center, and Joop Wiegant and Annelies van der Laan for their assistance. We thank Kitty Joore for generating artist impressions. E.N. and A.N. were supported by the EU Horizon 2020 program under project 674983 (Mimic) and 641639 (Biopol) respectively.

Competing financial interest

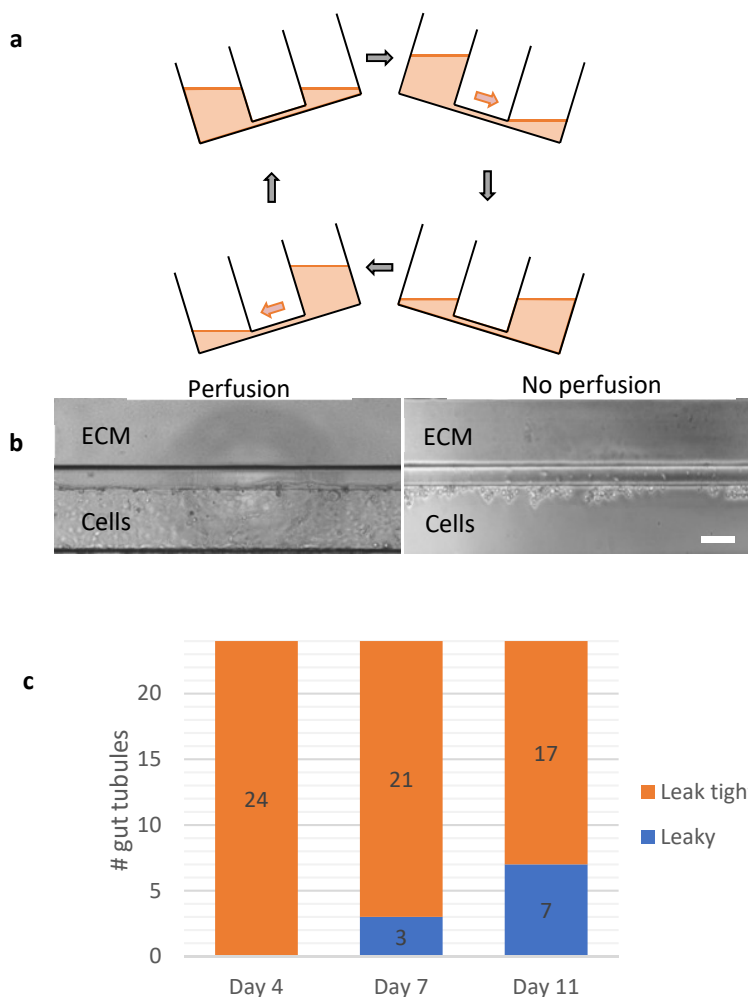
S.J.T., E.N., M.C.S., M.K.V., K.J.W., H.L.L., A.N., C.P.N., D.K., J.J., and P.V. are employees of MIMETAS BV, the Netherlands, that is marketing the OrganoPlate. P.V., J.J., T.H. and S.J.T. are shareholders of that same company. OrganoPlate® is a trademark of MIMETAS. A.B.R., S.K. and A.M. are employees of F. Hofmann-LaRoche Ltd and A.M. is a shareholder of F. Hofmann-LaRoche Ltd.

References

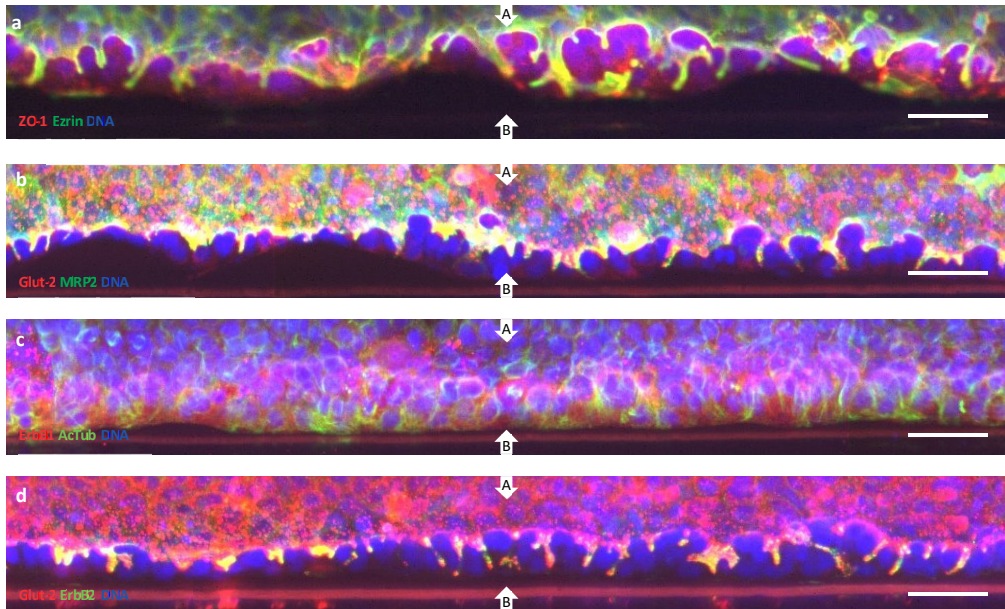
1. Pampaloni, F., Reynaud, E. G. & Stelzer, E. H. K. The third dimension bridges the gap between cell culture and live tissue. *Nat. Rev. Mol. Cell Biol.* 8, 839–45 (2007).
2. Weaver, V. M. et al. Reversion of the malignant phenotype of human breast cells in three-dimensional culture and in vivo by integrin blocking antibodies. *J. Cell Biol.* 137, 231–45 (1997).
3. van Duinen, V., Trietsch, S. J., Joore, J., Vulto, P. & Hankemeier, T. Microfluidic 3D cell culture: from tools to tissue models. *Curr Opin Biotechnol* 35, 118–126 (2015).
4. Tibbitt, M. W. & Anseth, K. S. Hydrogels as extracellular matrix mimics for 3D cell culture. *Biotechnol. Bioeng.* 103, 655–663 (2009).
5. Huh, D., Hamilton, G. A. & Ingber, D. E. From 3D cell culture to organs-on-chips. *Trends Cell Biol.* 21, 745–754 (2011).
6. Kim, H. J., Li, H., Collins, J. J. & Ingber, D. E. Contributions of microbiome and mechanical deformation to intestinal bacterial overgrowth and inflammation in a human gut-on-a-chip. *Proc. Natl. Acad. Sci.* 201522193 (2015). doi:10.1073/pnas.1522193112
7. Shah, P. et al. A microfluidics-based in vitro model of the gastrointestinal human–microbe interface. *Nat. Commun.* 7, 11535 (2016).
8. Junaid, A., Mashaghi, A., Hankemeier, T. & Vulto, P. An End-User Perspective on Organ-on-a-Chip: Assays and Usability Aspects. *Curr. Opin. Biomed. Eng.* (2017). doi:10.1016/j.cobme.2017.02.002
9. Trietsch, S. J., Israëls, G. D., Joore, J., Hankemeier, T. & Vulto, P. Microfluidic titer plate for stratified 3D cell culture. *Lab Chip* 13, 3548–3554 (2013).
10. Wevers, N. R. et al. High-throughput compound evaluation on 3D networks of neurons and glia in a microfluidic platform. *Sci. Rep.* 6, 38856 (2016).
11. Vulto, P. et al. Phaseguides: a paradigm shift in microfluidic priming and emptying. *Lab Chip* 11, 1596–602 (2011).
12. Giepmans, B. N. G. & van IJendoorn, S. C. D. Epithelial cell–cell junctions and plasma membrane domains. *Biochim. Biophys. Acta - Biomembr.* 1788, 820–831 (2009).
13. Liang, T. W. et al. Characterization of huJAM: evidence for involvement in cell-cell contact and tight junction regulation. *Am. J. Physiol. - Cell Physiol.* 279, (2000).
14. Lever, J. E. Inducers of mammalian cell differentiation stimulate dome formation in a differentiated kidney epithelial cell line (MDCK). *Proc. Natl. Acad. Sci. U. S. A.* 76, 1323–1327 (1979).
15. Chantret, I., Barbat, A., Dussaulx, E., Brattain, M. G. & Zweibaum, A. Epithelial Polarity , Villin Expression , and Enterocytic Differentiation of Cultured Human Colon Carcinoma Cells : A Survey of Twenty Cell Lines Epithelial Polarity , Villin Expression , and Enterocytic Differentiation of Cultured Human Colon Carcinoma C. *CANCER Res.* 48, 1936–1942 (1988).
16. Pfister, A. B., Wood, R. C., Salas, P. J. I., Zea, D. L. & Ramsauer, V. P. Early response to ErbB2 over-expression in polarized Caco-2 cells involves partial segregation from ErbB3

- by relocation to the apical surface and initiation of survival signaling. *J. Cell. Biochem.* 111, 643–52 (2010).
17. Johnson, L. R. *Physiology of the gastrointestinal tract*. (Academic Press, 2012).
 18. Belmokhtar, C. A., Hillion, J. & Ségal-Bendirdjian, E. Staurosporine induces apoptosis through both caspase-dependent and caspase-independent mechanisms. *Oncogene* 20, 3354–3362 (2001).
 19. Oshima, T., Miwa, H. & Joh, T. Aspirin induces gastric epithelial barrier dysfunction by activating p38 MAPK via claudin-7. *Am J Physiol Cell Physiol* 295, C800–806 (2008).
 20. Ricchi, P. et al. Effect of aspirin on cell proliferation and differentiation of colon adenocarcinoma Caco-2 cells. *Int. J. Cancer* 73, 880–4 (1997).
 21. Matsui, H. et al. The pathophysiology of non-steroidal anti-inflammatory drug (NSAID)-induced mucosal injuries in stomach and small intestine. *J. Clin. Biochem. Nutr.* 48, 107–11 (2011).
 22. Schindelin, J. et al. Fiji: an open-source platform for biological-image analysis. *Nat. Methods* 9, 676–82 (2012).

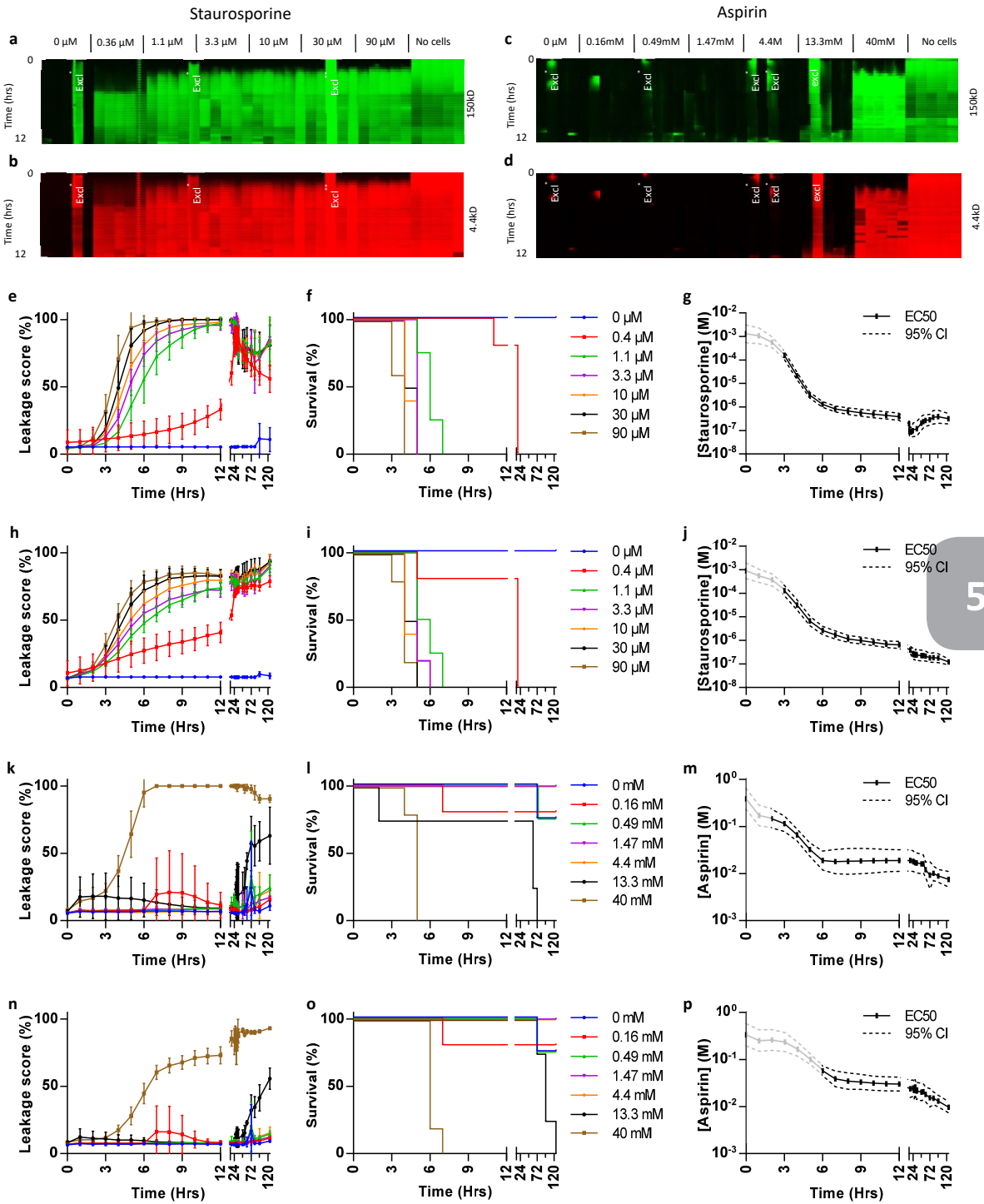
Supplementary information



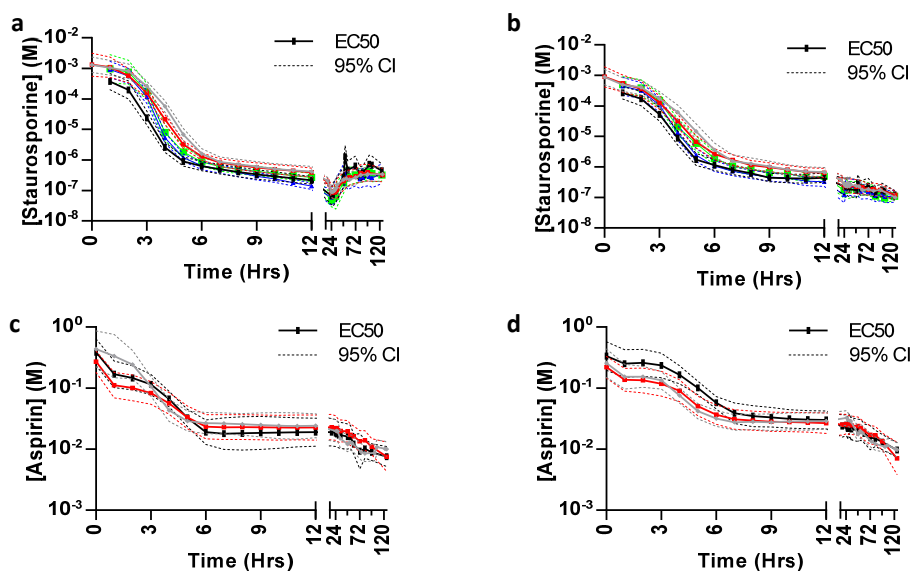
SI1 | Flow induction in OrganoPlate. **(a)** Flow is induced by leveling between two reservoirs that are connected by the perfusion channel. By placing the plate under an angle on an interval rocker that inverts the angle at regular intervals, a continuous bi-directional flow through the perfusion channel is induced. **(b)** Influence of flow on tube formation: A confluent tube of Caco-2 cells is formed within three days when perfused (left), while few cells survive culture without perfusion (right). Scale bars are 100 μ m. **(c)** Number of leak tight and leaky tubes in a single experimental run. Fluorescence intensity in the gel is measured and normalized to the fluorescence level in the tube channel. Upon crossing a threshold value of 0.4, a tube is considered leaky. At day 4 all tubes are leak tight, while at day 11 approximately 29% of tubes are leaking.



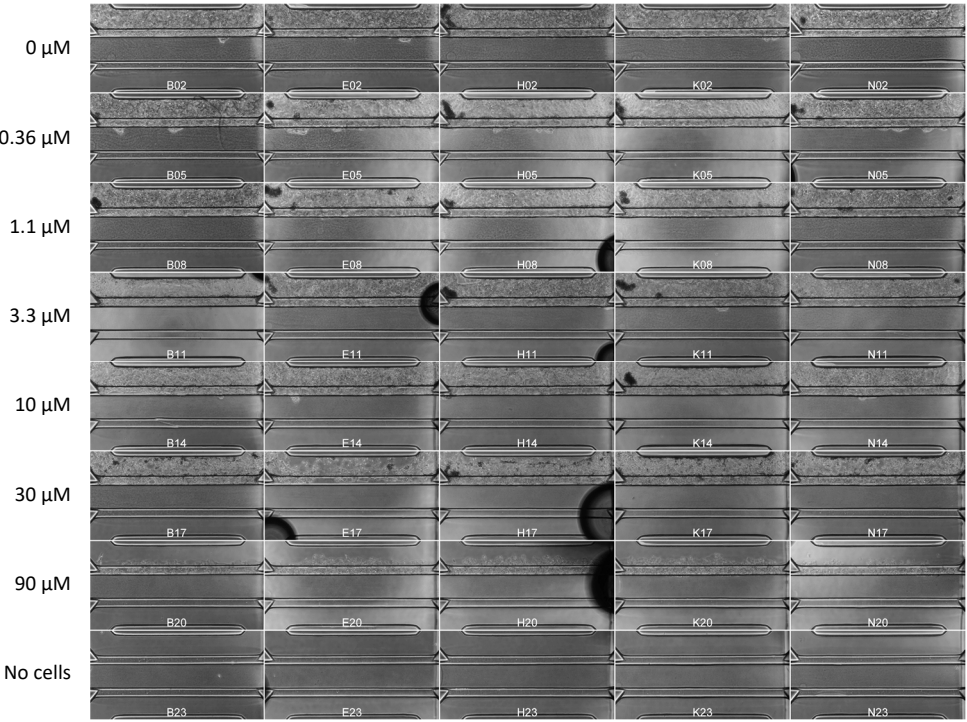
SI2 | Tubule characterization by immunofluorescent staining. Z-slices at higher magnification of confocal fluorescence micrographs of tubes from **fig. (2)** focusing on barrier morphology against ECM at approx. 50 μm above the bottom of the tube. An optical slice of the cells attached to the ECM is shown with white arrows indicating the apical (A) and basal (B) sides. The tube is stained for tight junctions (ZO-1 in red) and brush borders (Ezrin in green) showing apical positioning of Ezrin indicating polarization of the tube and invaginations expressing transport proteins. **(b)** expression of glucose and MRP2 transporters respectively stained with Glut-2 in red and MRP2 stain in green. Both stains clearly stain the apical side of the tube. **(c)** ErbB1 (red) and acetylated tubulin (green) expression. **(d)** Co-staining of Glut-2 transporter (red) and ErbB2 receptor (green); ErbB2 is primarily expressed pericellularly (here appearing as yellow). All tubes are fixated after four days in culture. Scale bars in white are 50 μm.



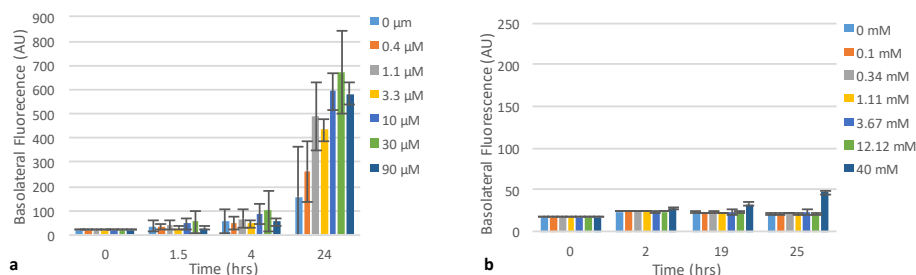
SI3 | Full replicate of the experimental series in Figure 4 in which loss of barrier integrity is observed over time in a concentration-dependent manner for staurosporine (a, b, e-j) and aspirin (c, d, k-p). (a-d) Array of fluorescence micrographs of the gel region showing distribution of the 150kDa FITC-Dextran (a, c) and 4.4kDa TRITC-Dextran (b, d) over time and as a function of compound concentration; the loss of barrier integrity is shown by an increased fluorescent signal. Measurements are taken at 1-hour intervals up to 12 hours, at 16 hours, from 24 to 36 hours at 1 hour interval, and at 48, 53, 60, 72, 82, 96 and 125 hours. In between each interval, the OrganoPlate was placed back into the incubator on the interval rocker platform. Five replicates of each concentration of a compound were measured on one single plate. Seven experimental runs were excluded from further data analysis, because the tubes appeared leaky at the first measurement (indicated with "Excl") and one run was excluded because of a pipetting error (indicated with "Excl**"). (e, h, k, n) The progression of the loss of barrier function over time is plotted as the ratio between fluorescent signal in apical and basal regions for the various concentrations of staurosporine (e, h) and aspirin (h, n); (e, k) show barrier integrity measurement using 150 kDa FITC dextran as a leakage marker, while (h, n) show barrier integrity measurement using 4.4 kDa TRITC-dextran as a leakage marker. The plotted line is the mean of 5 replicate exposures minus excluded datapoints and error bars depict the standard deviation (f, i, l, o) Kaplan-Meier curves were generated where survival was defined as showing a leakage score below 40%. Overlapping curves were shifted by 1% for clarity purposes. (g, j, m, p) EC50 values as a function of exposure time. EC50 values were obtained by fitting a concentration response curve at each time point based on non-linear regression of normalized leakage scores using standard slope. EC50 values obtained from time points before the first event in the Kaplan-Meier plot, as indicated by grayed out line, should be interpreted with caution as the curve fit could be dominated by noise rather than biological effect.



SI4 | Overlay of EC50 time curves of staurosporine and aspirin. The robustness of the assay was evaluated by multiple replicate series of the experimentals series depicted in figure 4 and SI3 executed on different days. The EC50 time curves were generated for 5 independent staurosporine studies (a, b) and 3 independent aspirin studies (c, d). Figures a, c show results for 150kDa FITC-Dextran and figures b, d show results for 4.4kDa TRITC-Dextran. Independent experimental series show comparable results, confirming the robustness of the assays. The EC50 curves represent a total of 330 Caco tubes and over 18,000 datapoints.



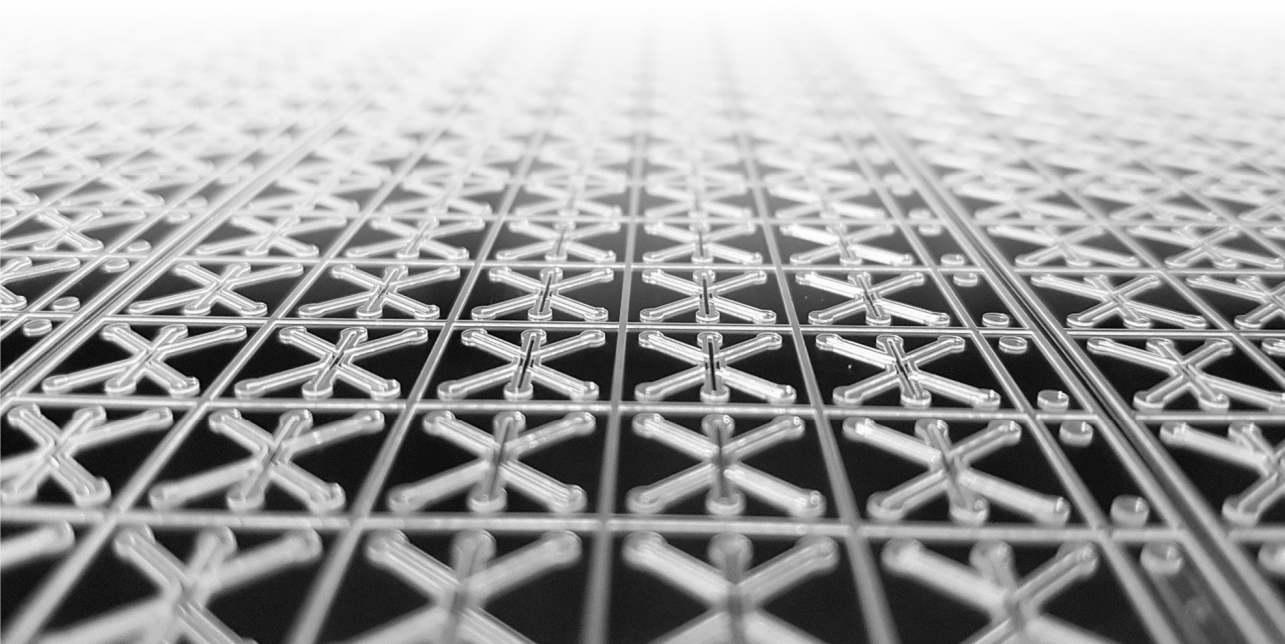
S15 | Phase contrast images of Caco-2 tubes after 96 hours of staurosporine exposure. Even though all concentration already show leakage at this time point, a confluent monolayer is still observed at all but the highest concentration. At 90 μM tubes have fully deteriorated. Dead cells detach and are flushed away by the perfusion flow.



SI6 | Barrier integrity on Caco-layers in conventional Transwell systems exposed to (a) staurosporine and (b) aspirin. Caco-2 cells were seeded at a density of 60×10^3 cells/cm² on 6.5 mm polyester Transwell inserts with 0.4 μm pores. Media was replaced three times per week (DMEM, 10% FCS, 1% NEAA, glutamax, p/s) for three weeks. After three weeks, the apical medium was replaced with 250 μL of medium containing a fluorescent probe (150kD FITC dextran) and staurosporine **(a)** or aspirin **(b)** at varying concentrations. The basolateral media was replaced with 550 μL fresh medium. At various time points, 75 μL basolateral medium was sampled to perform fluorescence measurements using a Fluoroskan FL plate reader. 75 μL fresh medium was added after the aspirin 2hr timepoint to maintain sufficient sample for the remaining sampling time points. Fresh medium was used for 0 hour measurements. Four replicates were used for aspirin at 0 to 0.34 mM and three replicates for the remaining concentrations. For staurosporine 4, 3, 3, 3, 4, 3, and 4 replicates were performed at 0, 0.4, 1.1, 3.3, 10, 30 and 90 μM respectively.

Chapter 6

Model development on the OrganoPlate



Introduction

There is an urgent need for more predictive models in preclinical drug development. While 3D cell cultures and complex co-cultures can offer more physiologically relevant tissue models, they have been generally associated with cumbersome techniques, low throughput and poor compatibility with established assays. Microfluidic techniques and especially organ-on-a-chip technology, show great potential to enable the application of complex, perfused 3D cell culture in a high throughput setting.

The field of microfluidics and organ-on-a-chip has offered many impressive feats of engineering and provided ingenious model systems. A wide range of models has been designed to capture particular aspects of the modelled tissues including detailed geometrical characteristics of e.g. vasculature¹, combinations of multiple tissue types² including the microbiome³, mechanical actuation as pioneered by Ingber et al⁴ or specific readouts⁵. The various application in the field have been extensively reviewed showing a multitude of devices that offer high flexibility and programmability of the devices and exquisite control of the tissues and liquids in the devices.^{6–8} Most platforms use tubing or other off-chip actuators to achieve the needed control, one exception being the surface tension driven platform developed by Beebe et al.⁹ In spite of these great achievements, a lack of widespread adoption of these platforms is apparent.

At the same time, there is a need for robust organ-on-chip platforms as the impressive developments in stem cell research and developmental biology will allow breakthroughs in biomedical and pharmaceutical research. For example, induced pluripotent stem (iPS) cells will allow to create different cell types and tissues from individuals.¹⁰ Organoid technology is rapidly setting new standards in cell culture, with a focus of maintaining the stem cell niche, while allowing tissues to proliferate and differentiate at the same time.¹¹ These techniques are being expanded to model diseases and for usage in the clinic. We are convinced that these biological progress is greatly complemented by the precise control that is made possible with application of microfluidic techniques.

The OrganoPlate is a microfluidic 3D cell culture platform based on a 384 well plate footprint¹². A single titerplate has 40 to 96 microfluidic networks embedded in the bottom layer of the device. Each of the microfluidic networks connects with various wells of the titerplate that are functioning as in- and outlets for the microfluidics. These inlets are either used to administer an extracellular matrix gel or growth medium that is perfused alongside the gel. The gel is patterned using phaseguide-

based capillary pinning, resulting in stratification into lanes for either gel or perfusion flow.

The platform departs from the trend in the field of microfluidics and organ-on-a-chip towards more complex, low throughput devices and aims at providing a robust, easy to use, high throughput system. The passive liquid routing technology of phaseguides is leveraged in combination with gravity driven flow to provide a stand-alone platform that can be used without any specialized equipment or interfaces to the outside world.

The OrganoPlate was first used for (co-)cultures of solid tissues embedded in an extracellular matrix (ECM) including liver and fibroblast cell lines. After proofs of principle were demonstrated for different readouts and dose response curves generation, the scope of tissue types was broadened to include membrane free, perfused barrier type tissues starting with Caco-2 epithelial tubes.¹³

The OrganoPlate was designed as a generic culture platform for complex 3D, perfused (co-)cultures. Moreover, the platform was designed for transfer to and adoption by end-users that are not experts in the field of microfluidics. In this chapter, we will demonstrate the generic aspects of the platform by discussing a number of tissues that were developed as part of or parallel to this thesis. Also, the success of transfer to the end-user is discussed by means of these examples.

It is not the intention to give a comprehensive review of the organ on a chip field or of all platforms being developed by different groups and companies, but rather to give an impression of the potential applications of the OrganoPlate platform and the research efforts that have been undertaken with it.

Liver

One of the earliest tissue types implemented on the OrganoPlate was the liver.¹² This effort was quickly adopted by the Korea Institute of Science and Technology (KIST) in Germany. Mi Jang et al. (Andreas Manz' group) applied the OrganoPlate to develop a liver model and showed the enhanced functionality and metabolism in the OrganoPlate compared to conventional 2D and 3D cell culture.¹⁴ They showed enhanced physiological relevance based on visualization of the morphology and proliferation of cell clusters as well as bile canaliculi formation. Metabolic competence was further demonstrated for albumin and urea production as well as cytochrome P450 1A induction and acetaminophen sensitivity. Increase in sensitivity to toxic compounds, enhance metabolic function and improved morphology was observed when compared to conventional 2D culture, but also

compared to conventional 3D culture, further showing the added value of the organ-on-a-chip model developed. The comparable performance of the platform for the same tissue model in a different lab was one of the first steps towards widespread acceptance and validation of the OrganoPlate platform. Research with a focus on the liver has since been pursued by multiple other groups in Europe and the United States including both academic groups and pharma companies.

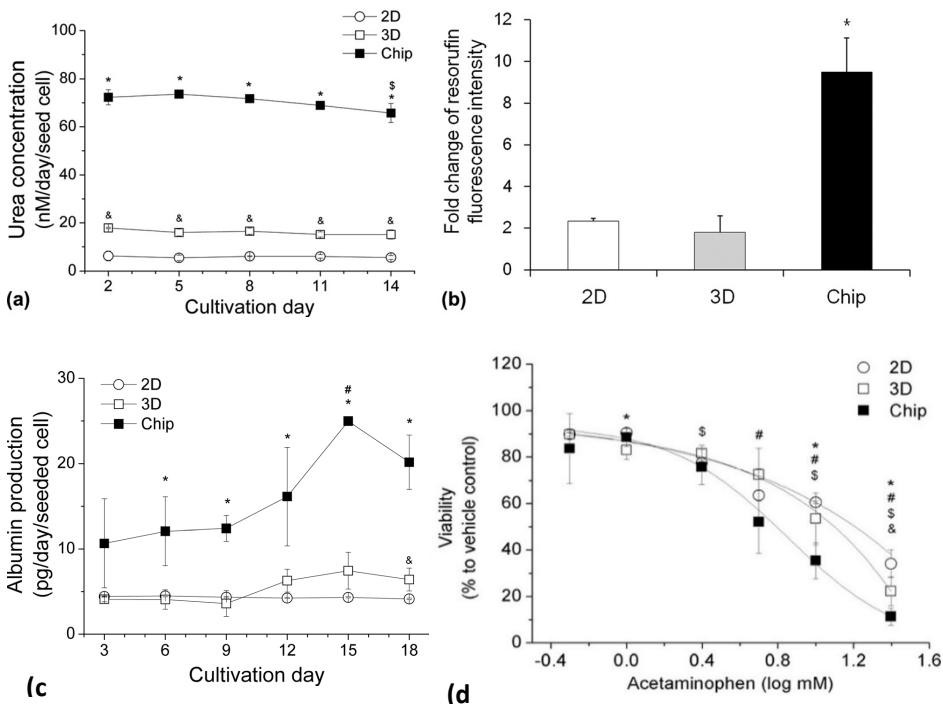


Figure 1 | Characterization of hepatocytes cultured in the OrganoPlate based on urea production (a), cytochrome P450 activity (b), albumin production (c), and acetaminophen sensitivity (d). (* $p < 0.05$). Figures adapted from ref 14.

Neurons

The culturing of neurons has always suffered from a poor availability of primary material and lengthy and sensitive culture methods. The use of iPS derived neurons has the promise to alleviate a part of these issues, but the desire for faster, more robust and more reagent-efficient culture techniques has remained strong. Because of this, multiple initiatives were started to use the OrganoPlate for neuronal models.

At the Luxembourg Center for Systems Biology, Lucumi Moreno et al. (Ronan Fleming group) used the OrganoPlate to differentiate iPS derived neuroepithelial stem cells into functional dopaminergic neurons.¹⁵ After a 30 day differentiation protocol in the OrganoPlate, the cells were characterized based on morphology, immunocytology and electrophysiology. The high biological fidelity of these cells in combination with automation compatibility and low reagent consumption made the use of this platform highly favorable for neuronal culture.

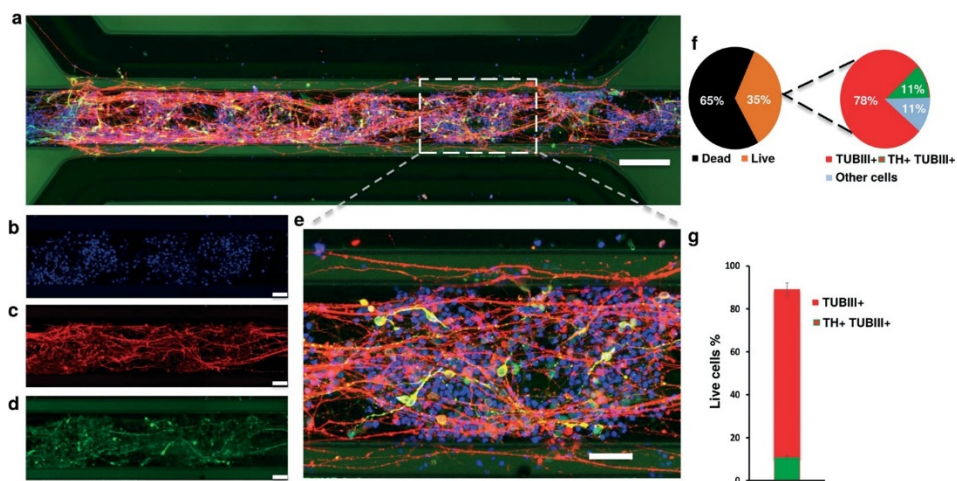


Figure 2 | hiPS derived neurons after 30 days of culture in an OrganoPlate (a,e), stained for nuclei with Hoechst (b), class III β tubulin (TUBIII) as a neuronal marker (c), and tyrosine hydroxylase (TH) as a marker for dopaminergic neurons (d); (a-d: scale bar 50 μ m, e: scale bar 100 μ m). Viability and differentiation efficiency (f,g). Figure reprinted with permission¹⁵.

In the work described by Wevers et al. (MIMETAS labs in collaboration with Westerink Group University of Utrecht, GSK, Sanofi, AbbVie and BASF) this research was followed up by the co-culture of iPS derived neurons with glia cells.¹⁶ The use of various commercially available cells eases adoption of the described protocols by end-users. A protocol was developed where network formation was observed within 24 hrs. Analysis of the network formation over time was demonstrated and the cells were further characterized using immunofluorescence. Calcium imaging was used to further characterize the networks formed by the neurons by visualizing the spontaneous activity of the neurons. The usability of this platform for compound evaluation and toxicity testing. Several model compounds with known mode of action on viability, neurite outgrowth and electrophysiological activity patterns were assayed including methyl mercury, endosulfan, 2,5-hexanedione, GABA and TTX.

The developed neuronal models enable research into various disease areas as well as neurotoxicity using relevant but available cells and scalable readouts to meet a largely unmet need in drug development.

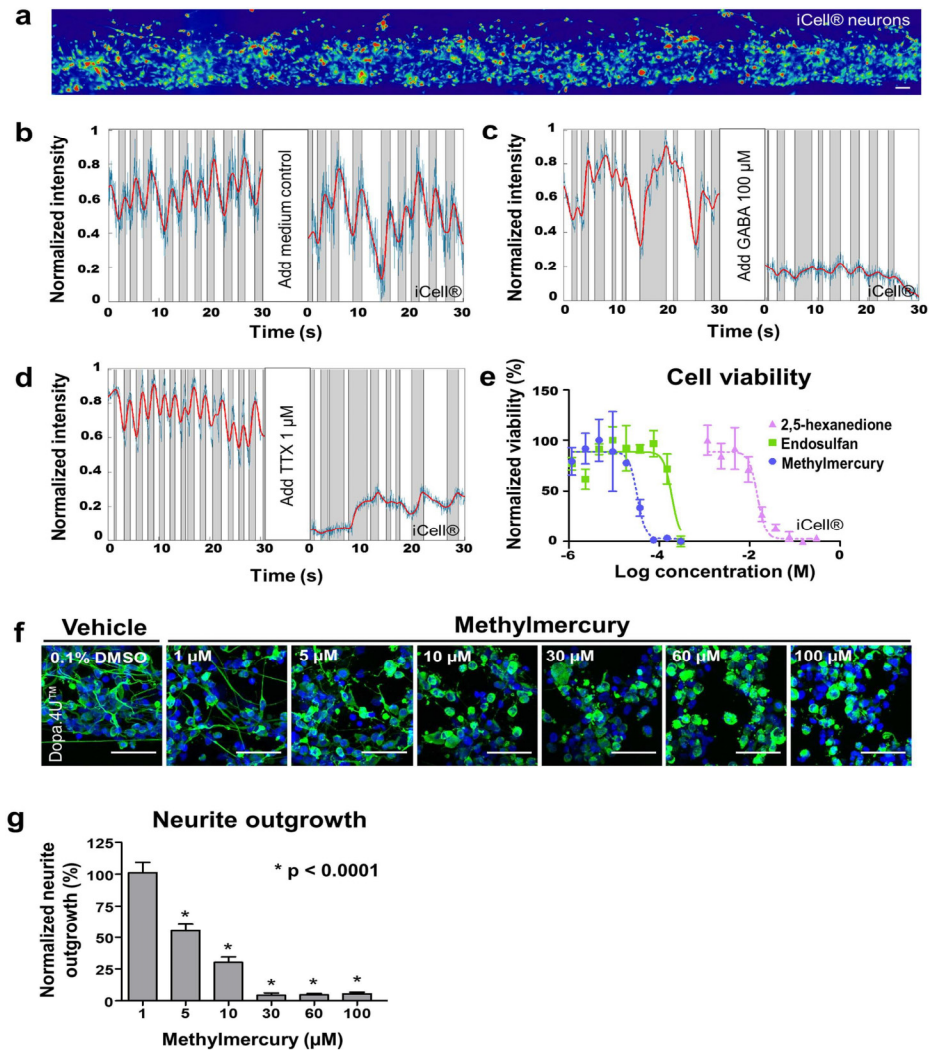


Figure 3 | Overview of assays performed on neuronal models including calcium imaging (a) and spike train analysis of spontaneous and compound modulated activity. Blue and red lines depict unfiltered and filtered traces of an individual neuron, with gray areas indicating inferred spike trains (b-d), and cell viability and neurite outgrowth visualization and analysis after compound exposure. Cells were fixed and stained with β 3-tubulin (neurites, green) and DraQ5 (nuclei, blue) (e-g).¹⁶

Cancer

Clinical use of the OrganoPlate platform was assessed by culturing tumor tissue and evaluating their response to chemotherapeutic treatments. In work described by Lanz et al.¹⁷ (MIMETAS labs and Wang group at Mayo Clinic), protocols were developed to culture breast cancer models in the OrganoPlate. ECM, perfusion and medium conditions were optimized for robust cell culture, and used to grow tumors with known BRCA1 and p53 status. Exposure to various anti-cancer drugs, including paclitaxel, olaparib, and cisplatin, showed an attenuated response. To show the applicability of the platform on primary material, rather than cell lines, cells from patient derived xenografts (PDX) were screened in the platform, showing attenuated response to cisplatin. Based on these protocols, a workflow was proposed for using tumor biopsies in microfluidic devices as an alternative to Xenograft transplantation. This microfluidic protocol would yield results in 21 days instead of 5-9 months showing its potential for future treatment selection in patients.

A wide range of oncological applications are envisioned for the platform. Culture of tumor tissues in a relevant (and modifiable) microenvironment can assist in gaining mechanistic insights in the pathophysiology. Furthermore, the downscaling and parallelization of 3D culture of these tissues can enable efficient study of combination treatments for different types of tumors, or ultimately for (combination) treatment selection or diagnostic stratification of patient populations.

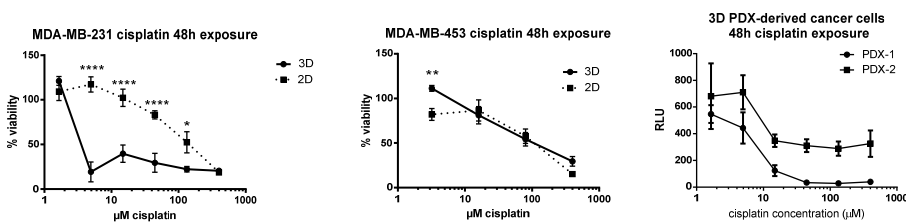


Figure 4 | Response to 48h cisplatin exposure of cell lines in 2D vs 3D and in two PDX derived models show an attenuated effect in some cell lines but not others. The difference in response rate between different PDX derived cells could guide treatment selection. Viability was measured using the luminescent CellTiter-Glo assay (Promega). Adapted from¹⁷

Endothelium

Blood vessels are a crucial constituent of nearly all tissues and play a major role in most complex diseases. Therefore, incorporation of endothelium is an important step towards physiological relevance. Including vasculature enables an *in-vivo* like supply of oxygen and nutrients even into larger and denser tissues. In addition, the signaling molecules excreted by the endothelial cells provide important cues for the surrounding tissue aiding differentiation and functionality.

Van Duinen et al. (MIMETAS labs, Hankemeier and van Zonneveld groups Leiden University) developed a high throughput methodology for culturing and assaying membrane free, perfusable endothelial tubes in a way akin to the methods described in this thesis for intestinal tubules.¹⁸ Van Duinen et al. cultured 96 tubules in parallel from endothelial cells that were fully leaktight for 150kDa TRITC dextran and showed limited permeability for 20 kDa FITC-dextran. The barrier integrity of the endothele tubes was quantified in the cross-platform standard of the apparent permeability (P_{app}) in cm/s. This eases comparison of the data acquired in the microfluidic platform with conventional assays. Moreover, authors show response of the endothele barrier to several cytokines including Vascular Endothelial Growth Factor (VEGF), Interleukin 1 beta (IL1 β), Interleukin 8 (IL8), Interferron gamma (INF γ), Tumor Necrosis Factor alpha (TNF α) and retinoic acid (RA)

In recent work by van Duinen et al. (MIMETAS labs, Hankemeier and van Zonneveld groups, Leiden University, *in preparation*) tubes are exposed to cocktails of growth factors to induce angiogenesis. In the 3-lane design, gradients of signaling molecules are formed and maintained in a stable manner to induce a directional network of perfusable sprouts into the gel. The effect of different combinations of medium components and the characteristics of the gradient is quantified based on the level of sprouting and the morphology of the sprouts. Recently, this work has been applied to co-culture endothelial cells with other cell types: the vascularization from a larger vessel into ECMs is combined with the culture of other tissues to provide perfused vascularization of complex 3D tissue constructs.

Another possibility of this platform is the combination of endothelium with other cell types. Endothelium can be co-cultured with pericytes to construct a comprehensive model of microvasculature. Endothelium is also being combined with neuronal tissues to mimic the neurovascular unit and kidney epithelium towards mimicking the entire kidney clearance pathway.

Finally, co-culture with monocytes is being explored to study monocyte recruitment and transmigration. The range of models comprising a vasculature component thus shows that endothelial models are not only important for vascular research purposes, but for nearly any tissue model, diseased or healthy.

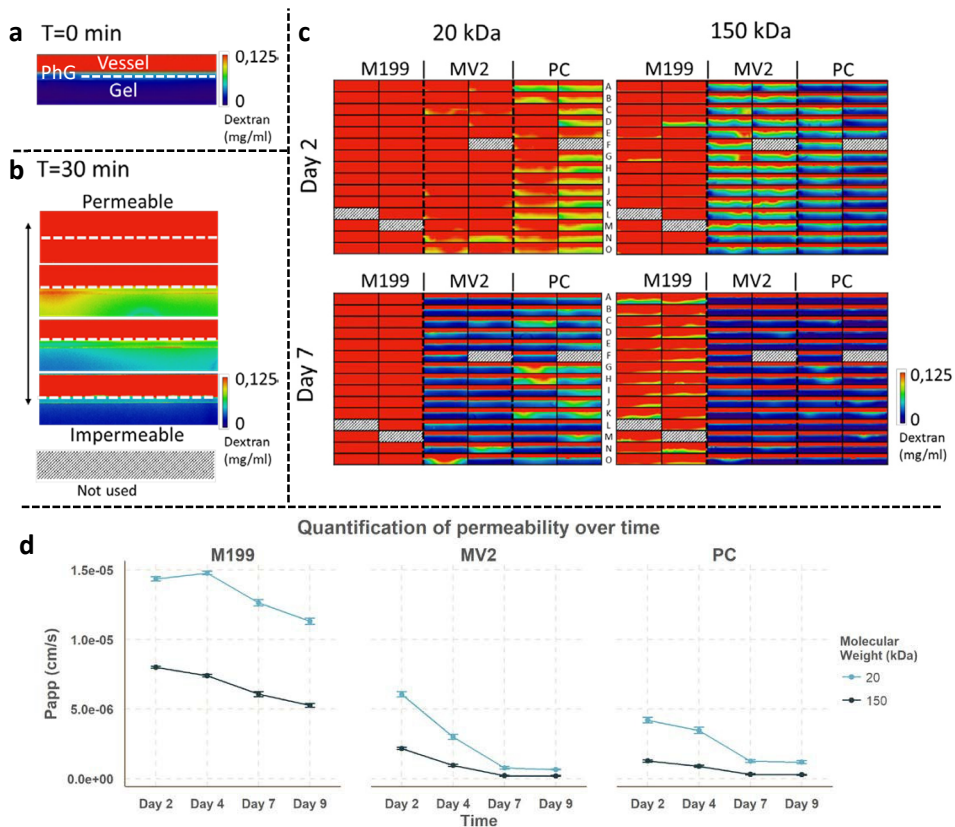


Figure 5 | Representation of the optimization of endothelial culture as described by van Duinen et al including an illustration of the barrier integrity assay with a fluorescent probe diffusion from the vessel into adjacent gel in more permeable vessels. The PhaseGuide (PhG) position is indicated by the white dashed line (**a,b**). Permeability of 86 tubes cultured in three media types is illustrated by the diffusion of fluorescent probes of 20 and 150 kDa at day 2 and 7 in culture. Each rectangle enclosed by a solid black line is an individual chip, with the perfused vessel in the top and gel in the bottom position. PhaseGuide™ location is not indicated in these images. (**c**) The progression of the permeability over time is depicted for each condition by plotting the extracted P_{app} (**d**).

Kidney

The kidney is amongst the critical organs for attrition of new drugs as a result of nephrotoxic events. Notwithstanding this, no models are available to predict such adverse events in humans other than animals. For this purpose, the MIMETAS lab in collaboration with Wilmer Group (Nijmegen University), Masereeuw group (Utrecht University), Suter Group (FHNW, Switzerland) and pharmaceutical companies Roche, GSK and Pfizer set off to develop a kidney model in the OrganoPlate. In a parallel effort to this thesis and similar to the approach described for culture of Caco-2 tubules in Chapter 5, models have been developed to mimic the proximal tubule. Vormann et al. (MIMETAS labs, in prep) developed and validated a nephrotoxicity screening model based on proximal tubules grown in 3D. In addition to developing culture protocols for several different proximal tubule cell sources and assays for measuring barrier integrity and apparent permeability, active transport has been a significant focus within these projects.

Assays were developed to monitor active influx and efflux transport. Fluorescent substrates, and agonists or antagonists for the transporters of interest are used in combination with automated image analysis protocols, to monitor transporter activity. An example of an automated image analysis pipeline is depicted in figure 6. Measuring transporter activity upon exposure to different compounds can give insight into transporter mediated nephrotoxicity and especially drug-drug interaction

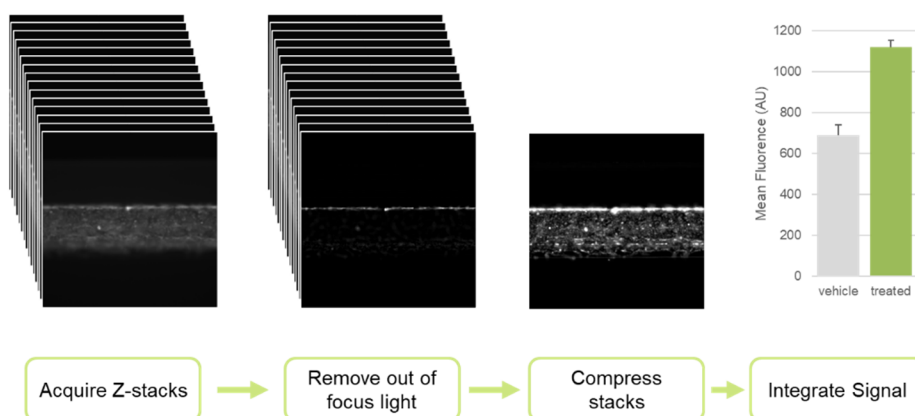


Figure 6 | Automated analysis pipeline to monitor compound uptake into cells. A stack of images is acquired along the z-axis of each tubule. Out of focus light is filtered from each slice and the resulting images are projected into a single image. The signal in the final image is analyzed and represents the uptake of the fluorescent compound into cells throughout the tube.

Organoids

In work described by Schutgens et al. (Clevers group, Hubrecht Institute), their groundbreaking work on organoids is combined with tubular culture in the OrganoPlate¹⁹. The work elaborated on previous achievements in culturing and expansion of adult intestinal *Lgr5*⁺ stem cells that was also translated to other organoid systems.^{11,20–22} In the work by Schutgens, an organoid culture system is described for mouse and healthy and diseased human kidney tissue. By combining this method with the OrganoPlate, the normally spheroidal organoids have been cultured in a tubular fashion as depicted in figure 7. The kidney tubules were leak-tight and polarized, with maintained transporter activity. The change from spheroidal to tubular culture yield access to the basal and apical side of the epithelium, enabling transporter and drug disposition studies.

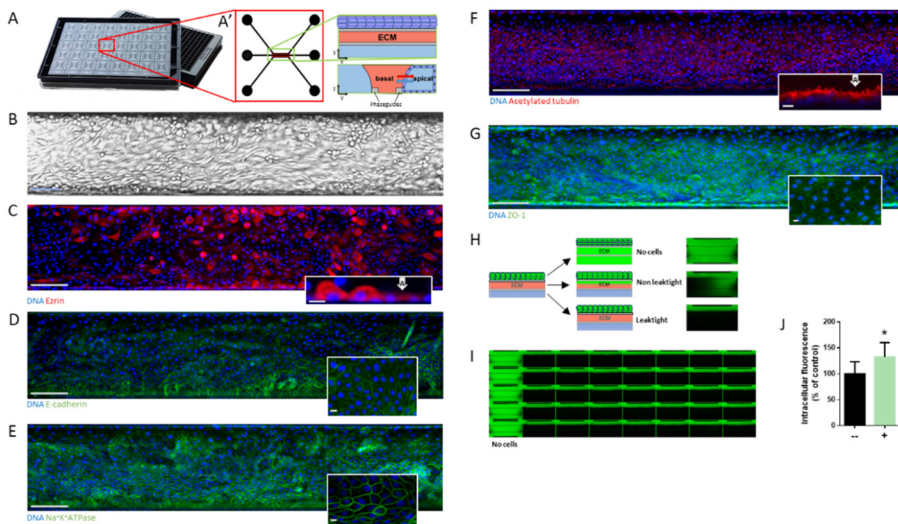


Figure 7 | Organoid derived kidney tubules. Cells are seeded in a manner similar to the process previously described for cell line based epithelial tubes¹³ (A), yielding leaktight, polarized tubes with maintained transporter activity (B-G). The tubes show robust performance in barrier integrity assays and respond appropriately in transporter studies (H-J).

Co-culture

One of the strengths of microfluidic 3D cell culture is the ability to perform complex co-cultures. Figure 8 depicts three examples of possible co-culture configurations. In various collaborations, different co-culture methods are being explored. Vasculature has been added to various models including liver, cancer, kidney, and brain. Other combinations include the addition of pericytes and fibroblasts to endothelium, of various non-parenchymal cells including Kupffer cells to hepatic models and glia to neuronal models. Lastly, co-culture of tissue with circulatory cells such as monocytes or non-mammalian cells such as bacteria is being explored as a method to mimic the interaction of tissues with the immune system and microbiome.

It is expected that co-culture of different cell types will become a standard in micro physiological systems. The membrane-free combination of various cell types enables mimicking of the intimate interaction between cells that is crucial in *in vivo* tissues and can yield vast improvement in physiological relevance of models.

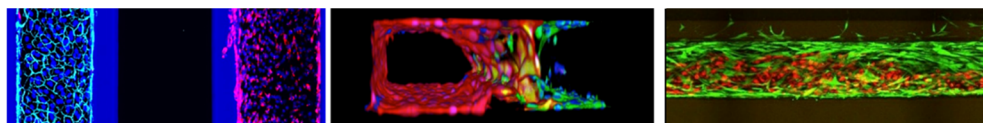


Figure 8 | Examples of co-cultures being explored including adjacent culture of two tubules consisting of kidney epithelium and endothelium (Vascular Endothelial-cadherin labeled Human Umbilical Vein Endothelial cells (HUVEC), green; Acetylated Tubulin labeled Renal Proximal Tubule Endothelial cells (RPTEC), Red, DraQ5 labeled nuclei, blue) (l). Endothelium was cocultured with astrocytes towards mimicking the blood-brain-barrier (RFP labeled HUVECs, red; Vimentin labeled astrocytes, green; DraQ5 labeled nuclei, blue) (m). Another method of coculture was demonstrated by culturing a tubule with an outer layer of pericytes lining an inner tubule of endothelium. (RFP labeled HUVECs, GFP labeled pericytes derived from kidney mesenchymal stem cells, green) (r).

Assays

The application of the OrganoPlate in a screening setting relies heavily on the availability of relevant and compatible readouts for assays performed on the models. The work in this thesis describes the use of widefield and confocal imaging of cells, reporting their morphology and expression of proteins. In addition, a dedicated readout for barrier integrity is described for perfused intestinal epithelium tubes. In addition to these readouts, a plethora of on-plate assays has

been developed including calcium imaging, transport assays, absorption spectroscopy, luminescence spectroscopy, 3D morphological analysis, and invasion assays. All of these assays use an optical readout to optimally leverage the high quality optical access to the plate without overly suffering from downscaling.

In addition to on-plate optical readouts, efforts are ongoing to enable electrical readouts of the models in the OrganoPlate. For example, direct electrophysiological evaluation of neurons in the OrganoPlate is made possible by integrating sensing electrodes inside the microfluidic channel. To maintain ease of implementation, the envisioned plate is designed to be compatible with commercially available multi-electrode array instruments. A second electrical readout that is being developed is the use of impedance spectroscopy to assay barrier function. By making electrical contact with the apical and basal side of a barrier type tissue, impedance measurements can be performed across this barrier. The extracted transepithelial electrical resistance (TEER) is a well-accepted characteristic to describe the barrier function of a cell layer. Enabling such readout will ease the comparison between conventional culture models and data acquired using the OrganoPlate as well as allowing for a non-invasive, high throughput method to evaluate barrier function.

In another research effort, aliquots of the medium are taken for mass spectrometric profiling of metabolites, drugs or drug metabolites.

The range of assays performed on models developed in the microfluidic 3D cell culture platform is expected to continue to grow as more tissues are being constructed. The compatibility with standard equipment and high quality optical access, ensure an easy translation of standard assays to on-plate assays. In addition, the ongoing development of peripheral equipment can further increase the range of assays that can be performed on the platform without sacrificing throughput.

Automation

The OrganoPlate was designed with a focus on throughput and compatibility with current lab instrumentation and robotic systems. The standard 384 well plate layout, glass bottom, and gravity driven perfusion not only make it easy to use manually, but also allow their implementation in a fully automated workflow.

One example of the integration of the titerplate for microfluidic 3D cell culture has been recently described by Kane et al.²³ In this work, a fully automated cell culture platform is presented that includes all steps required for cell culture maintenance, compound exposure and optical readout of cellular parameters over time. The use

of the platform is demonstrated by the successful automation of the generation of personalized *in vitro* models from neuroepithelial stem cells. This level of automation enables the characterization of large numbers of microtissues with increased reproducibility and throughput.

It is envisioned that fully automated workflows including plate handling, liquid handling for cell maintenance, exposures and assays, automated incubator hotels providing rocking and high throughput readouts such as high content imaging systems, will provide all the means necessary to perform large scale screens in the preclinical drug discovery pipeline.

Discussion

The research described above shows a wide range of applications of the OrganoPlate. The standalone and high throughput nature of the platform allows easy adoption by end-users, but of course also has forced some compromises and prerequisites.

One prerequisite of the system is the need for ECM. The presence of ECM is often advantageous for mimicking the *in vivo* microenvironment, but some research efforts have also been focused on culturing cells in 3D without any ECM, for example using hanging drop methods.²⁴ The fundamentals of phaseguide-based, membrane free culture require however the use of an ECM to maintain the architectures as patterned during seeding.

The dimensions and design of the cell culture compartment have been chosen to be a compromise between ease of imaging and 3D cell culture. Where macroscopic ECM embedded cultures can grow a lot larger¹¹ and allow for easy reclamation of cells from this culture, the dimensions of the microfluidics channels limit the maximum size of the tissues to hundreds of micrometers and the glass prevents easy physical access to the tissues. The benefit from this setup is, however, that higher throughput is more easily obtained using optical readouts.

The use of phaseguides for patterning cells in the OrganoPlate allows for side by side layering of different cell types, as well as the creation of perfuseable tubes in channels. This method, however, is limited to side by side patterns that are largely predetermined by the plate geometry. While being easy to adopt in a standard laboratory, and not requiring exogenous compounds or some bioinks, this method allows less freedom than 3D printing approaches that allow for the free patterning

of different cell types in three dimensions.²⁵ On the other hand, however, the achievable resolution is much higher than with current 3D printing methods.

The choice to manufacture OrganoPlates from glass enables high quality optical access, but the result is a rigid device. This is beneficial for handling and robustness, but less compatible with approaches for inducing mechanical cues to the system. Systems using external pressure sources to move flexible membranes incorporated in the microfluidics, such as the ones described by Ingber et al^{26,27}, are much more adept at providing these cues that can be valuable for certain models.

A final compromise that has been made in the OrganoPlate is the choice for gravity driven, bidirectional flow. Systems using integrated² or external pumps²⁸ to achieve active perfusion are commonly able to achieve much higher flow rates and shear combined with truly unidirectional flow. The gravity driven approach of the OrganoPlate yields a laminar flow that reverses direction at a preset interval. This has been a deliberate choice as it is to our knowledge the only manner to perfuse 40 to 96 tissues in parallel in a manner that is still workable for a non-expert end-user and is compatible with high throughput screening set ups. However, the range of flow profiles that can be achieved is more limited than what is possible with active perfusion.

Conclusion

The microfluidic 3D cell culture platform, the OrganoPlate, has been adopted for the development of a wide range of tissue models including mono and co-cultures of both solid and barrier type tissues. ECM embedded 3D cell culture, continuous perfusion and membrane free patterning of tissues is leveraged to yield models of the liver, brain, tumors, kidney, gut, vasculature and many more. Assays have been developed to make use of the parallel setup of the microfluidic devices and provide data in high throughput.

The ease of use and compatibility with standard equipment, combined with a high flexibility for developing complex tissue models has prompted a shift from engineering of complex devices, to the development of complex biology. This transition marks the onset of real adoption of the platform for biological research, rather than microfluidic engineering.

The most important validation of the usability of the OrganoPlate platform is the fact that it has been adopted by a multitude of end-users in laboratories around the world. Currently the OrganoPlate is being used by over 50 companies, institutes or research groups including most of the top 20 pharmaceutical companies. It is thus expected that the OrganoPlate platform will become an industry standard and will help to improve drug development efficiency and to bring better therapies to patients by using patient derived human cell models.

References

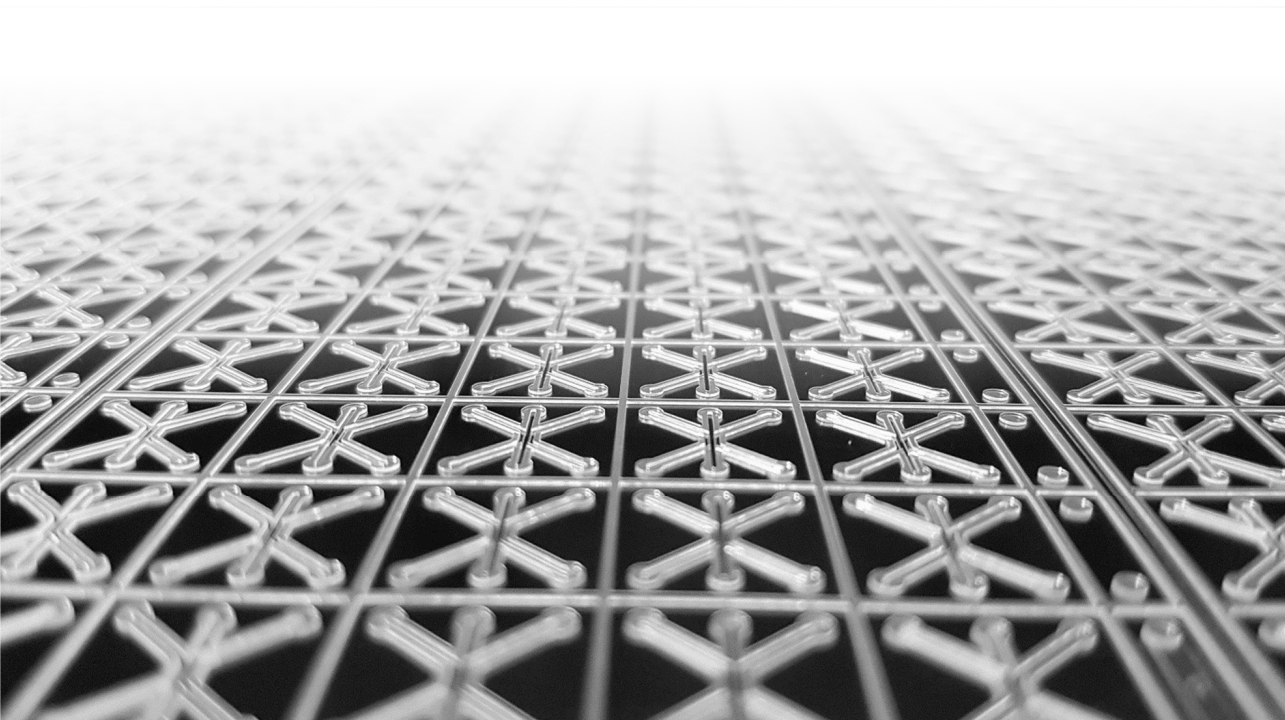
- Costa, P. F., Albers, H. J., Linssen, J. E. A., Middelkamp, H. H. T., van der Hout, L., Passier, R., van den Berg, A., Malda, J., van der Meer, A. D. Mimicking arterial thrombosis in a 3D-printed microfluidic in vitro vascular model based on computed tomography angiography data. *Lab Chip* 18, 1–7 (2017).
- Maschmeyer, I., Lorenz, A. K., Schimek, K., Hasenberg, T., Ramme, A. P., Hübner, J., Lindner, M., Drewell, C., Bauer, S., Thomas, A., Sambo, N. S., Sonntag, F., Lauster, R., Marx, U. A four-organ-chip for interconnected long-term co-culture of human intestine, liver, skin and kidney equivalents. *Lab Chip* 15, 2688–2699 (2015).
- Shah, P., Fritz, J. V., Glaab, E., Desai, M. S., Greenhalgh, K., Frachet, A., Niegowska, M., Estes, M., Jäger, C., Seguin-Devaux, C., Zenhausem, F., Wilmes, P. A microfluidics-based in vitro model of the gastrointestinal human–microbe interface. *Nat. Commun.* 7, 11535 (2016).
- Huh, D., Matthews, B. D., Mammoto, A., Montoya-Zavala, M., Hsin, H. Y., Ingber, D. E. Reconstituting Organ-Level Lung Functions on a Chip. *Science* (80-.). 328, (2010).
- Gaio, N., van Meer, B., Solano, W. Q., Bergers, L., van de Stolpe, A., Mummery, C., Sarro, P. M., Dekker, R. Cytostretch, an Organ-on-Chip platform. *Micromachines* 7, (2016).
- van Duinen, V., Trietsch, S. J., Joore, J., Vulto, P., Hankemeier, T. Microfluidic 3D cell culture: from tools to tissue models. *Curr Opin Biotechnol* 35, 118–126 (2015).
- Bhatia, S. N., Ingber, D. E. Microfluidic organs-on-chips. *Nat. Biotechnol.* 32, 760–772 (2014).
- Junaid, A., Mashaghi, A., Hankemeier, T., Vulto, P. An End-User Perspective on Organ-on-a-Chip: Assays and Usability Aspects. *Curr. Opin. Biomed. Eng.* (2017). doi:10.1016/j.cobme.2017.02.002
- Meyvantsson, I., Warrick, J. W., Hayes, S., Skoien, A., Beebe, D. J., Rodriguez-Zas, S. L., Wheeler, M. B., Bhatia, S. N. Automated cell culture in high density tubeless microfluidic device arrays. *Lab Chip* 8, 717 (2008).
- Park, I. H., Lerou, P. H., Zhao, R., Huo, H., Daley, G. Q. Generation of human-induced pluripotent stem cells. *Nat Protoc* 3, 1180–1186 (2008).
- Sato, T., Vries, R. G., Snippert, H. J., van de Wetering, M., Barker, N., Stange, D. E., van Es, J. H., Abo, A., Kujala, P., Peters, P. J., Clevers, H. Single Lgr5 stem cells build crypt-villus structures in vitro without a mesenchymal niche. *Nature* 459, 262–5 (2009).
- Trietsch, S. J., Israëls, G. D., Joore, J., Hankemeier, T., Vulto, P. Microfluidic titer plate for stratified 3D cell culture. *Lab Chip* 13, 3548–3554 (2013).
- Trietsch, S. J., Naumovska, E., Kurek, D., Setyawati, M. C., Vormann, M. K., Wilschut, K. J., Lanz, H. L., Nicolas, A., Ng, C. P., Joore, J., Kustermann, S., Roth, A., Hankemeier, T., Moisan, A., Vulto, P. Membrane-free culture and real-time barrier integrity assessment of perfused intestinal epithelium tubes. *Nat. Commun.* 8, 262 (2017).
- Jang, M., Neuzil, P., Volk, T., Manz, A., Kleber, A. On-chip three-dimensional cell culture in phaseguides improves hepatocyte functions in vitro. *Biomicrofluidics* 9, 34113 (2015).

15. Moreno, E. L., Hachi, S., Hemmer, K., Trietsch, S. J., Baumuratov, A. S., Hankemeier, T., Vulto, P., Schwamborn, J. C., Fleming, R. M. T. Differentiation of neuroepithelial stem cells into functional dopaminergic neurons in 3D microfluidic cell culture. *Lab Chip* 15, 2419–28 (2015).
16. Wevers, N. R., van Vught, R., Wilschut, K. J., Nicolas, A., Chiang, C., Lanz, H. L., Trietsch, S. J., Joore, J., Vulto, P. High-throughput compound evaluation on 3D networks of neurons and glia in a microfluidic platform. *Sci. Rep.* 6, 38856 (2016).
17. Lanz, H. L., Saleh, A., Kramer, B., Cairns, J., Ng, C. P. N., Yu, J., Trietsch, S. J. T., Hankemeier, T., Joore, J., Vulto, P., Weinshilboum, R., Wang, L. Therapy response testing of breast cancer in a 3D high-throughput perfused microfluidic platform. *BMC Cancer*
18. van Duinen, V., van den heuvel, A., Trietsch, S., Lanz, H., van Gils, J., van Zonneveld, A., Vulto, P., Hankemeier, T. High-throughput permeability assay in vitro on perfused 3D microvessels. *Circ. Res.* submitted, (2017).
19. Schutgens, F., Gijzen, L., Jansn, J., Ammerlaan, C., Vormann, M. K., Lanz, H. L., Rookmaaker, M., Masereeuw, R., Verhaar, M. C., Clevers, H. Kidney organoid-derived cells on a chip and on a hollow fiber. submitted (2017).
20. Huch, M., Gehart, H., Van Boxtel, R., Hamer, K., Blokzijl, F., Verstegen, M. M. A., Ellis, E., Van Wenum, M., Fuchs, S. A., De Ligt, J., Van De Wetering, M., Sasaki, N., Boers, S. J., Kemperman, H., De Jonge, J., Ijzermans, J. N. M., Nieuwenhuis, E. E. S., Hoekstra, R., Strom, S., et al. Long-term culture of genome-stable bipotent stem cells from adult human liver. *Cell* 160, 299–312 (2015).
21. Clevers, H. Review Modeling Development and Disease with Organoids. *Cell* 165, 1586–1597 (2016).
22. Huch, M., Bonfanti, P., Boj, S. F., Sato, T., Loomans, C. J. M., van de Wetering, M., Sojoodi, M., Li, V. S. W., Schuijers, J., Gracanin, A., Ringnald, F., Begthel, H., Hamer, K., Mulder, J., van Es, J. H., de Koning, E., Vries, R. G. J., Heimberg, H., Clevers, H. Unlimited in vitro expansion of adult bi-potent pancreas progenitors through the Lgr5/R-spondin axis. *EMBO J.* 32, 2708–21 (2013).
23. Kane, K. I. W., Moreno, E. L., Hachi, S., Walter, M., Jarazo, J., Hankemeier, T., Vulto, P., Schwamborn, J., Thoma, M., Fleming, R. M. T. Automated microfluidic cell culture of stem cell derived dopaminergic neurons in Parkinson ' s disease. (2017).
24. Bader, E., Migliorini, A., Gegg, M., Moruzzi, N., Gerdes, J., Roscioni, S. S., Bakhti, M., Brandl, E., Irmier, M., Beckers, J., Aichler, M., Feuchtinger, A., Leitzinger, C., Zischka, H., Wang-Sattler, R., Jastroch, M., Tschöp, M., Machicao, F., Staiger, H., et al. Identification of proliferative and mature β -cells in the islets of Langerhans. *Nature* 535, 430–434 (2016).
25. Norotte, C., Marga, F. S., Niklason, L. E., Forgacs, G. Scaffold-free vascular tissue engineering using bioprinting. *Biomaterials* 30, 5910–7 (2009).
26. Kim, H. J., Li, H., Collins, J. J., Ingber, D. E. Contributions of microbiome and mechanical deformation to intestinal bacterial overgrowth and inflammation in a human gut-on-a-chip. *Proc. Natl. Acad. Sci.* 201522193 (2015). doi:10.1073/pnas.1522193112

27. Huh, D., Leslie, D. C., Matthews, B. D., Fraser, J. P., Jurek, S., Hamilton, G. a, Thorneioe, K. S., McAlexander, M. A., Ingber, D. E. A human disease model of drug toxicity-induced pulmonary edema in a lung-on-a-chip microdevice. *Sci. Transl. Med.* 4, 159ra147 (2012).
28. Roest, M., Reininger, A., Zwaginga, J. J., King, M. R., Heemskerk, J. W. M. Flow chamber-based assays to measure thrombus formation in vitro: requirements for standardization. *J. Thromb. Haemost.* 9, 2322–2324 (2011).

Chapter 7

Conclusion and outlook



Conclusion and outlook

In this thesis, microfluidic technology was leveraged to develop a high throughput 3D cell culture platform. This 3D cell culture platform was designed to be used in the discovery and preclinical phases of the drug discovery pipeline. It should improve the predictivity of models that are used for efficacy and toxicity testing of compounds. These models are comprised of human cell cultures that are cultured in the relevant microenvironment. Critical factors to mimic human physiology comprise extracellular matrix embedment, 3D morphology, interaction with multiple cell types and flow. Such complex tissue models should enable selection of better drug candidates in a more efficient manner. Primary constraints to satisfy criteria of physiological relevance of these tissues were following:

- 3D tissue morphology
- Extracellular matrix embedment
- Co-culture of multiple cell types
- Integration of tubules and vessels
- Absence of artificial membranes
- Continuous flow

In addition to constraints of physiological relevance, an equally important aspect in the design of the platform was the fact that the platform could be adopted by end-users that are not necessarily an expert in microfluidics. Therefore, strong emphasis was put on the ease of use of the platform and compatible with standard laboratory equipment and routines. This led to a set of additional design constraints:

- Multiple data points in parallel
- Compatible with high throughput applications
- Stand-alone operation
- Compatibility with standard liquid handlers and imaging equipment
- Inert and biocompatible materials
- Usability by non-experts

To achieve the goal of designing a microfluidic 3D cell culture platform for use in preclinical drug development and screening, we had to select the most appropriate technology to suit these demands. A review of the state of the art in the field of microfluidics in chapter 2 showed a strong trend towards the development of complex operations in microfluidic systems. Categorizing the efforts in the field by fluid control mechanisms and detection methods gave clear insights into the trends in the field: a focus on complex, flexible systems with advanced readout. During this review of the literature the value of gaining throughput by parallel operations was clearly observed. It became, however, also clear that widespread implementation of these technologies in biomedical or pharmaceutical research had not yet occurred. We are convinced that this lack of implementation can be overcome by focusing more on ease of use and ease of adoption of microfluidic technologies. Based on these observations we concluded that for widespread adoption of any microfluidic platform, one should deviate from the search for ever more complex devices, as these are usually low throughput, require dedicated infrastructure and require specialized skills from end-users. Instead, a focus is needed on devices that can be used by non-experts using standard equipment, while maintaining and increasing the throughput in the experimentation needed for research.

Triggered by the conclusions of Chapter 2, in Chapter 3 a passive microfluidic device for screening purposes was developed. The mechanism and possibilities of phaseguide-based microfluidics were studied and extended. Both empirical studies and simulations were used to define the relation between phaseguide shape and stability. The acquired insights were used to guide the design of microfluidic networks with unprecedented passive liquid routing complexity. Selectively filling hundreds of chambers according to predetermined patterns provided a proof of principle for stand-alone, passive microfluidic devices of a complexity previously only achieved with active actuation. The detailed understanding of the functioning of phaseguides, as well as the demonstration of complex operations using passive elements only, further showed the possibilities of performing advanced microfluidic operations without increasing complexity of interfacing the device to the outside world or reducing ease of use. These complex networks can be useful for many applications in the life sciences. We expect that these networks can be used for handling of cells, chemical reactions, sample handling, sample preparation, single cell analysis, 3D cell culture, and probably many more.

The knowledge of passive liquid control gained in chapter 3 was further leveraged in the development of a microfluidic platform using a microtiter plate interface for stratified 3D cell culture in chapter 4. The so-called OrganoPlate was designed on a 384 wells plate footprint and contained up to 96 individual microfluidic networks. Phaseguides were used to pattern extracellular matrix and cells for 3D cell culture, leaving adjacent channels open for perfusion with medium. Gravity was utilized to drive flow by means of reciprocal passive leveling between two reservoirs. This eliminated the need for tubing and pumps. (Co-)culture of various cell types was demonstrated to create organized tissue architecture without usages of artificial membranes. Instead, phaseguides were used to control tissue architecture. A dose dependent response to a known toxic compound was observed and proofs of principle for transmitted light, epifluorescence and confocal microscopy based readouts were shown. The platform developed in this chapter demonstrated the range of applications that can in principle be achieved using a passive, stand-alone microfluidic device. The combination of perfused microfluidic 3D cell culture with high throughput readouts and compatibility with standard equipment formed the basis for the development for a plethora of tissue models.

In chapter 5 of this thesis, the scope of applications developed on the microfluidic platform as described in chapter 4 was expanded from (co-)culture of solid tissues to include barrier type tissues in the form of perfused tubules. The OrganoPlate was utilized to culture human Caco-2 cells as intestinal tubules, with membrane-free basal and apical access. Perfusion in these tubules was prolonged using an interval rocker platform.

In addition to immunohistochemical characterization of the tubes, an assay was developed to monitor their barrier function. The permeability of the tubule could be monitored by perfusing the lumen of the tube with a fluorescent marker. At increased permeability, diffusion of the probe across the cell barrier could be observed. Monitoring of the barrier function during exposure to toxic compounds yielded EC50 curves over time. Such dose response curves could be generated by real time imaging of the barrier integrity up to 8 hours, or be expanded into chronic exposure by intermittent monitoring for over a week. As part of this single study, over 20.000 data points based on more than 350 gut tubes were generated. This yielded the largest published organ-on-chip dataset to date according to our knowledge. The drug-induced loss of epithelial integrity by staurosporine and aspirin was demonstrated, and proved the good predictivity of this model to human physiology.

The platform and culture strategies described in chapter 4 and 5 have been expanded to a multitude of tissue models as described in chapter 6. These include models for solid tissues such as liver, neurons and cancer, but also epithelial and endothelial models including (micro-)vasculature, kidney and gut. In addition to this, complex cultures including organoid and double and triple co-cultures are being developed towards models for e.g. the blood brain barrier, renal clearance and vascularized tissues. These tissue models demonstrated that the platform is generic in nature and many more tissue models are expected to be developed in the future. End-users can decide to use any combination of cells, ECMs and levels of interaction between them to model their tissue of interest. The challenge of building the most physiologically relevant models has thus become one of biological insights and understanding, instead of microfluidic engineering.

As with any design, decisions made to increase ease of use, robustness and throughput of the platform also enforce some limitation such as a limit to the maximum size of the tissues, the maximum achievable flow, absence of mechanical cues and direct access to the tissues. The wide application of the OrganoPlate shows that this combination of strengths, including the limitation imposed by them, has a valuable place between the other platforms and research efforts in the organ-on-a-chip field.

For the various models that were developed on the OrganoPlate, a wide spectrum of assays has been, and is continuously being developed including complex morphological analysis, angiogenesis, neuronal activity, mitochondrial, metabolic function and mass spectrometric molecular analysis. The compatibility with high quality optical readouts is used in high throughput, high content assays, but other types of readout including off-plate (bio-)chemical analysis or e.g. electrical readout have also been developed.

The combination of the unprecedented level of robustness and throughput demonstrated by the platform, combined with the fact that it can be easily adopted by non-expert end-users has enabled wide spread implementation of the OrganoPlate platform developed in this thesis.

Current OrganoPlate models are comprised of human cells that are used to create healthy or diseased models. Cell sources may be a cell line, primary cells, induced pluripotent stem cells or organoids. All these techniques have been shown compatible. Primary cells, organoids and iPS derived cells offer the promise to generate disease models for some of today's most complex diseases, including

Alzheimer's and Parkinson's Disease. Techniques such as Crispr/CAS could be exploited as well to induce specific disease phenotypes. In a next stage, we predict that the OrganoPlate will become a useful tool in diagnostics: patient-derived material can be transferred to the OrganoPlate and used to establish organotypic 3D cell culture models to diagnose the presence of a disease, to predict the development of a disease, and probably most important, to predict the treatment outcome by exposing them to a panel of treatment options. First steps towards these applications have been shown in Chapter 6.

Probably the most valuable outcome of the research in this thesis is the wide spread adoption of the OrganoPlate in both academic labs, pharmaceutical industry, consumer-goods companies and chemical industry. The platform is well underway to become an industry standard and prove its value to increase efficiency in drug development and select better therapies for patients.

Addendum

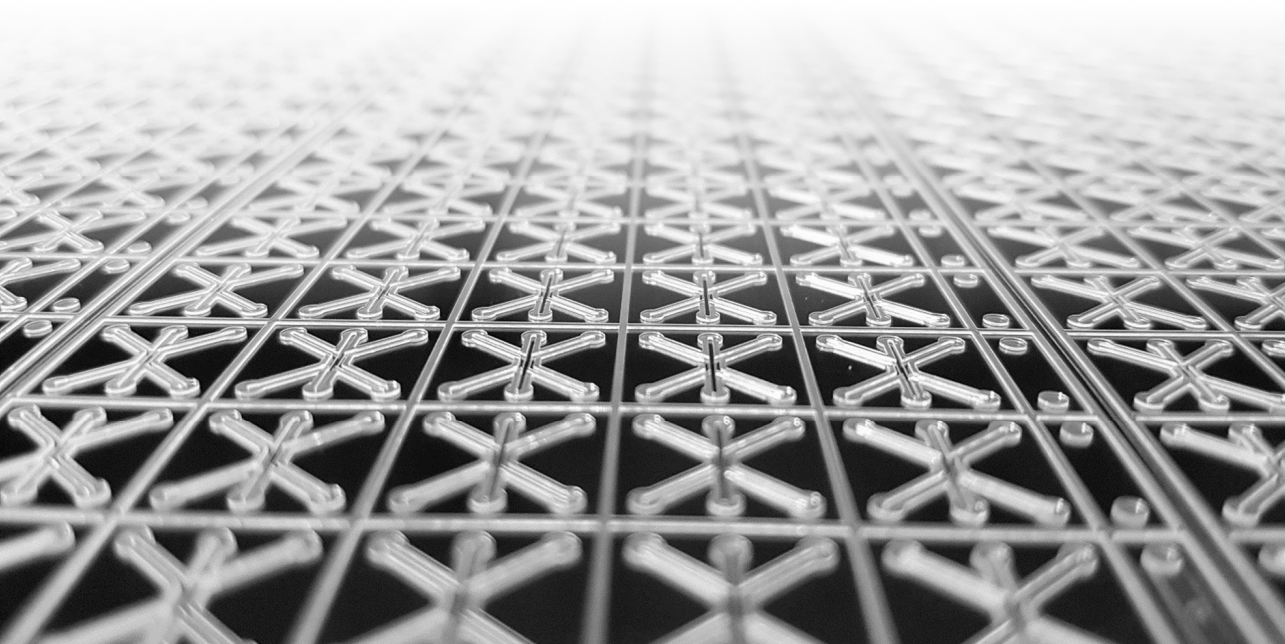
Summary

Nederlandse Samenvatting

Curriculum Vitea

List of publications

Acknowledgements



Summary

In **Chapter 1**, the general introduction, an overview is given of the current drug delivery pipeline and the huge associated developmental cost per drug that reaches the market. The main method to reduce these costs is seen in better selection of drug candidates in early phases of the development, by using more physiologically relevant cell culture models.

Cells cultured in 3D have been recognized to more closely resemble the physiological situation, but widespread adoption in drug discovery is lacking due to limited compatibility and limited recapitulation of complex tissue aspects such as complex co-culture and perfusion.

The field of microfluidics offers tools to control liquid flows and patterns and is applied in the Organ-on-a-Chip field to build complex tissue models with tightly controlled microenvironments. An overview of the state of this field shows a focus on highly advances, but often complex and low throughput models systems.

The scope of the thesis is to develop a microfluidic platform that enables enhanced physiology in cell culture models including 3D cell culture, co-culture and perfusion flow, whilst maintaining throughput, compatibility and usability by end-users.

In **Chapter 2**, a review is performed of the state of the art in lab-on-a-chip (LOC) technology. The review is written to introduce the field of LOC to scientists from different disciplines, but was also used by the authors to understand the focus of the field and decide what technologies could be used to benefit the platform envisioned in this thesis.

Lab-on-a-chip (LOC) technology focusses on improving experimentation and analysis in the life sciences through miniaturization. The developments in the field have led to significant increases in analysis throughput, more than billion-fold sample volume reductions and increased separation efficiency. Despite this, the existence and the implications of LOCs are not widely known outside its community.

Some of the most important LOCs, their physical operating principles and the unique benefits that can be gained through miniaturization are discussed, and the chapter is concluded by a discussion of the potential of LOCs for massive parallel data generation and the life sciences.

After observing the focus of the LOC field it was realized that a platform needed to be developed that allowed for preprogrammed, stand-alone, easy operation. **Chapter 3** describes the development of the phaseguiding principle into a microfluidic passive valving platform with full control of the stability of each valve. Phaseguides, which are small ridges at the bottom of a channel acting as pinning barriers are used as burst valves with predetermined stability. The angle between the wall and a phaseguide is shown to determine its stability and this relationship is characterized numerically, analytically and experimentally. It is demonstrated that liquid routing can be performed by using multiple phaseguide with different stability values. Controlled filling of complex matrices of chambers is demonstrated leading up to the use of a 400-chamber network as a pixel array. The use of this elegant method for liquid routing shows its potential for implementation in microfluidic devices for the life sciences.

In **chapter 4**, the technology refined in chapter 3 is implemented for 3D cell culture. A stratified 3D cell culture platform, the OrganoPlate, is proposed that uses phaseguides to better recapitulate heterogeneity of human tissues and organs. Adjacent lanes of gels and liquids are patterned by phaseguides to capture the inherent heterogeneity of human tissues and organs. Membrane free stratification of 3D cell (co-)cultures under perfusion is used to mimic the interplay between different cell types in tissues, their secondary tissue architecture, vascular system and gradients of signaling molecules and metabolites. 3D cell culture of HepG2 hepatocytes under continuous perfusion is demonstrated as well as a rifampicin toxicity assay and co-culture with fibroblasts. 4T1 breast cancer cells are used to demonstrate invasion and aggregation models. The incorporation of the platform in a microtiter plate format ensures compatibility with automation and high-content screening equipment. The combination of functionality, ease of use and compatibility enable widespread adoption of this platform in academia as well as a screening setting.

Where chapter 4 focusses on embedded 3D cell culture, **chapter 5** extends the use of the OrganoPlate to perfused tubules. Perfused extracellular matrix-supported intestinal tubules, exhibiting tissue polarization and transporter expression are demonstrated. Forty leak tight tubules are cultured in parallel on a single plate and their response to pharmacological stimuli is recorded over 125 hours using automated imaging techniques. A study comprising 357 gut tubes is performed of which 93% are leak tight before exposure. EC50-time curves are extracted that provide insight in both concentration and exposure time response. The study in this chapter represents the largest organ-on-a-chip dataset known to the authors, demonstrating its scalability both in biological applications and in throughput.

In **Chapter 6**, the adoption of the developed platform for a wide range of applications is described. A brief overview of the research efforts in the field of organs-on-chips is provided showing a focus on impressively complex, but low throughput model systems. The applicability of a platform with more focus on ease of use, compatibility and throughput is demonstrated with examples of models developed on the OrganoPlate by different researchers. Models are described for a range of tissues or diseases including liver, neurons, cancer, endothelium, and kidney. Complex models including the use of organoids, and co-culture is described as well as the possibilities for developing complex assays and implementation of automation. Its wide adoption for across different tissue models as well as different users is possibly the most valid proof of the utility of the system.

In **Chapter 7**, the conclusion and outlook of the thesis, the initial design criteria of the platform are described to include both biological and usability aspects. The biological aspects focus on ECM embedded 3D co-culture, including perfused tubules, while the usability aspects focus on throughput, ease of use and compatibility. Throughout the thesis, these design criteria have been heeded, yielding a platform that is widely used and is on its way to become an industry standard in preclinical drug development.

Nederlandse Samenvatting

In **hoofdstuk 1**, de algemene introductie, wordt een overzicht gegeven van de huidige drug delivery pipeline en de enorme bijbehorende ontwikkelingskosten per geneesmiddel dat op de markt komt. Een van de meest veelbelovende manieren om deze kosten te verlagen, is een betere selectie van kandidaat-geneesmiddelen in vroege fase van de ontwikkeling, door meer fysiologisch relevante weefselkweek modellen te gebruiken.

Het is bekend dat 3D gekweekte weefsel meer representatief zijn voor de fysiologische situatie. Toch worden deze modellen niet veel gebruikt vanwege beperkte compatibiliteit met andere technieken en het deels ontbreken van complexe weefselaspecten zoals complexe co-cultuur en perfusie.

Het veld van de microfluidica biedt precieze controle over hoe vloeistoffen zich in chips gedragen. Dit wordt toegepast in zogenaamde Organs-on-Chips om complexe weefselmodellen met onder strak gedefinieerde omstandigheden te bouwen. Een overzicht van de status van dit veld toont een focus op zeer geavanceerde, maar vaak complexe systemen met een lage doorvoersnelheid.

Het doel van het proefschrift is om een microfluidisch platform te ontwikkelen dat verbeterde fysiologie mogelijk maakt in weefselmodellen, inclusief 3D-celkweek, co-kweek en perfusie, terwijl de doorvoer, compatibiliteit en bruikbaarheid door eindgebruikers behouden blijven.

In **hoofdstuk 2** wordt een overzicht gegeven van de nieuwste technieken in lab-on-a-chip (LOC) technologie. De review is geschreven om het veld van LOC te introduceren bij wetenschappers uit verschillende disciplines. Tegelijkertijd hebben de auteurs de focus van het veld bekeken om te zien welke technieken er toepasbaar zouden zijn in het beoogde 3D kweek platform.

Lab-on-a-chip technologie richt zich op het verbeteren van experimenten en analyses in de levenswetenschappen door middel van miniaturisatie. Ontwikkelingen in dit veld hebben geleid tot een aanzienlijke toename van de analyse-doorvoer, meer dan een miljardvoudige vermindering van benodigde monstervolumes en een verhoogde scheidingsefficiëntie. Desondanks krijgt het veld en zijn toepassingen weinig aandacht buiten de gemeenschap. Enkele van de belangrijkste labs-on-chips, hun werkingsprincipes en de voordelen die kunnen worden behaald via miniaturisatie worden besproken.

Het hoofdstuk wordt afgesloten met een bespreking van de potentie van LOC's voor het parallel genereren van grote hoeveelheden data en toepassingen voor de levenswetenschappen.

Na het observeren van de focus van het LOC-veld, werd het duidelijk dat er een platform moest worden ontwikkeld met de focus op bruikbaarheid door daadwerkelijke eindgebruikers.

Hoofdstuk 3 beschrijft de verdere ontwikkeling van phaseguides tot een platform waarin ze als voorgeprogrammeerde kleppen worden gebruikt om vloeistoffen te sturen. Phaseguides zijn ribbels op de bodem van een microfluidisch kanaal. Doormiddel van oppervlaktespannen kunnen ribbels vloeistoffen tegen houden. Het wordt aangetoond dat de hoek tussen de wand van het kanaal en de phaseguide de stabiliteit van de phaseguide bepaald. Deze relatie wordt numeriek, analytisch en experimenteel gekarakteriseerd.

Er wordt aangetoond dat het vulpatroon van een microfluidisch gestuurd kan worden met behulp van meerdere faseguide met verschillende stabiliteitswaarden. Een complexe matrix van kamers worden gecontroleerd gevuld. De ultieme demonstratie van de controle over het vulgedrag is het gebruik van een netwerk van 400 kamers als een pixel array.

Het gebruik van deze elegante methode om vloeistofstromen te sturen toont zijn potentieel voor implementatie in microfluidische apparaten voor de levenswetenschappen.

In **hoofdstuk 4** wordt deze techniek geïmplementeerd voor 3D-celkweek in de OrganoPlate. In dit gelaagde 3D-celkweekplatform wordt gedemonstreerd dat met behulp van phaseguides de heterogeniteit van menselijke weefsels en organen beter na te bootsen valt. Met behulp van phaseguides worden laantjes van gels en vloeistoffen naast elkaar gepatroneerd om de inherente heterogeniteit van menselijke weefsels en organen te weerspiegelen. Op deze manier kunnen de aangrenzende laantjes zonder tussenliggende membranen met elkaar in verbinding staan en geperfundeerd worden.

HepG2-hepatocyten worden onder continue perfusie in 3D gekweekt. Een toxiciteitstest wordt gedemonstreerd aan de hand van rifampicine en co-kweek mogelijkheden in combinatie met fibroblasten. 4T1 borstkankercellen worden gebruikt om invasie- en aggregatiemodellen te demonstreren.

De integratie van het platform in het formaat van een standaard microtiterplaat zorgt voor compatibiliteit met automatisering en screeningapparatuur. De combinatie van functionaliteit, gebruiksgemak en compatibiliteit maakt wijdverspreide acceptatie van dit platform in de academische wereld en een screeningomgeving mogelijk.

Waar hoofdstuk 4 focust op ingebedde 3D-celculturen, breidt **hoofdstuk 5** het gebruik van de OrganoPlate uit naar geperfundeerde buizen. Extracellulaire matrix-ondersteunde darmbuisjes onder perfusie resulteert in gepolariseerde weefsels met de correcte transporter expressie.

Op een plaat kunnen tegelijkertijd veertig lekdicte buizen worden gekweekt. Gedurende 125 uur wordt hun respons op farmacologische stimuli geregistreerd met behulp van een geautomatiseerde microscoop. In dit experiment worden 357 buizen gekweekt waarvan 93% lekdicht was bij aanvang. Door te meten over de tijd kan er een curve worden gebouwd van de verandering van de EC50 door de tijd. Dit geeft in een keer inzicht in het effect van doses als blootstellingsduur.

Voor zover bekend bij de auteurs is dit de grootste gepubliceerde organ-on-a-chip dataset. Dit toont de schaalbaarheid in zowel de biologische toepassingen als in de doorvoer.

In **hoofdstuk 6** wordt de invoering van het ontwikkelde platform voor een breed scala van toepassingen beschreven. Een kort overzicht van de lopende onderzoeken op het gebied van organs-on-chips toont een focus op modellen met een indrukwekkende complexiteit, maar dit gaat vaak ten koste van de doorvoer en bruikbaarheid.

De potentie van een platform met meer focus op gebruiksgemak, compatibiliteit en verwerkingscapaciteit wordt aangetoond aan de hand van voorbeelden van modellen die door verschillende onderzoekers op de OrganoPlate zijn ontwikkeld.

Er wordt een overzicht gegeven van verschillende weefsels die op de OrganoPlate zijn gemodelleerd, waaronder lever, neuronen, kanker, endotheel en nier. Complexe modellen zoals het gebruik van organoïden en co-cultuur worden beschreven, evenals de mogelijkheden voor het ontwikkelen van complexe assays en implementatie van automatisering.

De brede acceptatie van dit systeem voor verschillende weefselmodellen door verschillende gebruikers is mogelijk het sterkste bewijs van het nut ervan.

In **Hoofdstuk 7**, de conclusie van het proefschrift, wordt beschreven dat de initiële ontwerpcriteria van het platform zowel biologische als bruikbaarheidsaspecten omvatte. De biologische aspecten waren gericht op ECM-ondersteunde 3D-co-kweek, inclusief geperfundeerde buizen, terwijl de bruikbaarheidsaspecten zich richtten op doorvoer, gebruiksgemak en compatibiliteit. Gedurende het proefschrift zijn deze ontwerpcriteria opgevolgd, wat een platform heeft oplevert dat op grote schaal wordt gebruikt en op weg is om een industriestandaard te worden in de preklinische ontwikkeling van geneesmiddelen.

Curriculum Vitae

Sebastiaan Johannes Trietsch werd geboren op 9 augustus 1985 in Den Haag. In 2003 behaalde hij zijn VWO diploma op Dalton Den Haag, waarna hij zijn studie Biofarmaceutische wetenschappen in Leiden begon. Tijdens zijn studie was hij voorzitter van de L.P.S.V. „Aesculapius”. Voor zijn masterscriptie heeft hij 6 maanden onderzoek gedaan naar de invloeden van elektrostatische lading op de dosering van inhalatiemedicijnen aan de Faculty of Pharmacy van de University of Sydney. Na het afronden van zijn master is hij zijn promotieonderzoek bij prof. Dr. Thomas Hankemeier begonnen aan de divisie Analytical Biosciences van het Leiden Academic Center for Drug Research. Als onderdeel van het Netherlands Metabolomics Center heeft hij hier meerder microfabricage processen opgezet, waarvan een deel toegepast is in dit proefschrift. Het onderzoek dat hier is uitgevoerd in samenwerking met Paul Vulto heeft geleid tot de ontwikkeling van de OrganoPlate. Op basis van dit platform heeft hij samen met Paul Vulto, Jos Joore, Thomas Hankemeier en Herbert Heineker het bedrijf Mimetas opgericht. Mimetas is in korte tijd uitgegroeid tot een bloeiend bedrijf en hij is hier tot op heden werkzaam als head of research.

List of publications

In this thesis

Trietsch, S. J., Hankemeier, T., Van der Linden, H. J. Lab-on-a-chip technologies for massive parallel data generation in the life sciences: A review. *Chemom. Intell. Lab. Syst.* 108, 64–75 (2011).

Yildirim, E. *, **Trietsch, S. J. ***, Joore, J., van den Berg, A., Hankemeier, T., Vulto, P. Phaseguides as tunable passive microvalves for liquid routing in complex microfluidic networks. *Lab Chip* 14, 3334–40 (2014).

Trietsch, S. J., Israëls, G. D., Joore, J., Hankemeier, T., Vulto, P. Microfluidic titer plate for stratified 3D cell culture. *Lab Chip* 13, 3548–54 (2013).

Trietsch, S. J., Naumovska, E., Kurek, D., Setyawati, M.C., Vormann, M.K., Wilschut, K.J., Lanz, H.L., Nicholas, A, Ng, C.P., Joore, J., Kustermann, S., Roth, A., Hankemeier, T, Moisan, A. *, Vulto, P. * Membrane-free culture and real-time barrier integrity assessment of perfused intestinal epithelium tubes, *Nature Communications* 262 (2017)

Other publications

Kwok, P. C. L., **Trietsch, S. J.**, Kumon, M., Chan, H.-K. Electrostatic charge characteristics of jet nebulized aerosols. *J. Aerosol Med. Pulm. Drug Deliv.* 23, 149–159 (2010).

Quist, J., **Trietsch, S. J.**, Vulto, P., Hankemeier, T. Elastomeric microvalves as tunable nanochannels for concentration polarization. *Lab Chip* 13, 4810–4815 (2013).

van der Maaden, K.*, **Trietsch, S. J.***, Kraan, H., Varypataki, E. M., Romeijn, S., Zwier, R., van der Linden, H. J., Kersten, G., Hankemeier, T., Jiskoot, W. Novel hollow microneedle technology for depth-controlled microinjection-mediated dermal vaccination: a study with polio vaccine in rats. *Pharm. Res.* 31, 1846 (2014).

Phurimsak, C., Yildirim, E., Tarn, M. D., **Trietsch, S. J.**, Hankemeier, T., Pamme, N., Vulto, P. Phaseguide assisted liquid lamination for magnetic particle-based assays. *Lab Chip* 14, 2334–2343 (2014).

Moreno, E. L., Hachi, S., Hemmer, K., **Trietsch, S. J.**, Baumuratov, A. S., Hankemeier, T., Vulto, P., Schwamborn, J. C., Fleming, R. M. T. Differentiation of neuroepithelial stem cells into functional dopaminergic neurons in 3D microfluidic cell culture. *Lab Chip* 15, 2419–28 (2015).

van Duinen, V., **Trietsch, S. J.**, Joore, J., Vulto, P., Hankemeier, T. Microfluidic 3D cell culture: from tools to tissue models. *Curr. Opin. Biotechnol.* 35, 118–126 (2015).

Wevers, N. R., van Vught, R., Wilschut, K. J., Nicolas, A., Chiang, C., Lanz, H. L., **Trietsch, S. J.**, Joore, J., Vulto, P. High-throughput compound evaluation on 3D networks of neurons and glia in a microfluidic platform. *Sci. Rep.* 6, 38856 (2016).

Lanz H. L., Saleh A., Kramer B., Cairns J., Ng C. P., Yu J, **Trietsch S. J.**, Hankemeier T., Joore J., Vulto P., Weinshilboum R., Wang L. Therapy response testing of breast cancer in a 3D high-throughput perfused microfluidic platform. *BMC Cancer* 17, 709 (2017)

*authors contributed equally

Patents

Vulto, P., **Trietsch, S.J.**, Arnaud, N., Michel, Y., Apparatus for inducing microfluidic flow (2017)

Vulto, P., **Trietsch, S.J.**, Lanz, H.L., Vormann, M.K. barrier function measurements (2017)

Vulto, P., **Trietsch, S.J.**, Yilderim, E. Improvements relating to capillary pressure barriers, (2015)

Vulto, P., **Trietsch, S.J.**, Microfluidic plate (2016)

Vulto, P., **Trietsch, S.J.**, Yilderim, E. Fluid Triggerable Valves (2015)

Vulto, P., **Trietsch, S.J.**, van der Linden, H.J., Joore, A.J., Hankemeier, T. Apparatuses for and methods of processing cells and related structures (2014)

van der Maaden, K., **Trietsch, S.J.**, van der Linden, H.J., Bouwstra, J.A., Hankemeier, H. Process and device for minimally invasive deep tissue probing (2014)

Trietsch, S.J., Quist, J., Vulto, P., Hankemeier, T. Method and apparatus for processing a liquid (2014)

Acknowledgements

I owe many people thanks for the completion of this thesis.

Thomas, for getting me back to Leiden and enabling everything there.

My colleagues and friends at ABS for setting a stage filled with science and good fun.

Collaborators in the early years, for chasing down many ideas, however farfetched.

Paul, for dropping by and changing the journey into the great adventure it has become.

The OrganoPlate early birds, for joining while we were still embryonic and nursing it into a great team.

The entire team at Mimetas, for taking this all the way and making it unforgettable.

Family and friends, old and new, who have made what is in this book possible, by keeping everything that is not in it interesting.

My paranymphs, for their support in the finale.

And, of course, Daphne.

